ISSN 1410-1675

BULLETIN OF THE MARINE GEOLOGY

VOLUME 38 • NUMBER 2 • DEC. 2023

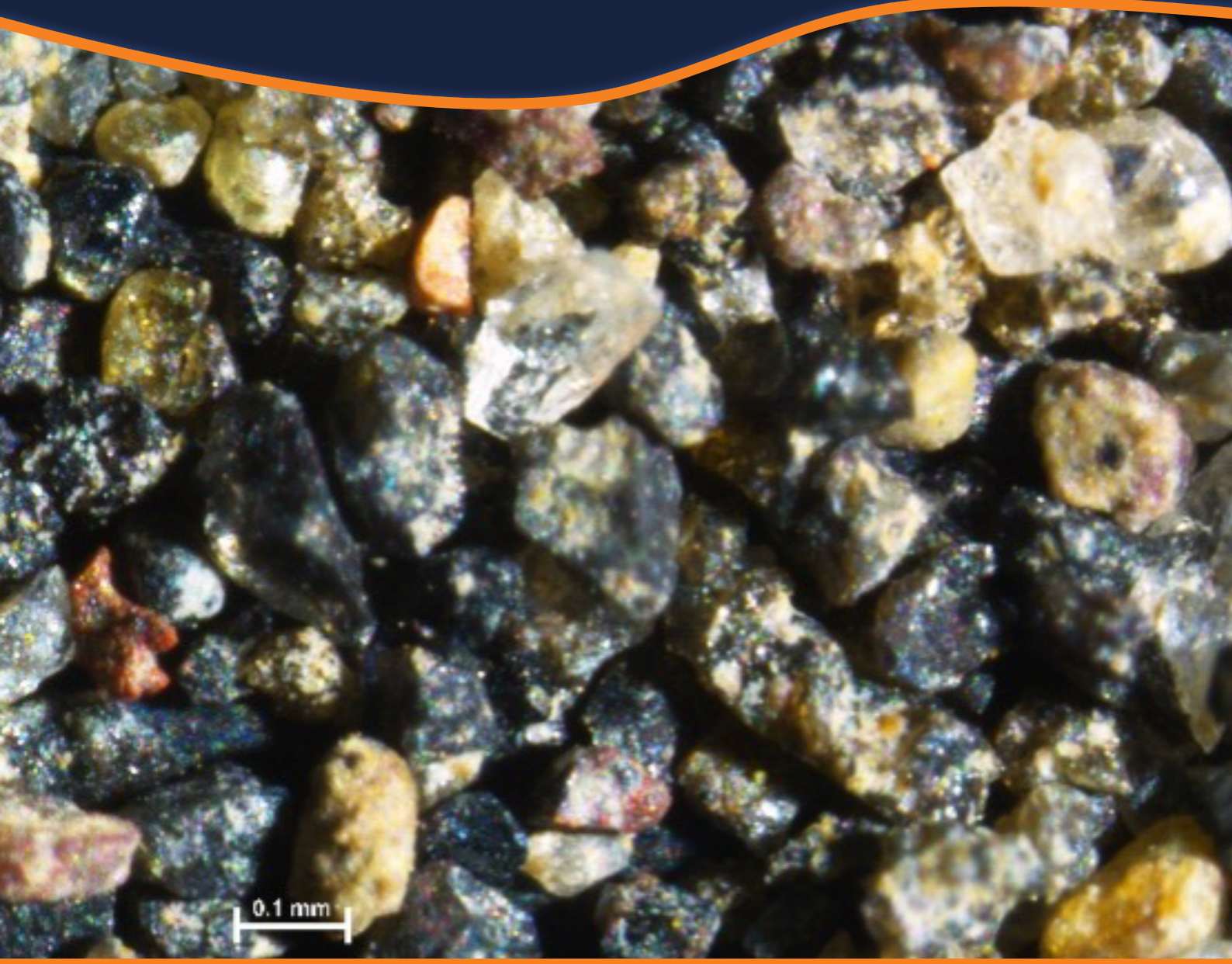

BoMG	VOL. 38	NO. 2	PAGE 54-116	BANDUNG, DEC. 2023	ISSN 1410-6175

Accredited : RISTEK-BRIN 200/M/KPT/2020

MARINE GEOLOGICAL INSTITUTE
GEOLOGICAL AGENCY
MINISTRY OF ENERGY AND MINERAL RESOURCES

BALAI BESAR SURVEI DAN PEMETAAN GEOLOGI KELAUTAN
BADAN GEOLOGI
KEMENTERIAN ENERGI DAN SUMBER DAYA MINERAL

BULLETIN OF THE MARINE GEOLOGY

Vol. 38, No. 2, December 2023

For communication of this publications, please contact :
MARINE GEOLOGICAL INSTITUTE
Dr. Junjunan 236, Bandung-40174, Indonesia
Telephone : +62-22-6032020, 6032201, Fax : +62-22- 6017887
E-mail : ejournal.p3gl@gmail.com

Cover Figure : Megascopically of second paleotsunami deposits (Source: Yudhicara, 2023)

Preface

The second edition of our journal, Bulletin of the Marine Geology (BOMG) in 2023 contains six papers from various scientific disciplines written by experts in each field. The Editorial Board appreciates those who have contributed to submitting papers or reviewing them.

The first paper describes the examination of surface microtexture with well-preserved foraminifera specimens using SEM-EDS which is considered good for knowing small-scale carbonate diagenesis products beyond the traditional binocular microscope. This tool is recommended to aid amino acid dating in detecting reworked fossils.

In the second article, the focus discussion is on the geological interpretation of the sedimentary basins in northern Madura waters based on the gravity data analysis.The area of north Madura offshore is one of the sedimentary basins which has interesting paleogeographical developments. Gravity analysis consists of spectrum analysis, optimum upward continuation filtering, spectral decomposition analysis, 2D forward modeling and 3D inversion of gravity data. The next author elaborates the Granulometric Analysis of Paleotsunami candidate deposits in Ternate Island. Variations in mean, sorting, skewness and kurtosis values indicate changes in tsunami wave energy which cause changes in grain size.

The fourth article reveals a three-dimensional baroclinic circulation model study for the Musi coastal area. Coastal areas and river estuaries are areas where freshwater sources from land and sea meet. This ecosystem is influenced by several factors such as river water discharge, sea tides and bathymetry. This model helps in understanding the properties of water masses in space and time, as well as the interactions between various components.

The fifth paper discusses the provenance and distribution of Middle Baong Sand in the Malacca Strait. The results research show that the provenance of Middle Baong sand on land is predicted to originate from southwest Sumatra, contrary to general assumptions. Validation was carried out by comparing Malay Peninsula data with Kutacane research data and wells using REE analysis.

The last article presents the exploring marine geology and oceanography in Manggar waters: a prelude to the burgeoning Belitong geopark. This survey gather information about marine geology and oceanography around Manggar Waters, East Belitung, which is useful for coastal and marine planning areas as well as enriching geological heritage data.

Finally, the Editorial Board is always looking forward to receiving papers in marine geology from various scientific disciplines to diversify contributions and enhance the quality of our journal. We also invite critiques for improving this journal. Enjoy reading this publication, and welcome to seeing you again in the first edition next year.

Bandung, December 2023
Warm regards,

Editorial Board

ISSN 1410-6175

BULLETIN OF THE MARINE GEOLOGY

Vol. 38, No. 2, December 2023

Contents

THE APPLICATION OF SEM-EDS FOR THE SURFACE TEXTURE OF FORAMINIFERA: IDENTIFICATION OF EARLY DIAGENESIS OF REWORKED L. DIMIDIATUS WITHIN MODERN COASTAL DEPOSITS

PENERAPAN SEM-EDS UNTUK TEKSTUR PERMUKAAN FORAMINIFERA: IDENTIFIKASI DIAGENESIS AWAL PADA FOSIL ROMBAKAN L. DIMIDIATUS DI ENDAPAN PANTAI MODERN

Rahmadi Hidayat[1*], Sarju Winardi[1], and Akmaluddin[1]

[1] Geological Engineering Department, Faculty of Engineering, Gadjah Mada University, Yogyakarta

*Corresponding author: rahmadihidayat@ugm.ac.id

(Received 23 May 2023; in revised from 7 June 2023; accepted 25 July 2023)

DOI : http://dx.doi.org/10.32693/bomg.38.2.2023.831

ABSTRACT: Sediment recycling has been known to occur within Quaternary coastal barriers of the greater Coorong Coastal Plain, southern Australia. A high degree of reworking of skeletal carbonates from Late Pleistocene deposits (Robe Range) is evident based on the novel application of amino acid dating of the single-foraminifera species *Lamellodiscorbis dimidiatus*. More importantly, some apparently transparent, well-preserved tests indicate anomalously high extents of amino acid racemization, implying that reworked fossils could not be easily distinguished based on taphonomic signatures such as corrosion. Here, we examine the surface microtexture of this species, constrained with well-preserved specimens, on a modern beach of Canunda, southern Australia, using scanning electron microscopy coupled with energy dispersive spectroscopy (SEM-EDS). The aim is to identify surface features of foraminifera in more detail, capturing signs of early diagenesis associated with weakly consolidated Late Pleistocene coastal barriers. The results reveal that some well-preserved tests show localized blocky calcite cementation, most notably within intraseptal spaces or impact sites. The EDS spectra of cement indicate lower Mg content than unaltered foraminifera surface. This suggests low-Mg calcite precipitation due to meteoric diagenesis experienced by the onshore Late Pleistocene coastal barrier. It implies that these foraminifera shells are reworked fossils originated from older successions and were subsequently redeposited within the present-day beach. SEM-EDS used in this study demonstrates its capability in examining small-scale carbonate diagenesis products beyond the traditional binocular microscope. Thus, this tool is recommended to aid amino acid dating in detecting reworked fossils.

Keywords: scanning electron microscope, sediment reworking, foraminifera, *L. dimidiatus*

ABSTRAK: *Perombakan sedimen sangat umum ditemukan pada lingkungan pantai berumur Kuarter di Dataran Pesisir Coorong, Australia bagian selatan. Proses perombakan yang sangat intensif pada partikel karbonat dari endapan Pleistosen Akhir (Robe Range) telah terbukti berdasarkan aplikasi geokronologi asam amino dengan metode analisis foraminifera tunggal Lamellodiscorbis dimidiatus. Lebih penting lagi, beberapa foraminifera yang transparan dan terpreservasi baik menunjukkan tingkat rasemisasi asam amino yang sangat tinggi, mengindikasikan bahwa fosil yang mengalami perombakan tidak dapat dibedakan hanya berdasarkan ciri taphonomik seperti korosi. Pada studi ini, kami melakukan analisis mikrotekstur pada permukaan pada spesimen foraminifera dengan preservasi tinggi di pantai Canunda, Australia bagian selatan, menggunakan mikroskop elektron yang dipadukan dengan spektroskopi dispersi energi (SEM-EDS). Tujuan penelitian ini yaitu mengidentifikasi fitur permukaan secara detil untuk melihat tanda-tanda diagenesis awal pada endapan pesisir pantai berumur Pleistosen Akhir yang terkonsolidasi lemah. Hasil penelitian menunjukkan bahwa beberapa foraminifera dengan tingkat preservasi tinggi memiliki sementasi blok kalsit yang terlokalisir pada intraseptal, pori atau area bekas tumbukan. EDS*

spektra pada semen menunjukkan konsentrasi Mg yang relatif lebih rendah daripada permukaan foraminifera yang belum teralterasi. Hal ini menunjukkan pengendapan kalsit dengan Mg rendah hasil diagenesis meteorik yang dialami oleh endapan pantai berumur Pleistosen Akhir. Foraminifera tersebut kemungkinan merupakan fosil rombakan hasil erosi dari suksesi yang lebih tua, yang kemudian diendapkan kembali di pantai Canunda pada saat ini. Pada penelitian ini, SEM-EDS dinilai baik untuk mengetahui produk diagenesis karbonat secara lebih rinci dibandingkan dengan mikroskop binokular untuk membantu geokronologi asam amino dalam mendeteksi butiran karbonat hasil rombakan.

Kata Kunci: *mikroskop elektron, perombakan sedimen, foraminifera, L. dimidiatus*

INTRODUCTION

Scanning electron microscopy (SEM) has been extensively applied to geological samples because of the versatility of this instrument in providing direct, high-resolution images with excellent depth of focus at a minimal cost and time for sampling preparation (Chen et al., 2015). In the study of sedimentology, SEM is commonly used to examine micro-characteristics of grains, mainly quartz, to understand the specific transportation and inferred environments (Krinsley and Doornkamp, 1973; Vos et al., 2014). SEM, coupled with elemental analysis such as energy dispersive spectroscopy (EDS), is also important in deciphering the diagenesis route of Quaternary coastal dune deposits (Loucks and Patty, 2017). In terms of calcareous microfossils, several studies have relied on EDS instrument to determine unusual elemental compositions that lead to abnormal shells influenced by contaminated marine environments, particularly foraminifera and ostracoda (Dewi et al., 2016, 2015).

It has been suggested that Holocene skeletal particles act as the primary carbonate sediment source for the accumulation of modern beaches along the Limestone Coast (Joury et al., 2018). The basis of this interpretation is the assumption of high preservation of skeletal particles determined from an optical microscope that is in line with inferred age. In this case, the well-preserved appearance of skeletal carbonate grains is defined as modern to the Holocene, whereas brownish iron-stained particles indicate relict grains from preceding successions, particularly older than the last glacial period (Joury et al., 2018; Rivers et al., 2007). However, using optical luminescence dating, Oliver et al. (2019) mentioned the possibility of enhanced sediment delivery not only from Holocene-modern carbonate factories but also a reworking process based on the relatively rapid shoreline progradation since middle Holocene in this region of up to 74,000 m^3/yr. A subsequent study by Hidayat (2022) has supported this argument, suggesting that these reworked carbonate particles were derived primarily from the eroded Late Pleistocene Robe Range and thus, it plays a significant role in supplying sediments for present-day beaches in this region based on the results from amino acid dating of the single-foraminifera method. Moreover, some apparently pristine foraminiferal tests are reworked fossils due to the unusually high amino acid racemization, which could not be assigned as Holocene or modern specimens. This challenges conventional optical microscopes to provide more detailed characteristics of skeletal particles to be confidently given as reworked fossils from Late Pleistocene succession.

Here, we apply SEM-EDS to provide further evidence of diagenetic features within reworked benthic foraminifera *Lamellodiscorbis dimidiatus* from Late Pleistocene Robe Range successions that show relatively pristine conditions from binocular microscopy. *L. dimidiatus*, a member of the genus *Lamellodiscorbis*, is regarded as one of the key faunal assemblages supplying beach deposits in the Limestone Coast, having typically inner shallow-marine habitat associated with temperate carbonate environments, mainly in seagrass meadows (James and Bone, 2011). The selection of this species is based on its robustness and relatively high abundance within the beach deposits (Joury et al., 2018; Oliver et al., 2020), acting as one of the primary carbonate sources from shallow-marine environments. The meteoric diagenetic signatures experienced by Late Pleistocene successions within the southern part of the Coorong Coastal Plain have been noted by James et al. (2018) based on the slight increase of low-Mg calcite proportion compared to Holocene deposits. The significantly higher magnification provided by SEM performed in this study may be suitable to determine possible small-scale (microns in size) of early diagenetic products from subaerially exposed Robe Range coastal dune deposits found within foraminiferal tests, which could not be previously seen in conventional microscopy.

Coastal Setting

Canunda Beach (140°13'17.1"E, 37°39'31.7"S) is located south of Rivoli Bay, southern Australia. It has characteristically long elongated beach landform, around 45 km, with extensive and partially vegetated Holocene coastal dunes up to 4 km in cross-section (Fig. 1). The beach shows large foredunes around 10 m tall, whereas the Holocene coastal dune may reach 30 m high. The earliest development of the Holocene dunes is thought to begin ~8 ka ago (Ohmori et al., 1987). In contrast to the shoreline north of Rivoli Bay (Beachport to Robe), eroded remnants of the Late Pleistocene coastal barrier, termed the Robe Range, such as sea stacks (Fig. 1), nearshore islands, shore platforms, and pocket beaches, are only present locally in this area. It is suggested that limited erosional remnants from older deposits with high accumulations of Holocene coastal dunes may be related to the higher degree of

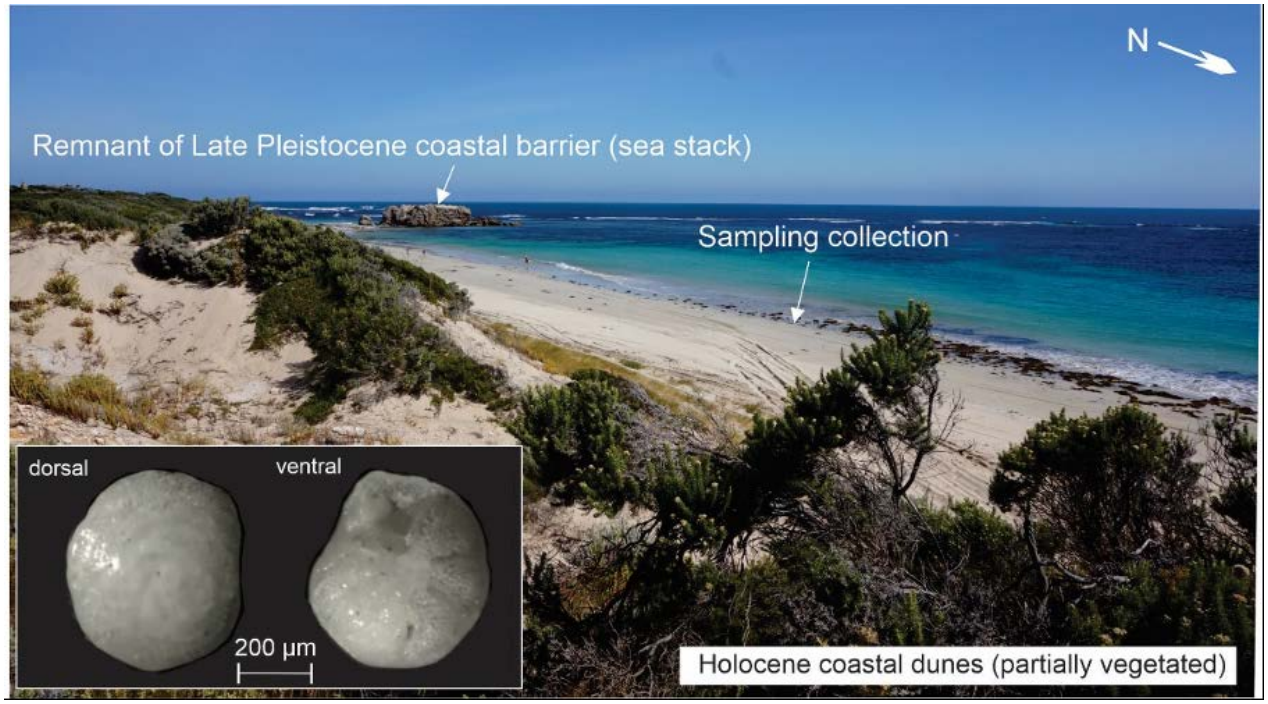

Figure 1. Location of sampling sites at Canunda Beach, southern Australia, showing coastal landform with partially vegetated Holocene onshore dunes and an erosional remnant of older successions associated with Late Pleistocene Robe Range coastal barrier. Inset: representation of *L. dimidiatus* taken from the sample.

coastal erosion. This is supported by the high proportion of reworked *L. dimidiatus* tests and the relatively high extent of racemization from the whole-rock and foraminifera samples previously reported in this region, particularly in prograding ridges of Guichen Bay, 70 km northwest of Canunda Beach (Murray-Wallace et al., 2001; Oliver et al., 2020).

From a hydrodynamic perspective, Canunda Beach is considered one of the most energetic beaches on the southern Australian coast (Short, 2020). Joury et al. (2018) modeled the conditions of Canunda Beach, suggesting that the relatively steep bathymetry immediately offshore of this area generates optimum bottom velocity outside the surf zone up to 1.1 m/s at 15 m of water depth, providing a high chance of waves to scour seafloor sediments. This results in the typically unconsolidated bare sand blanketing the nearshore zone of Canunda (Miller et al., 2009).

MATERIALS AND METHODS

The sediment sampling of foraminifera *L. dimidiatus* was carried out 20 cm from the beach surface. Ten transparent and well-preserved tests were collected from the binocular microscope with a typical size of around 500 microns. Following this, an ultrasonic bath for 1 minute and 2 hours of hydrogen peroxide soak were established to remove adhering particles. Collected *L. dimidiatus* tests were mounted on adhesive-taped SEM stubs for surface micromorphology. After that, specimens were coated using gold to avoid the charging effect. Microtextures were analyzed using a JEOL JSM-6490LV instrument, combined with a large EDS X-ray detector (80 mm^2) at the Electron Microscopy Centre, the University of Wollongong, Australia. We generally used secondary electron imaging between 15 and 20 kV depending on magnification, with a 10 mm working distance and spot size at 60. Elemental spot analyses, covering an area of around 1 μm^2, from the EDS tool focused on carbonate diagenetic features within the surface of identified *L. dimidiatus* and compared them with the fresh or unaltered part to determine any relative difference in Mg intensity. Chave (1954) noted that the genus of this species commonly has around ~15% $MgCO_3$ and is considered as intermediate to high Mg-calcite carbonate skeletons.

RESULTS

In this study, we opted to select four *L. dimidiatus* tests (CB/LD-1 to CB/LD-4) for further discussion regarding microtextural characteristics. The description of each foraminifera is based on a general overview of the overall conditions, followed by a more detailed image of the focus area with associated EDS analysis. EDS spectra were also established in the fresh, unaltered part to understand the typical Mg intensity compared with diagenetic features found on the foraminiferal tests.

Generally, the well-preserved foraminifera shell (CB/LD-1) displays minor physical breakages, around 20 to 80 microns, and some pittings resulting from bioturbation (Fig. 2a, 2b). Small pits may be formed by the energetic hydrodynamic setting of offshore Canunda, as previously suggested by Joury et al. (2018). Despite the relatively clean and smooth surface of *L. dimidiatus* coded

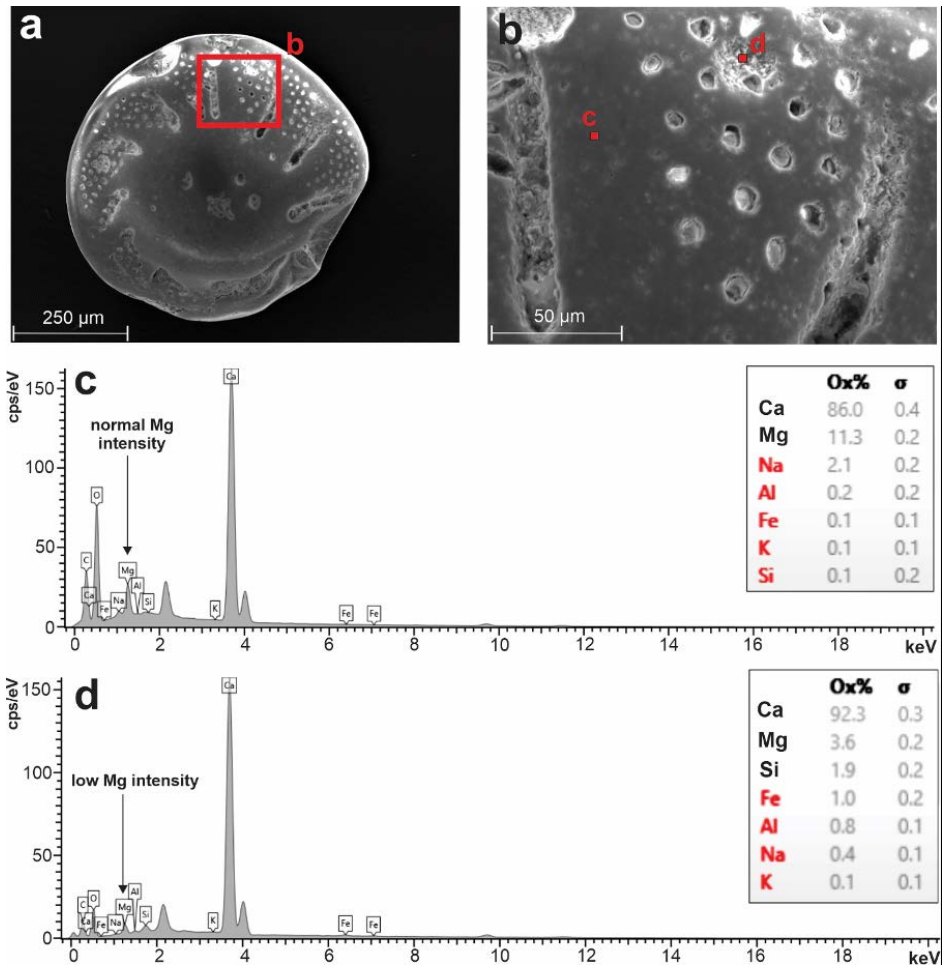

Figure 2. (a) SEM image of overall foraminiferal test CB/LD-1. (b) Localized blocky cement occurs within the impact zone and intraseptal spaces. (c) The EDS spectrum of the fresh surface indicates relatively high Mg intensity as opposed to (d) the EDS spectrum of cement within the impact zone.

CB/LD-1, some isolated blocky calcite crystals can be seen within a small impact pit (Fig. 2b). The more detailed EDS spectrum of this crystal indicates a significantly lower Mg intensity than the unaltered test wall (Fig. 2d), possibly associated with low-Mg calcite precipitation from meteoric diagenesis. It shows that the blocky crystal has a content of Mg at 3.6%, significantly less than the unaltered part at 11.3% (Table 1). Similarly, within the intraseptal space of *L. dimidiatus* coded CB/LD-2, some features of blocky calcite can be seen within the smooth depression region (Fig. 3b). Further assessment from the EDS tool suggests a comparatively low Mg concentration (Fig. 3d), whereas the intensity of Mg from the fresh surface shows similar values with foraminiferal test CB/LD-1, at 9.7% of normalized oxide (Table 1).

Despite the apparently well-preserved microtexture, the SEM image of *L. dimidiatus* CB/LD-3 indicates more substantial diagenetic alteration than other specimens (Fig. 4b). Some subtle depressions occur as a result of slight dissolution, possibly happened during the vadose subaerial exposure after deposition of Late Pleistocene Robe Range dune complexes. This was followed by extensive precipitation on the majority of the outer surface by low-Mg calcite, as recorded from the low intensity of Mg peak determined from EDS analysis (Fig. 4d) compared to surfaces lacking diagenetic features. The precipitate contains almost entirely Ca with low Mg (5.0%) whereas the unaltered part has a substantially higher Mg concentration at 10.5% (Table 1). In contrast to other *L. dimidiatus* tests selected in this study, foraminiferal test CB/LD-4 yields an overall unaltered surface with limited impact pits (Fig. 5a, 5b). There is no visible localized calcite precipitation within pores or intraseptal spaces, where the EDS analysis of these regions often demonstrates consistently high Mg intensity, showing 12.2% respectively (Table 1). Interestingly, within depression area, many parts contain silica globules as evidenced by elevated Si intensity based on EDS spot check (Fig. 5d), resulting in 2.1% of normalized oxide (Table 1). Based on the insufficient evidence of meteoric diagenesis products, it is suggested that this foraminiferal test may be modern or Holocene in origin and unlikely to be reworked fossils.

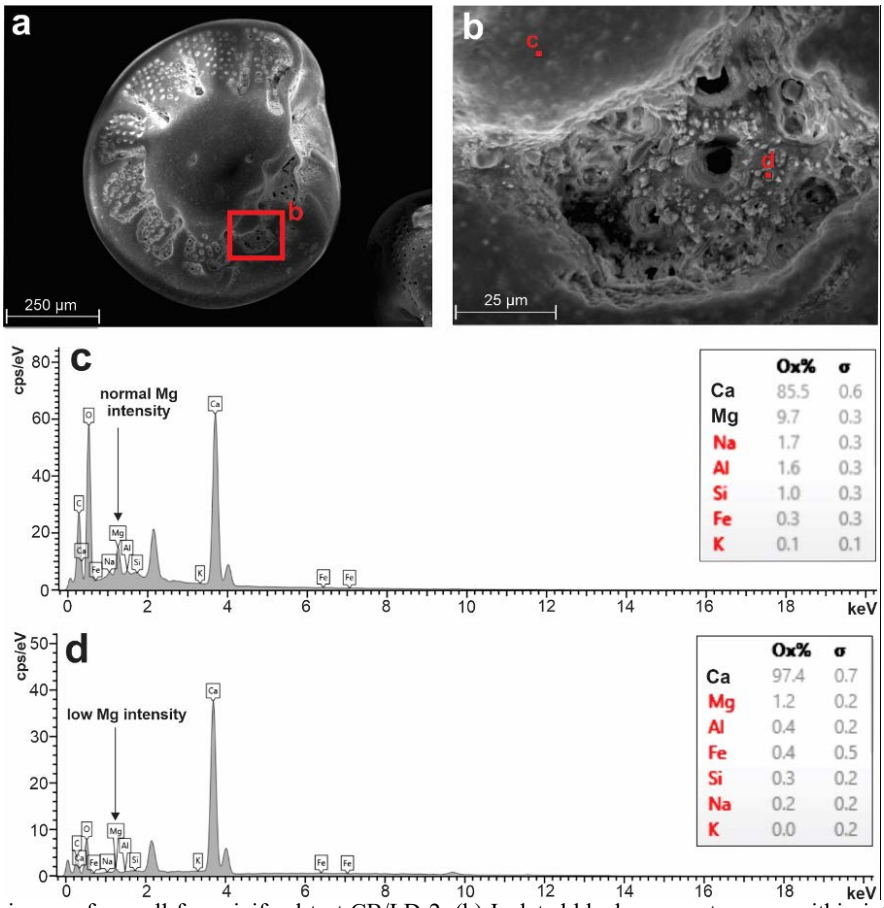

Figure 3. a) SEM image of overall foraminiferal test CB/LD-2. (b) Isolated blocky cement occurs within intraseptal spaces. (c) The EDS spectrum of the unaltered surface indicates relatively high Mg intensity as opposed to (d) the EDS spectrum of cement within intraseptal space.

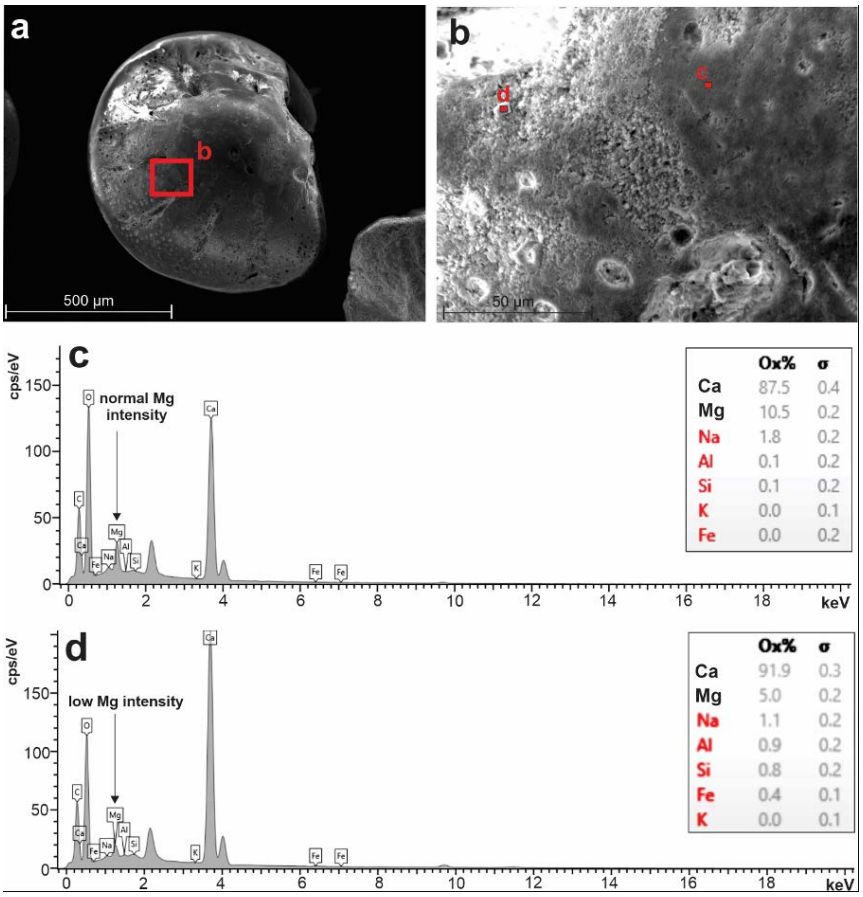

Figure 4. (a) SEM image of overall foraminiferal test CB/LD-3. (b) Broad cementation occurs within the subtle depression, likely created by dissolution. (c) EDS spectrum of fresh surface indicates relatively high Mg intensity as opposed to (d) EDS spectrum of cement within the depression.

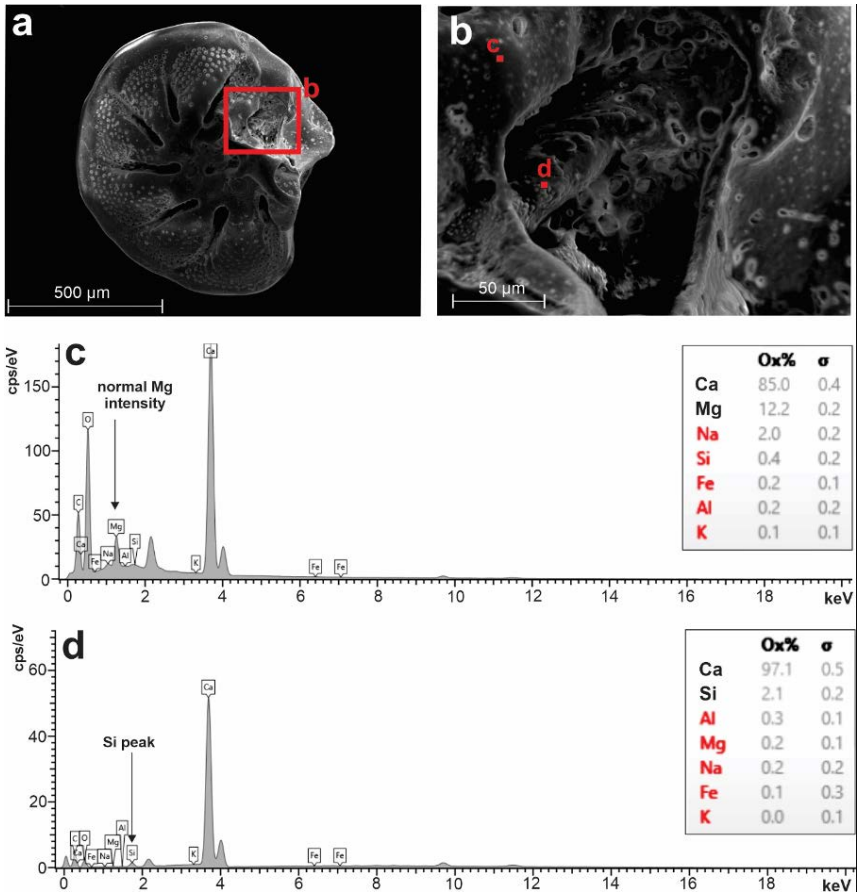

Figure 5. (a) SEM image of overall foraminiferal test CB/LD-4. (b) Silica globules on the intraseptal spaces but no indication of blocky calcite cementation. (c) EDS spectrum of the fresh surface indicates relatively high Mg intensity, whereas (d) the EDS spectrum of silica globules with a notable peak of Si.

Table 1. Chemical composition foraminifera *L. dimidiatus* resulted from EDS spectra shown in Figure 2-5.

Sample	Features	CaO	MgO	SiO_2	Al_2O_3	Fe_2O_3	NaO	K_2O
CB/LD-1 (Fig. 2c)	Unaltered surface	86.0	11.3	0.1	0.2	0.1	2.1	0.1
CB/LD-1 (Fig. 2d)	Precipitates on impact zone	92.3	3.6	1.9	0.8	1.0	0.4	0.1
CB/LD-2 (Fig. 3c)	Unaltered surface	85.5	9.7	1.0	1.6	0.3	1.7	0.1
CB/LD-2 (Fig. 3d)	Precipitates on intraseptal space	97.4	1.2	0.3	0.4	0.4	0.2	n.d.
CB/LD-3 (Fig. 4c)	Unaltered surface	87.5	10.5	0.1	0.1	n.d.	1.8	n.d.
CB/LD-3 (Fig. 4d)	Precipitates on depression area	91.9	5.0	0.8	0.9	0.4	1.1	n.d.
CB/LD-4 (Fig. 5c)	Unaltered surface	85.0	12.2	0.4	0.2	0.2	2.0	0.1
CB/LD-4 (Fig. 5d)	Globules	97.1	0.2	2.1	0.3	0.2	0.2	n.d.

n.d.: note detected

DISCUSSION

The surface microtexture of benthic foraminifera *L. dimidiatus* provides supporting evidence of amino acid dating from previous studies (Oliver et al., 2020) that the determination of reworked sediments based on the visual taphonomic assessment by using a conventional microscope should be used with caution. Here, the well-preserved foraminiferal tests may experience diagenesis based on the presence of calcite precipitates, localized to mainly depression areas such as impact pits or intraseptal spaces (Fig. 2b, 3b). The consistently low intensity of Mg compared to the unaltered part based on EDS spot analyses suggests the regular route of early vadose diagenesis associated with blocky low-Mg calcite. Thus, despite their pristine appearance, these foraminifera are considered a product of sediment recycling from currently eroded Late Pleistocene coastal deposits. Hidayat et al. (2023) noted that the development of onshore Late Pleistocene Robe Range barrier structure correlates with marine isotope stages (MIS) 5c–5a and early MIS 3. During glacial sea levels, particularly MIS 4 and MIS 2, the more arid conditions may induce precipitation of low-Mg calcite on this coastal barrier. Calcretization also developed extensively at this stage, covering and protecting the morphology of Late Pleistocene sedimentary units, mainly landward-advancing eolianite facies, prior to the formation of overlying Holocene coastal dunes (Murray-Wallace, 2018). In Late Pleistocene eolianites in Warrnambool, Victoria, the typical precipitation of blocky low-Mg calcite is also common, filling some of the voids and dissolving shells, particularly with aragonitic skeletons (Reeckman and Gill, 1981). The small scale of these precipitates may not be seen with the low resolution of binocular microscopy, reducing the reliability of identifying reworked skeletal carbonate grains.

It has been known that the iron-oxide coating of grains of the coastal dune is attributed to the prolonged pedogenic-related weathering process (Khadkikar and Basavaiah, 2004); thus, the majority of bioclasts show a brown-staining or corroded appearance. Based on an amino acid dating study (Hidayat, 2022), overall brown-stained *L. dimidiatus* yielded exclusively high extents of amino acid racemization corresponding to the Late Pleistocene age. However, given the nature of the general characteristics of the internal part of Robe Range eolian dune outcrops that are weakly consolidated (Hidayat et al., 2023), the influence of pedogenesis is possibly limited temporally and not as spatially extensive to the overall stratigraphical succession. Except for the uppermost part associated with protosol or *terra rossa* paleosol and associated calcrete layer, it is possible that some bioclasts within the Robe Range, particularly away from the pedogenized interval, have a minimal influence of iron-oxide staining or excessive vadose diagenetic precipitation. This may explain the occurrence of some well-preserved reworked skeletal grains derived from erosion of Robe Range barrier structures. During the coastal erosion that started since the end of post-glacial marine transgression, both preserved and iron-oxide-stained bioclasts within Robe Range eolianites were scoured, remixed, retransported by wave action, and ultimately redeposited in the modern beach deposits.

The imaging of SEM-EDS results can also be used to characterize Holocene foraminifera specimens. As opposed to the reworked fossils, the overall exterior of the shell does not show features associated with low-Mg calcite formation (Fig. 5a). In depression regions, the surface remains entirely smooth without any development of small calcite crystals (Fig. 5b). Some undulations are observed in some areas, probably linked to the formation of amorphous silica derived from ocean water. The occurrence of silica globules is possible due to silica precipitations where the foraminifera experienced wetting-drying around the intertidal zone (Chakroun et al., 2009). Moreover, wetting-drying is more effective in the coastal environments within the Mediterranean-type climate setting, as Chakroun et al. (2009) reported. In Canunda Beach, Hidayat (2022) also reported that many *L. dimidiatus* tests yield low extents of amino acid racemization, indicating a minor contribution of skeletal carbonate grains from the modern–Holocene carbonate factory. Based on visual inspection, these foraminiferal tests showed exclusively excellent preservation without signs of corrosion or iron-oxide staining (Hidayat, 2022). Since the incorporation of these Holocene skeletal grains into the present-day beach deposit took place in a relatively short period, it is unlikely that these grains have experienced sufficient subaerial weathering that leads to brown staining and shell corrosion in contrast to the relict counterpart.

CONCLUSIONS

The SEM-EDS established in this study has aided the previous amino acid racemization dating studies related to the presence of well-preserved reworked foraminiferal tests from the Late Pleistocene Robe Range coastal barrier that were re-deposited as present-day Canunda Beach. The capability of SEM to capture small-scale and localized calcite precipitations within depression areas such as intraseptal spaces, pores, and impact pits of these foraminiferal tests is essential to assigning foraminifera or other calcareous skeletons as relict or reworked more reliably than the optical microscope. More importantly, the semi-quantitative analysis of EDS provides valuable information that these precipitations consistently have lower Mg intensity as opposed to the unaltered or fresh surfaces. This implies typically early diagenetic calcite cementation (low-Mg) that is common in Late Pleistocene coastal dune deposits elsewhere with similar climatic settings, for instance, in Warrnambool, Victoria.

ACKNOWLEDGEMENTS

Professor Colin Murray-Wallace (the University of Wollongong) is thanked for assisting and for the essential discussion in collecting beach samples. We also thank the research staff of the Electron Microscopy Centre, University of Wollongong, for granting access to specimen preparation and the JSM-6490LV instrument.

REFERENCES

Chakroun, A., Miskovsky, J.-C., and Zaghbib-Turki, D., 2009. Quartz grain surface features in environmental determination of aeolian Quaternary deposits in northeastern Tunisia. *Mineralogical Magazine*, 73(4): 607–614.

Chave, K.E., 1954. Aspects of the Biogeochemistry of Magnesium 1: Calcareous marine organisms. *Journal of Geology*, 62(3): 266–283.

Chen, L., Xu, J., and Chen, J., 2015. Applications of scanning electron microscopy in earth sciences. *Science China Earth Sciences*, 58(10): 1768–1778.

Dewi, K.T., Priohandono, Y.A., and Masduki, A., 2016. Abnormal microfaunal shells as early warning indicator of environmental changes surrounding Berau Delta, East Kalimantan. *Bulletin of the Marine Geology*, 26: 31–40.

Dewi, K.T., Nurdin, N., Priohandono, Y.A., and Sinaga, A., 2015. Benthic foraminifera in marine sediment related to environmental changes off Bangka Island, Indonesia. *Berita Sedimentologi*, 33: 47–54.

Hidayat, R., 2022. *Late Quaternary evolution of Robe Range, southeast South Australia: An archive of deposition and destruction of a coastal barrier complex*. Unpublished Ph.D Thesis, University of Wollongong.

Hidayat, R., Murray-Wallace, C. V., and Jacobs, Z., 2023. Late Pleistocene evolution of Robe Range , southern Australia – The timing and carbonate source dynamics of coastal dune development. *Marine Geology*, 456: 106987.

James, N.P., and Bone, Y., 2011. *Neritic carbonate sediments in a temperate realm: Southern Australia.* Springer Netherlands, 254p.

James, N.P., Bone, Y., Joury, M., Malcolm, I., and Kyser, T.K., 2018. Diagenesis and compositional partitioning of Quaternary cool-water carbonate aeolianites: southeastern Australia. *Journal of Sedimentary Research*, 88(4): 431–448.

Joury, M.R.F., James, N.P., and James, C., 2018. Nearshore cool-water carbonate sedimentation and provenance of Holocene calcareous strandline dunes, southeastern Australia. *Australian Journal of Earth Sciences*, 65(2): 221–242.

Khadkikar, A.S., and Basavaiah, N., 2004. Morphology, mineralogy and magnetic susceptibility of epikarst-Terra Rossa developed in late Quaternary aeolianite deposits of southeastern Saurashtra, India. *Geomorphology* 58(1-4): 339–355.

Krinsley, D.H., and Doornkamp, J.C., 1973. *Atlas of quartz sand surface textures*. Cambridge University Press, 102p.

Loucks, R.G., and Patty, K., 2017. Vadose diagenetic dissolution textures, cementation patterns, and aragonite and Mg-calcite alteration in the Holocene Isla Cancun eolianite aragonitic ooids: modern analog for ancient ooid-grainstone pore networks. *Gulf Coast Association of Geological Societies*, 6: 1–20.

Miller, D., Westphalen, G., Jolley, A.M., Rutherford, H., Colella, D., and Holland, S., 2009. *Marine habitat within selected areas of the South East NRM Region*. Department for Environment and Heritage, Government of South Australia.

Murray-Wallace, C.V., 2018. *Quaternary history of the Coorong Coastal Plain, Southern Australia: An archive of environmental and global sea-level changes*. Springer International Publishing, Switzerland, 229p.

Murray-Wallace, C.V., Brooke, B.P., Cann, J.H., Belperio, A.P., and Bourman, R.P., 2001. Whole-rock aminostratigraphy of the Coorong Coastal Plain, South Australia: Towards a 1 million year record of sea-level highstands. *Journal of Geological Society London*, 158: 111–124.

Ohmori, H., Endo, K., Uesugi, Y., and Horikoshi, M., 1987. Stratigraphy and geomorphologic history of Holocene dunefield near Millicent along the southeastern coast of South Australia. *Journal of Geography (Chigaku Zasshi)*, 96(1): 1–22.

Oliver, T.S.N., Murray-Wallace, C. V., and Woodroffe, C.D., 2019. Holocene shoreline progradation and coastal evolution at Guichen and Rivoli Bays, southern Australia. *Holocene*, 30: 106–124.

Oliver, T.S.N., Tamura, T., and Murray-Wallace, C.V., 2020. Identification of reworked foraminifera in temperate carbonate sediments – A pilot study from the Coorong Coastal Plain, southern Australia. *Marine Geology*, 421: 106096.

Reeckman, S.A., and Gill, E.D., 1981. Rates of vadose diagenesis in Quaternary dune and shallow marine calcarenites, Warrnambool, Victoria, Australia. *Sedimentary Geology*, 30(3): 157–172.

Rivers, J.M., James, N.P., Kyser, T.K., and Bone, Y., 2007. Genesis of palimpsest cool-water carbonate sediment on the continental margin of southern Australia. *Journal of Sedimentary Research*, 77: 480–494

Short, A.D., 2020. *Australian Coastal Systems*. Springer International Publishing, 1256p.

Vos, K., Vandenberghe, N., and Elsen, J., 2014. Surface textural analysis of quartz grains by scanning electron microscopy (SEM): From sample preparation to environmental interpretation. *Earth-Science Reviews*, 128: 93–104.

GEOLOGICAL INTERPRETATION OF NORTH MADURA OFFSHORE SEDIMENTARY BASIN BASED ON GRAVITY DATA ANALYSIS

INTERPRETASI GEOLOGI CEKUNGAN SEDIMEN PERAIRAN UTARA MADURA BERDASARKAN ANALISIS DATA GAYABERAT

Restu Ningsih[1*], Imam Setiadi[2], Muh Sarkowi[1], and Akroma Hidayatika[1]

[1] Department of Geophysical Engineering, Faculty of Engineering, University of Lampung, Jl. Prof. Dr. Ir Sumantri Brojonegoro, Bandar Lampung, Lampung 35141

[2] Marine Geological Institute, Jl. Djunjunan No. 236, Husein Sastranegara Bandung 40174

*Corresponding author: restuningsih913@gmail.com

(Received 16 May 2023; in revised from 06 June 2023; accepted 22 August 2023)

DOI : http://dx.doi.org/10.32693/bomg.38.2.2023.828

ABSTRACT: The area of north Madura offshore is one of the sedimentary basins within the North East Java Basin which has interesting paleogeographical developments. These developments are the result of various sedimentation processes and changes in the depositional environments. The purpose of this study is to identify subsurface geological structures, delineate sedimentary sub-basins, and estimate sediment thickness. For that, we do spectrum analysis, optimum upward continuation filtering, spectral decomposition analysis, 2D forward modeling and 3D inversion of gravity data. The results of the spectral analysis show that the average thickness of sedimentary rocks in the study area is around 3.788 km. From the gravity data analysis, 10 sedimentary sub-basins were delineated, indicating structural patterns of basement high, grabens, and faults. 2D and 3D modeling revealed four layers of stratigraphy, in order from youngest to oldest are Tertiary-Neogene sedimentary rocks with a density value of 2.1 gr/cc, the Tertiary-Neogene sedimentary rocks with a density of 2.3 gr/cc, the Tertiary - Paleogene sedimentary rocks with a density of 2.45 gr/cc, and the basement layer identified as volcanic igneous rock with a density of 2.67 gr/cc.

Keywords: Gravity method, optimum upward continuation filter, modeling, spectral analysis decomposition, 2D forward modeling and 3D inversion

ABSTRAK: *Wilayah lepas pantai utara Madura merupakan salah satu daerah cekungan sedimen pada cekungan Jawa Timur Utara yang memiliki perkembangan paleogeografi yang menarik. Hal ini didasarkan pada proses sedimentasi yang bervariasi serta perubahan lingkungan pengendapan yang beragam. Tujuan dari penelitian ini adalah untuk mengidentifikasi struktur geologi bawah permukaan, mendelineasi subcekungan sedimen serta memperkirakan ketebalan sedimen. Analisis data gayaberat yang digunakan yaitu analisis spektrum, filter optimum upward continuation, analisis dekomposisi spektral, serta pemodelan 2D forward modeling dan inversi 3D. Hasil analisis spektral menunjukkan bahwa tebal batuan sedimen rata rata di daerah penelitian adalah sekitar 3.788 km. Delineasi sub-cekungan dari analisis data gayaberat ditemukan 10 sub-cekungan sedimen, pola struktur berupa tinggian batuan dasar, graben dan patahan. Adapun berdasarkan hasil pemodelan 2D dan 3D yang dilakukan diperoleh model lapisan yang terdiri atas empat lapisan dari lapisan paling muda ke lapisan paling tua yaitu batuan sedimen berumur Tersier-Neogen dengan nilai densitas 2.1 gr/cc, lapisan batuan sedimen TersierNeogen dengan densitas 2.3 gr/cc, batuan sedimen Tersier-Paleogen dengan densitas 2.45 gr/cc, serta lapisan basement yang berupa batuan beku vulkanik dengan densitas 2.67 gr/cc.*

Kata Kunci: *gayaberat,* filter optimum upward continuation*, analisis dekomposisi spektral,* 2D forward modeling*, inversi 3D*

INTRODUCTION

Geologically, the North East Java Basin is part of the back-arc basin located in the southeastern region of the Sunda microplate. This basin is flanked by a series of mountains (known as the volcanic arc) and the Indo-Australian plate to the south (Walidah, 2011). The formation of the North East Java Basin resulted from the collision of the Australian continent Plate which subducted to the northwest under the Asian plate (Walidah, 2011). Regarding its constituent rocks, this basin is a geosyncline comprising Tertiary deposits with a layer thickness of up to 6000 meters (Koesoemadinata, 1978).

As one of the main objectives of hydrocarbon exploration in Indonesia, the Middle Miocene sediment of the North East Java Basin have been studied extensively. However, studies on sub-basin delineation and basement configuration based on gravity analysis in the northern region of Madura have not been conducted. Nevertheless, from a stratigraphic and structural perspective, this area exhibits significant potential for oil and natural gas production. The diverse deposits ranging from fluvial faces to marine, along with deltaic and shallow sea depositional environments, suggest potential hydrocarbon sources. Furthermore, the structural history of the basin is characterized by significant influences from rifting and tectonic activities during the Cretaceous Age (Fatahillah, 2016).

Many geophysical methods can be used to explore sedimentary basins, including the gravity method. The gravity method is one of the geophysical methods that can be used to determine subsurface geological conditions based on the physical parameters of rock mass density. This technique, with its sensitivity to changes in both lateral and vertical directions, proves to be an applicable method for studying geological structures, bedrock, rock intrusions, and sedimentary basins (Grant and West, 1965). However, due to the significant ambiguity in gravity data, spectral analysis is conducted during the modeling to estimate the depth of the anomaly source (Setiadi et al., 2010).

In this study, spectral analysis was used (Setiadi and Marjiyono, 2018) to determine the depth of bedrock (basement) within the research area. Furthermore, spectral decomposition analysis was conducted (Setiadi et al., 2019) to reveal the anomalous structural patterns at different depths in the study area. To characterize the subsurface conditions, two-dimensional (2D) forward modeling was executed (Talwani et al., 1959) using Oasis Montaj software. Additionally, three-dimensional (3D) inverse modeling was conducted using Grablox software (Pirtijarvi, 2008). The study aimed to identify a sub-basin pattern, bedrock depth, basement high pattern, subsurface

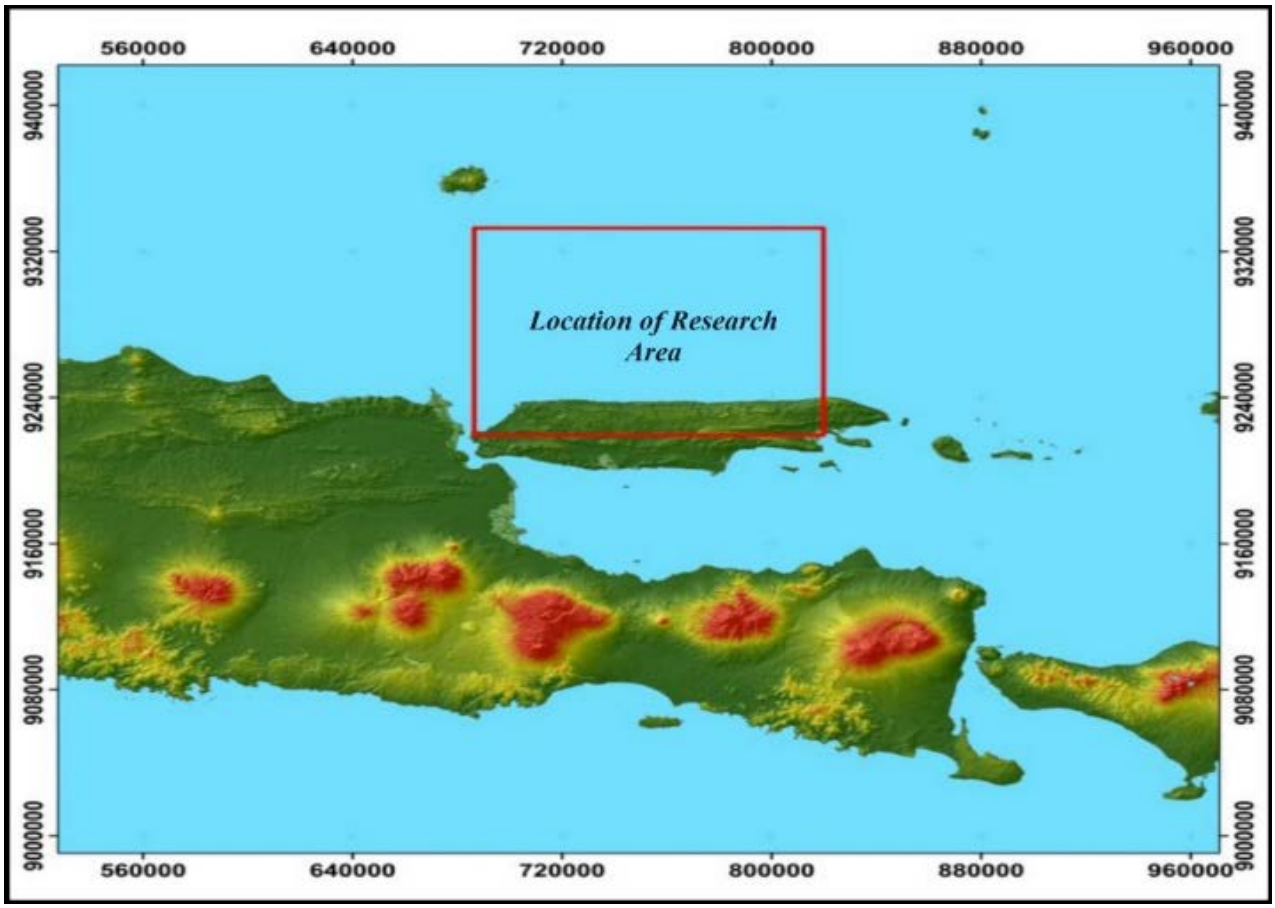

Figure 1. Location of research area of north Madura offshore.

structure pattern, 2D and 3D subsurface models that can be used as a reference or initial information in determining hydrocarbon sedimentary basin. The location of this study is in the offshore area of North Madura, North East Java Basin. Administratively, the research location is situated between coordinates (6º 03'34" - 7º 05' 38") S and (112º 41'10" - 113º 49' 32") E, including parts of Madura mainland and the north Madura offshore area (Figure 1).

METHOD

Ground gravity data used in this study was Geological Research and Development Centre data with a total of 526 data which measured using gravimeter G.826 as our primary data. The data was then integrated with free air anomaly (FAA) and bathymetry data from the Topex satellite. Spectral analysis was carried out to estimate the depth of sedimentary rocks and basement within the research area. Optimum upward continuation filters are applied to separate regional and residual anomalies from gravity data. This technique was carried out by doing an upward continuation of Bouguer anomaly data at several different heights, and then correlating it with the regional anomalies from other methods which are considered as references. The optimum height is obtained based on the highest correlation value. Moreover, spectral decomposition analysis was also conducted as an additional step to identify the structure and sub-basin patterns at specific depths and the depth determination was carried out sequentially from a shallower to a deeper depth. To obtain the expected basement depth, the cut-off value was set up from the graph of Ln A and K, which was then used to determine the window width for filtering.

2D forward modeling is used to calculate the effect of the subsurface model on gravity anomaly with an arbitrary in the form of a polygon, representing the subsurface state (Talwani et al., 1959). The density values utilized for generating sub-surface models in 2D forward modeling are based on Telford et al., (1990). Meanwhile, 3D inversion modeling is done by optimizing the Singular Value Decomposition approach on gravity anomaly. Singular Value Decomposition (SVD) is a matrix factoring method that is closely related to the singular value of the matrix, which is one of the well-known numerical analysis techniques for matrix diagonalization. The results of 3D inversion modeling appear as a distribution of rock mass density, providing a clearer depiction of the subsurface and enhancing the subsurface model information obtained from 2D forward modeling. Inversion modeling was carried out using Grablox 1.6 software (Pirttijarvi, 2008). The research flowchart is presented in Figure 2.

RESULTS AND DISCUSSION

Bouguer Anomaly

Bouguer anomaly illustrates the response to variations in subsurface rock mass density. Bouguer Anomaly values in the study area range between 8.9 - 49.5 mGal (Figure 3). The high anomaly is represented by a red color distribution in the southern and eastern parts of the area. These value are interpreted as uplifted bedrock and indicates the presence of high density rocks that occupy this area. The low anomaly values in the central to the northern areas are probably due to the presence of graben or depocenters, suggesting that the sedimentary rocks in that area are relatively thicker.

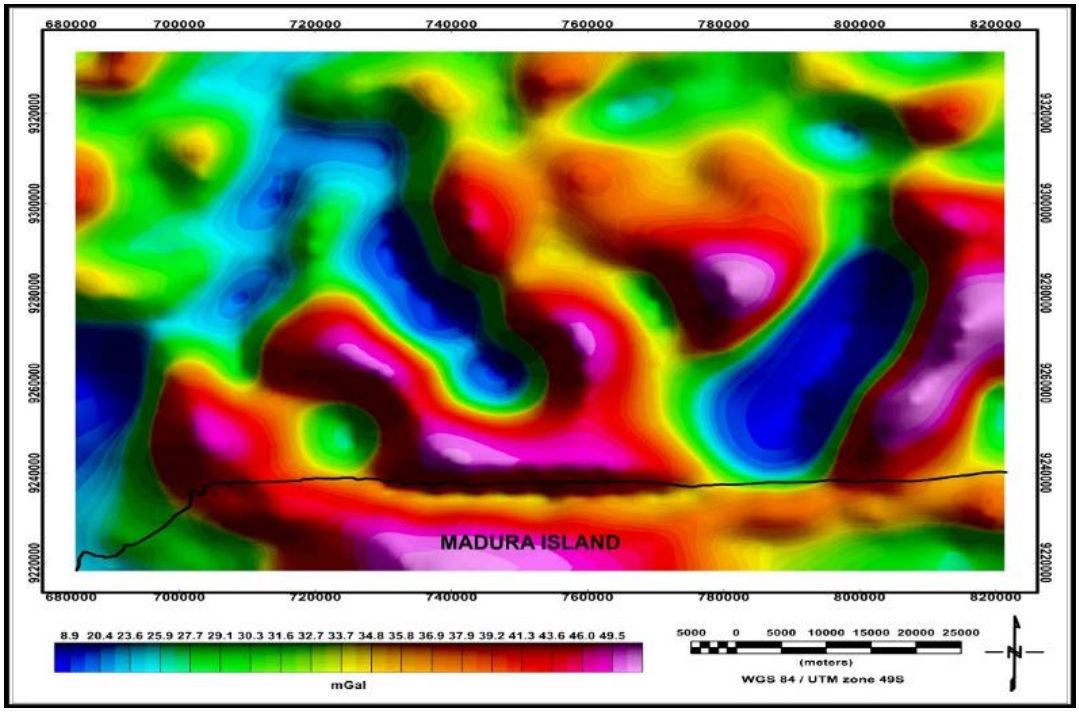

Figure 3. Bouguer anomaly map North Madura Offshore

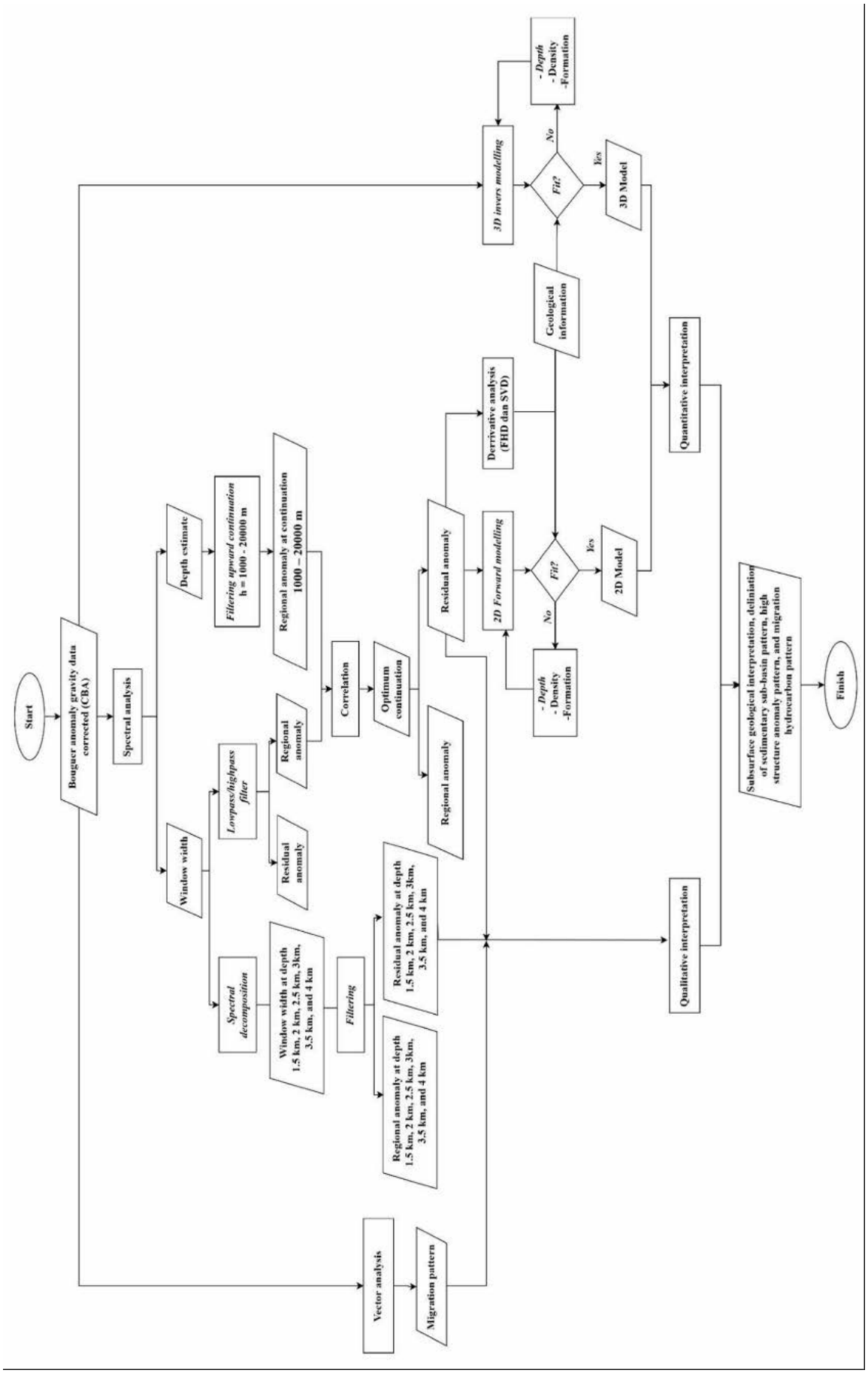

Figure 2. Research Flowchart

Spectral Analysis

Spectral analysis was carried out in order to estimate the depth of bedrock (basement) in the research area. In this study, 11 cross sections with northeast-southwest and northwest-southeast directions were analyzed by a Fourier transform (FFT) to determine the signal content along the lines (Figure 4(a)). The relationship between wave number (K) versus log normal amplitude (Ln A) is illustrated in Figure 4(b). On spectral analysis, the gradient or the slope of the line from the graph of ln A with respect to K is the depth of the discontinuity plane. A large gradient value reflects the discontinuity area of the regional (deep) anomaly, while a low gradient value indicates the discontinuity area of the residual (shallow) anomaly. The intersection of the regional and residual discontinuity plane gradients is the kc wave number (cut-off). The

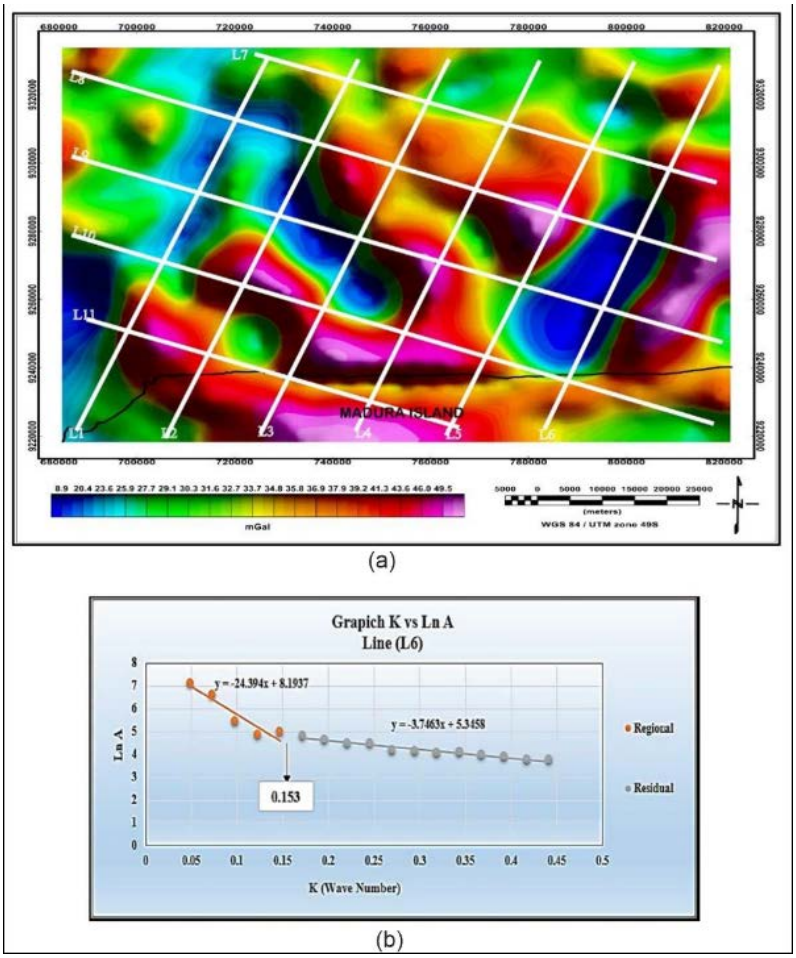

Figure 4. (a) Bouguer anomaly map and cross section direction of spectral analysis, and (b) Example of spectral analysis chart of the line L6

Table 1. Result of the calculation of regional and residual anomaly depth based on spectral analysis.

Line	Depth Reg (Km)	Depth Res (Km)	Kc	N	Window Width
L1	-22.62	-2.9727	0.151	21	40
L2	-18.443	-3.1577	0.181	19	36
L3	-14.578	-3.1216	0.181	19	36
L4	-24.325	-3.6123	0.158	21	40
L5	-22.801	-3.4334	0.172	19	36
L6	-24.394	-3.7463	0.153	21	40
L7	-24.764	-3.4386	0.158	21	40
L8	-17.79	-4.4386	0.151	21	40
L9	-27.457	-4.8654	0.141	23	44
L10	-38.97	-5.5182	0.147	23	44
L11	-24.604	-3.372	0.153	21	40
Average	**-23.704**	**-3.788**		**21**	**40**

average depth of the deep discontinuity field in the study area is -23.704 km which is estimated as the depth of the lower crustal discontinuity field (basement). The average depth of the shallow discontinuity field is -3.788 km, interpreted as the average depth of sedimentary rocks (border between bedrock and sedimentary rocks) in the study area (Table 1).

Optimum Upward Continuation

Filter upward continuation at an altitude of 1000 – 20000 m was conducted to determine the optimum regional anomaly. Upward continuation is calculated on the map at each altitude using the grid size (1.5 x 1.5) Km. The obtained regional anomaly was then correlated with regional anomaly from other methods (as a correlation reference), resulting in a regional anomaly from optimum upward continuation (Table 2). From Table 2, it can be seen that the highest correlation value is obtained at an altitude continuity of 5000 m (Figure 5). The height of this maximum correlation is the estimated optimum height of upward continuation that is used to calculate the residual anomaly. When the altitude upward continuation is lower than the optimum height, an anomaly upward continuation consists of two components, namely regional and residual anomaly. The residual anomaly decreases and almost disappears as it approaches the optimum value. In contrast, when the altitude of upward continuation is higher than the optimal height, the regional anomaly is attenuated and

Table 2. The correlation between the regional anomaly results of the continuation and the reference regional anomaly

UPWARD	HEIGHT	CORRELATION VALUE
UP_1000	1000	0.988182
UP_2000	2000	0.991887
UP_3000	3000	0.993896
UP_4000	4000	0.994779
UP_5000	5000	0.994959
UP_6000	6000	0.994679
UP_7000	7000	0.994121
UP_8000	8000	0.993402
UP_9000	9000	0.99254
UP_1000	10000	0.991711
UP_11000	11000	0.990875
UP_12000	12000	0.990008
UP_13000	13000	0.98911
UP_14000	14000	0.988418
UP_15000	15000	0.987724
UP_16000	16000	0.987008
UP_17000	17000	0.986311
UP_18000	18000	0.985696
UP_19000	19000	0.985156
UP_20000	20000	0.984623

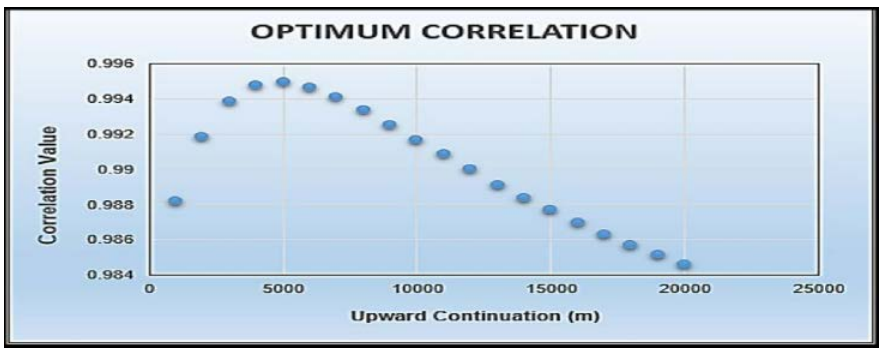

Figure 5. The optimum correlation curve between the regional anomaly of the continuation result and the reference regional anomaly

may reach a zero value. At the optimal height, this condition produces a regional component. Hence, the maximum correlation shows the optimum regional component because it is not affected by residual anomalies and has not experienced attenuation, as shown in Figure 5.

Regional and Residual Anomalies

Separation of regional and residual anomalies is carried out based on the results of the optimum upward continuation filtering of gravity data. The value of regional anomaly ranges from 19.4 to 43.3 mGal (Figure 6a). This anomaly pattern shows a relatively longer wavelength than the Bouguer anomaly, the regional anomaly reflects the rock structure with a deeper position. The high anomaly is suggested to be influenced by rock undulations at the depth of the lower crust or Moho which may rise upwards. The high anomaly pattern in the south is relatively west-east direction, while the high anomaly in the east part is relatively northeast-southwest ward. This high anomaly direction is estimated to be influenced by the RMKS fault zone (Rembang – Madura – Kendeng) and the Meratus pattern. Meanwhile, low anomalies are scattered in the central part to the southern part of the study area.

The residual anomaly pattern (Figure 6b) is obtained from the subtraction between the Bouguer anomaly and the regional anomaly resulting from optimum upward continuation filtering. From the figure, it can be seen that the anomaly value ranges from -11.7 to 7.2 mGal. The structural anomaly pattern is more complex than the Bouguer anomaly pattern because the residual anomaly represents an anomaly structure with a shallower depth

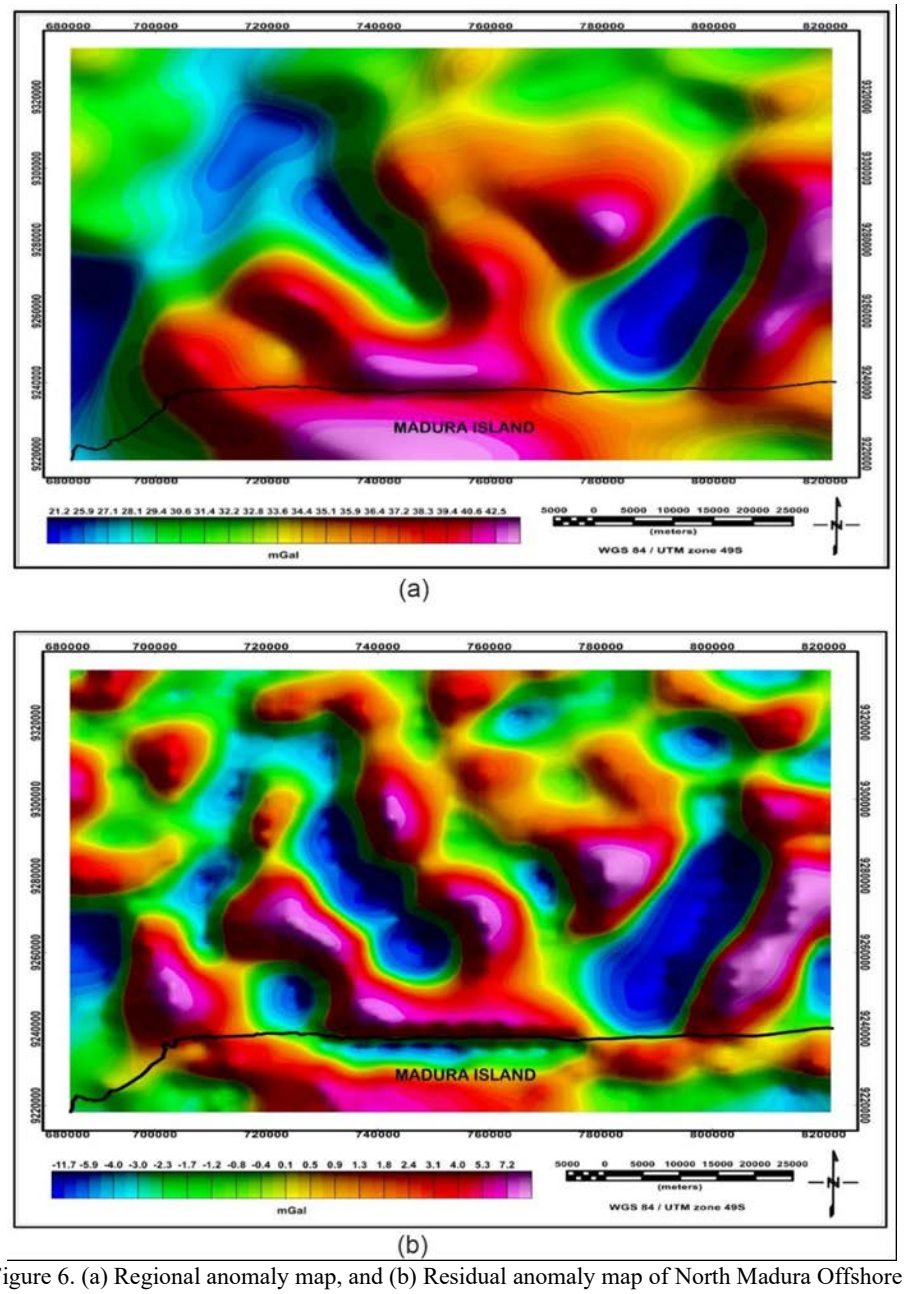

Figure 6. (a) Regional anomaly map, and (b) Residual anomaly map of North Madura Offshore

and shorter wavelength. The results of this residual anomaly will be used to make a qualitative interpretation.

Spectral Decomposition

Spectral decomposition analysis is carried out by parsing or making several cut-off wave numbers and window widths, which are divided into different depths. The purpose of spectral decomposition analysis is to identify patterns of anomalous structures at predetermined depths. In this analysis, the cut-off value is calculated based on the results of the Fourier transform on 11 paths that have been made previously in the spectral analysis. In this study, the depths of the residual anomalies selected for analysis were at depths of 1.5 km, 2 km, 2.5 km, 3 km, 3.5 km, and 4 km. The result reveals that shallower anomalies indicate more complex structures, in contrast, deeper anomaly reflects more homogeneous structure patterns (Figure 7).

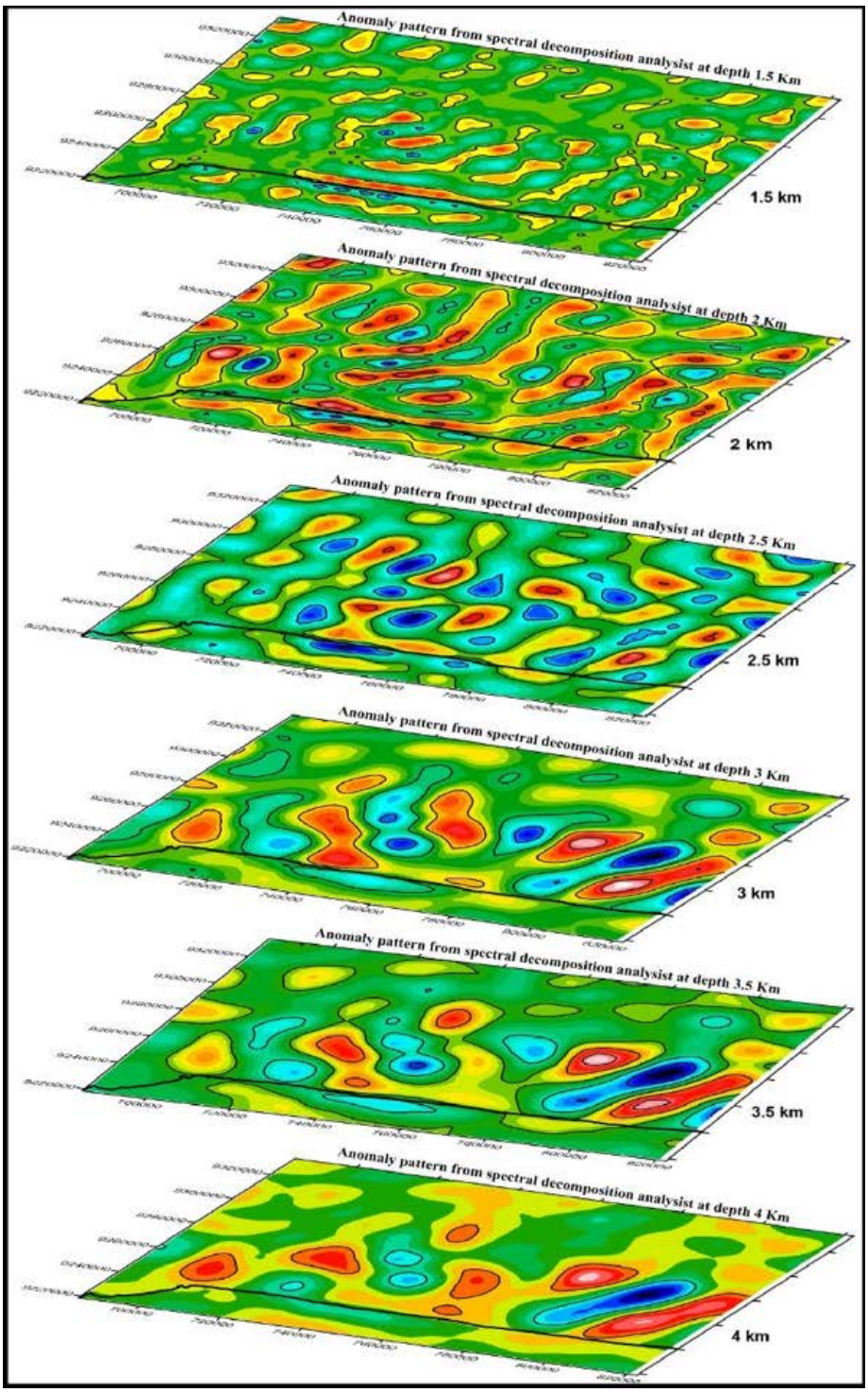

Figure 7. Anomaly pattern at 1.5 km, 2 km, 2.5 km, 3 km, 3.5 km, and 4 km depths based on spectral decomposition analysis

This result is in line with the theory suggesting that a deeper density of the subsurface rock characterizes a homogenous pattern (Febriansyah et al., 2017). Analyzing the anomaly pattern for each depth, the residual anomaly at 4 km depth appears more regional, while the anomaly pattern at 1.5 km depth still shows complexity, forming a closures pattern. The results of the residual anomaly in the spectral analysis show that the boundary of the discontinuity field between the sedimentary rock and the basement is at a depth of 3.78 km. This finding aligns with the results of spectral decomposition analysis, where at 4 km depth the anomaly pattern is similar to residual anomaly from spectral analysis. Meanwhile the residual anomaly pattern of the spectral decomposition analysis, at 3 km and 3.5 km depths exhibits relatively similar to the one that resulted from the separation of the anomaly with optimum upward continuation filtering.

Qualitative Interpretation of Sedimentary Basins

Qualitative Interpretation was conducted to determine the lateral changes of anomalies based on residual anomaly using optimum upward continuation filtering. Furthermore, the structural pattern, basement high and sub-basin delineation can be recognized by this qualitative interpretation. In general, the structural pattern in the study area (Figure 8c) consists of two main directions, namely east-west and northeast-southwest. The west-east trending structure might be affected by the RMKS fault zone (Rembang – Madura – Kendeng) (Satyana et al., 2004), while the northeast-southwest trending structure pattern might be affected by the Meratus pattern, which is the dominant structural pattern in the East Java region. The height pattern (basement high) as shown in the residual anomaly (Figure 8a) shows a relatively east-west and northeast-southwest direction.

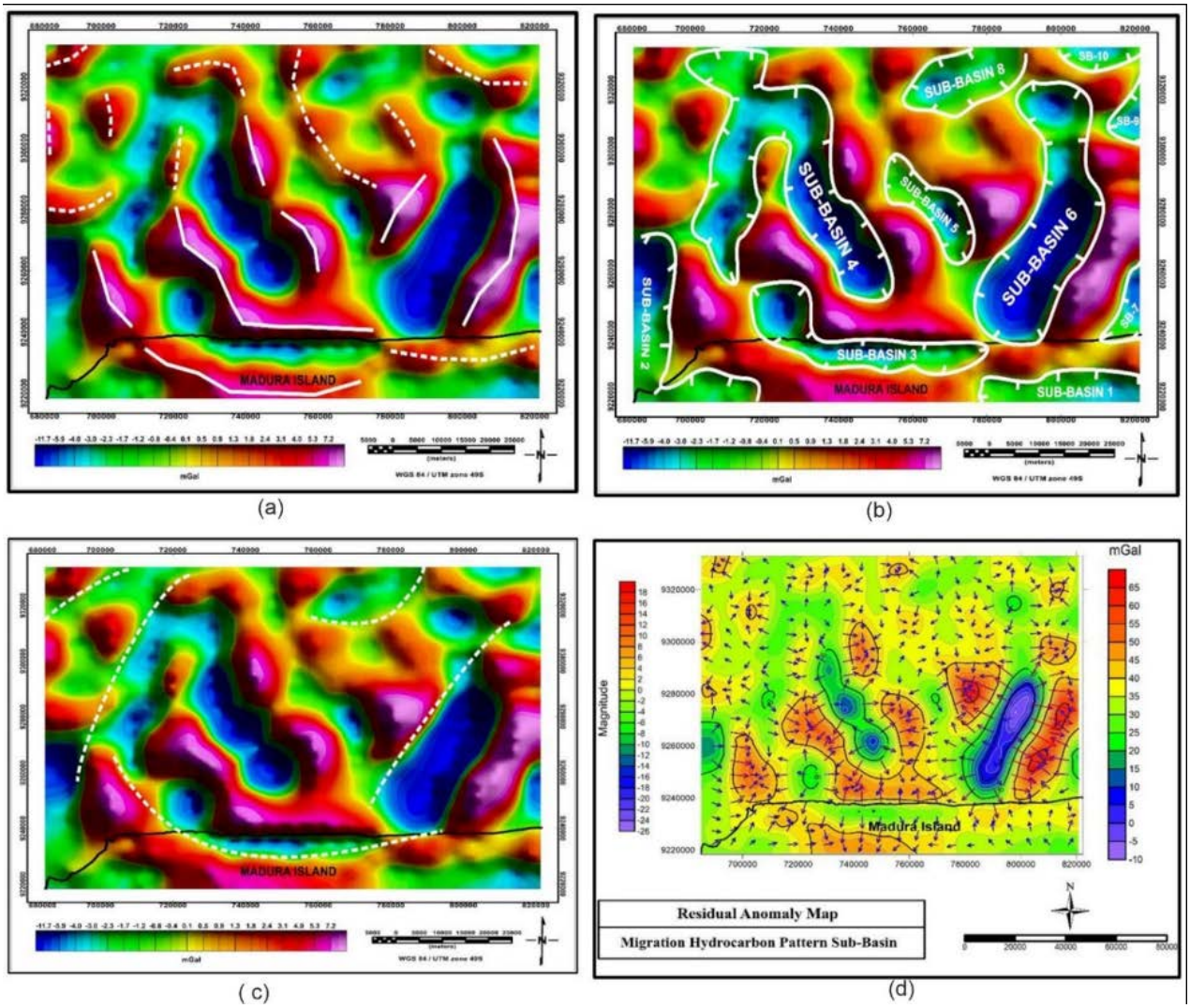

Figure 8. (a) Basement high pattern, (b) sub-basin delineation, (c) Lineament structure pattern, (d) Migration hydrocarbon pattern North Madura Offshore.

These basement high patterns will later be developed into anticlinal structures which are important for the petroleum system analysis. In the southern part of the study area, the relative basement high pattern appears to be oriented east-west, likely influenced by the RMKS fault zone (Rembang – Madura – Kendeng). Meanwhile, in the southern to the northern part of the study area, the high anomaly is relatively northeast-southwest direction. This might be due to the influence of the Meratus pattern.

The delineation pattern of the sedimentary sub-basins determined based on residual anomaly consists of 2 (two) large sub-basins and 8 (eight) small sub-basins (Figure 8b). These sub-basins are bounded by the surrounding basement high patterns, and characterized by low anomalies, indicated by blue to dark blue colors with the anomaly values ranging from -11.7 to 7.2 mGal. Figure 8(d) shows the alleged migration patterns of hydrocarbons identified based on vector analysis on the residual Bouguer anomaly map using Surfer software. Furthermore, the flow patterns can be predicted which tend to migrate from the low anomalies to the high anomalies, since the fluids move from high-pressure area to that of lower pressure.

Quantitative Interpretation

To determine the subsurface geological model, which includes the dimensions or size of the subsurface model, the types of constituent rocks based on the geology of the study area and rock density parameters, quantitative interpretation was conducted. The results are expected to reveal the bedrock depth and the composition of the sedimentary rock above it. This quantitative interpretation involved 3D inversion modeling using the Grablox program (Pirttijarvi, 2008) and visualizing the 3D model using rockwork. The inversion results (Figure 9a) show that the density values of the model range from 2.37 to 3.0 gr/cc which is an illustration of the subsurface rock mass density in the north Madura offshore area, North East Java Basin. While Figure 9(b) displays the cross-sectional direction of the 2D model.

In the 2D model, Line A-A' (Figure 9c) is a northeast-southwest ward, while Line B-B' shows a northwest-southeast direction (Figure 9d). Within this path, the

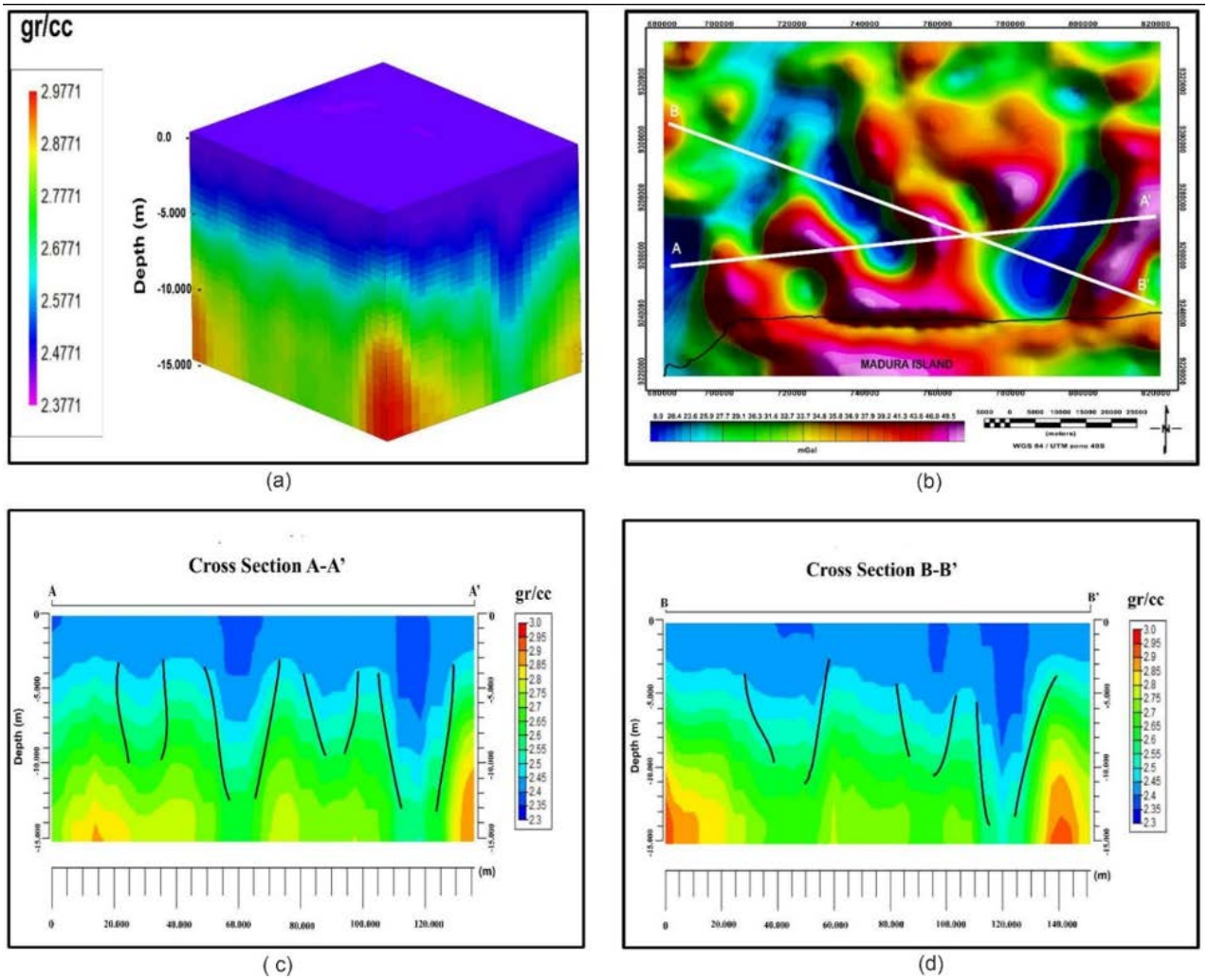

Figure 9. (a) 3D inversion modeling, (b) Line direction of 3D inversion modeling (c) 2D modeling of cross section A-A', (d) 2D modeling of cross section B-B'.

presence of highs and lows anomalies can be identified, resembling sub-basins as indicated by the anomaly patterns along the modeling trajectory. From the model (Figures 9c and 9d), low-density values represent sedimentary rocks, identified as sub-basins within the study area, while higher-density values correspond to the basement underlying the sedimentary layers. In the A-A' and B-B' cross sections, two large sub-basins are bounded by basement high, which are interpreted as depocenters. To validate the 3D inversion modeling result, 2D modeling is used with forward modeling. This modeling is done by creating a subsurface model with an arbitrary cross-section in the form of a polygon that is considered to represent the subsurface state (Talwani et al, 1959). The density values used for making subsurface models on 2D forward modeling are based on references from Telford et al., (1990). Figure 10 displays a cross-section of the 2D forward modeling path (A-A' and B-B'), which is in a similar position to the path in the 3D inversion modeling.

The 2D modeling of the residual anomaly on the Line A-A' was conducted along 132 km length (Figure 11a), while the length of the Line B-B' model was 148 km (Figure 11b). The model result exhibits a subsurface model consisting of four layers including the basement and some sedimentary rock layers. The topmost layer is interpreted as Tertiary-Neogene sedimentary rock with a density value of 2.1 gr/cc. This layer is indicated as the Lidah Formation which is dominated by marine shale with some limestones formed from the decomposition of older limestones. This formation is the result of rapid deposition from the Paciran and Kalibeng Formations to the northeast (Putra, 2007). According to the regional stratigraphy of the North East Java Basin by Pringgoprawiro (1983 in Sribudiyani et al., 2003), this formation is younger from the early Pliocene to the Pleistocene. The second layer is interpreted as Tertiary-Neogene sedimentary rock with a density value of 2.3 gr/cc. This layer consists of alternations between sandy claystone with sandstone and foraminiferal-rich limestone, belonging to the orbitoid group from the Tawun formation. It is also composed of orbitoid limestone and claystone at the bottom and sandstone with the insertion of orbitoid limestone at the top from the Ngrayong formation. Additionally, it consists of unlayered marl and claystone, with sandy limestone and calcareous sandstone at the bottom of the Wonocolo formation.

The third layer is interpreted as Tertiary-Paleogene sedimentary rock with density a value of 2.45 gr/cc. This layer age ranges from the Late Oligocene – Miocene, composed of carbonate platforms from the Late Oligocene Prupuh Formation and followed by the growth of reef limestones in the Early Miocene. The lowest part is the basement layer which comprises volcaniclastic igneous rock with a mass density value of 2.67 gr/cc. This volcaniclastic layer covers the southern part of the basin area, dominated by eroded rocks from "Old Andesite

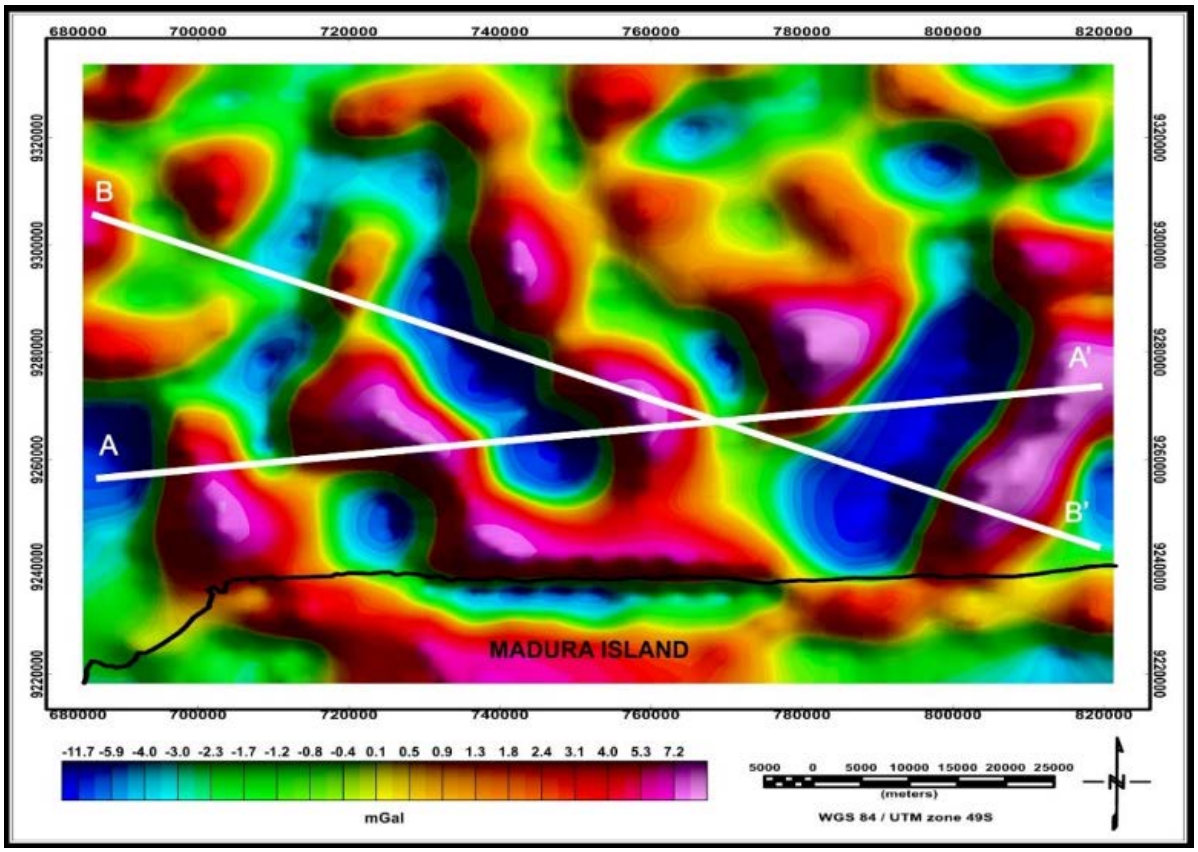

Figure 10. Line direction of 2D subsurface geological modeling of the North Madura Offshore

Formations" in the Cepu – Tuban area along the north coast and granite rock erosion, producing sandstone deposits from the Ngrayong Formation (Putra, 2007). Furthermore, to determine the fault structure, we conducted the second vertical derivative (SVD) analysis. Thrust faults are identified if the positive SVD value is lower than the negative SVD value, whereas, normal faults are identified when the positive SVD value is greater than the negative SVD value. The results indicate that the fault in the basin area is dominated by normal faults.

The results of qualitative gravity data analysis show two quite large sub-basins, namely sub-basin4 and sub-basin6 with a sedimentary rock thickness of around (5-6) Km. The results of the second vertical derivative analysis and 2D modeling in these two basins show the existence of a normal fault structure which is characteristic of back-arc basins. These sedimentary basins are something of interest for the development of the petroleum system in this area. The results of the spectral decomposition of gravity data show different structural patterns at several depths. The sub-basin pattern clearly appears at a depth of 4 km,

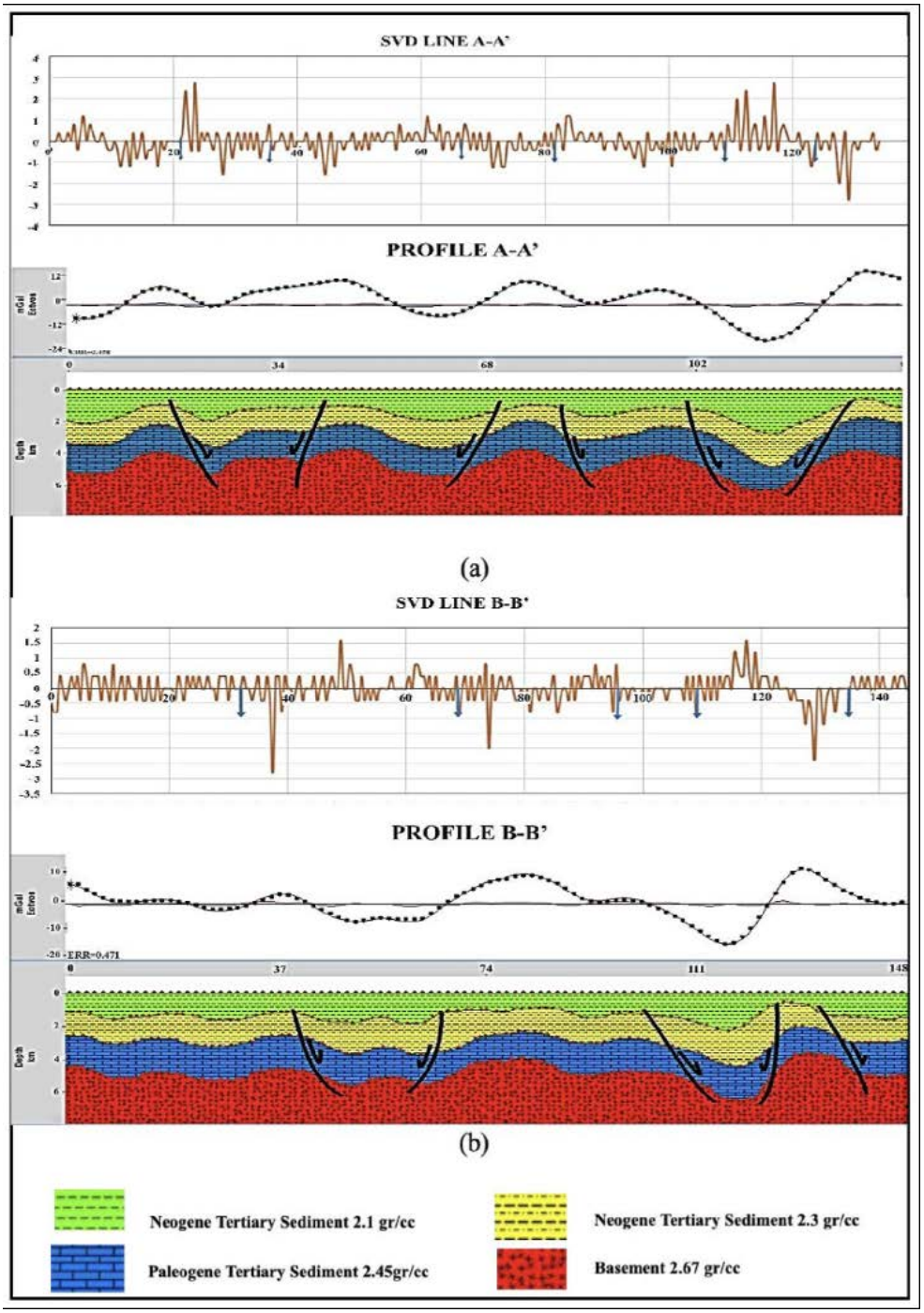

Figure 11. (a) 2D Model of subsurface geology A-A' line section, (b) 2D Model of subsurface geology B-B' line section of the North Madura Offshore.

characterized by a simpler structural pattern, more complex structures are visible at shallower depths. The basement highs pattern, fault structures, and depocenters are clearly visible in the 2D model (figure 11), the anticline structure appears at a depth of 1.5 km, this is in accordance with the anticline structure seen in the spectral decomposition results (figure 7). The existence of fault structures, sub-basins, and basement highs in the north Madura offshore basin is interesting for further study to determine the potential of the petroleum system in this area.

CONCLUSIONS

The Bouguer anomaly map shows that the high anomalies are scattered in the southern and eastern parts of the study area, while the central to northern parts exhibit low anomalies surrounded by high anomalies. The results from spectral analysis indicate an average depth of 23.704 km for deep discontinuities field (representing lower crust) and 3.788 km for shallow discontinuities field (basement). Filtering upward continuation identified the optimal height at 5000 m, used in determining regional and residual anomalies. Regional anomaly indicates a long wavelength anomaly which is usually interpreted as a regional (deep) structure while residual anomaly reflects shorter wavelength anomaly which is interpreted as a local (shallow) structure. Based on the qualitative interpretation, the height pattern of the study area is relatively west-east direction in the southern part and relatively northeast-southwest in the central to northern parts. This might be due to the influence of the RMK fault in the south and the Meratus pattern in the central to northern parts. Additionally, sub-basin delineation identified 2 large sub-basins and 8 smaller sub-basins characterized by low anomalies. These sub-basins are limited by the surrounding basement high. The bedrock that underlies the research area is volcaniclastic igneous rock with a mass density value of 2.67 gr/cc. The modeling results reveal several thick sedimentary basins, fault structures, and anticlines that are interesting for further exploration in petroleum studies.

ACKNOWLEDGEMENTS

The authors would like to thank the Center for Geological Survey of the Geological Agency for allowing us to use the data. We would like also to thank the Head of the Marine Geological Institute, the reviewers, and all parties whom helped in data processing and contributed to writing this paper.

REFERENCES

Fatahillah, Y., 2016. Penentuan Potensi Batuan Induk Menggunakan Model Log TOC, pada Formasi Ngimbang, Lapangan "Arrazi", Cekungan Jawa Timur Utara. *Bachelor thesis*. Institut Teknologi Sepuluh Nopember. Surabaya. *Unpublished.*

Febriansyah, D., Haerudin, N., Suharno, and Setiadi, I., 2017. Studi Pola Sub-Cekungan Hidrokarbon Menggunakan Analisis *Spectral Decomposition*, Pemodelan 2D Dan Pemodelan 3D Berdasarkan Data Gayaberat Daerah Longiram, Kalimantan Timur. *Jurnal Geofisika Eksplorasi*, 3 (3): 1-16.

Grant, F.S., and West, G.F., 1965. *Interpretation theory in applied geophysics*. New York: MC Graw-Hill Book Company.

Koesoemadinata, R.P., 1978. *Geologi Minyak dan Gas Bumi*. Bandung, ITB.

Pirttijarvi, M. 2008. *Gravity interpretation and modeling software based on 3-D block models. User's guide to version 1.6b.* Department of Physics Sciences. University of Oulu. Finland.

Putra, P. S., 2007. Sekuen Pengendapan Sedimen Miosen Tengah Kawasan Selat Madura. *Jurnal Riset Geologi & Pertambangan*, 17 (1): 20-36.

Satyana, A.H., Erwanto, E., and Prasetyadi, C., 2004. Rembang -Madura -Kangean -Sakala (RMKS) Fault Zone, East Java Basin: The Origin and Nature of a Geologic Border. *Proceeding the 33rd Annual Convention & Exhibition of Indonesian Association of Geologist.*

Setiadi, I., Setyanta, B., and Widijono, B, S., 2010. Delineasi Cekungan Sedimen Sumatera Selatan Berdasarkan Analisis Data Gayaberat. *Jurnal Geo-Sciences,* 20 (2): 93-106.

Setiadi, I., and Marjiyono. 2018. Interpretasi Geologi Bawah Permukaan dan Delineasi Cekungan Salawati wilayah Sorong dan Sekitarnya Berdasarkan Analsis Spektral serta Pemodelan 2D dan 3D Data Gayaberat. *Jurnal Geologi dan Sumber Daya Mineral*, 19 (3): 117-130.

Setiadi, I., Setyanta, B., Nainggolan, T. B., and Widodo, J., 2019. Delineation of Sedimentary Subbasin and Subsurface Interpretation East Java Basin in the Madura Strait and Surrounding Area Based on Gravity Data Analysis. *Bulletin of the Marine Geology*, *34* (1): 1-16.

Sribudiyani, Muchsin, N., Ryacudu, R., Kunto, T., Astono, P., Prasetya, I., Sapiie, B., Asikin, S., Harsolumakso, A. H., and Yulianto, I., 2003. The collision of the East Java microplate and its implication for hydrocarbon occurrences in the East Java basin. *Proceedings Indonesian Petroleum Association, 29th Annual Convention & Exhibition.*

Talwani, M. Worzel, J.L., and Ladisman, M. 1959. Rapid Gravity Computation for Two Dimensional

Bodies with Application to the Medicino Submarine Fractures Zone. *Journal of Geophysics Research*, 64 (1): 49 - 59.

Telford, W.M., Geldart, L.P., and Sheriff, R.E., 1990. *Applied Geophysics*. USA: Cambridge University.

Walidah, F. I. 2011. Penentuan Struktur Bawah Permukaan Berdasarkan Analisa dan Pemodelan Data Gayaberat untuk Melihat Potensi Hidrokarbon pada Daerah "FW1807" Cekungan Jawa Timur Utara. *Bachelor thesis*. Universitas Indonesia. Depok.

GRANULOMETRIC ANALYSIS OF PALEOTSUNAMI DEPOSITS CANDIDATE IN TERNATE ISLAND, NORTH MALUKU

ANALISIS GRANULOMETRIK TERHADAP KANDIDAT ENDAPAN TSUNAMI DI PULAU TERNATE, MALUKU UTARA

Yudhicara*

Center for Volcanology and Geological Hazard Mitigation – Geological Agency Jl. Diponegoro 57 Bandung, Indonesia

*Corresponding author: yudhicara966@gmail.com

(Received 30 January 2023; in revised from 3 February 2023; accepted 25 July 2023)

DOI : http://dx.doi.org/10.32693/bomg.38.2.2023.807

ABSTRACT: Ternate Island is a volcanic island located in the Maluku Sea. Tsunami ever hit Ternate before 1900 or occurred before the age of the people living in this island. The paleotsunami suspect have been found in the western coast of Ternate Island. The outcrop has 50 m length and 1 m width, was discovered beneath the Gamalama eruption product which occurred in 1907. The paleotsunami candidate consists of at least five layers originating from different tsunami events. The granulometric analysis was carried out for each layer. The results obtained were that paleotsunami sediments had poorly sorted which indicated that the grain sizes were mixed, this was due to the energy of tsunami wave varied in time when transporting and depositing the sediments. Skewness varies from very fine to very coarse, indicating a change in the energy of the tsunami wave that occurs from very high when rising inland to decreasing as it returns to sea. Kurtosis varies from leptokurtic, platykurtic, and mesokurtic. Variations in mean, sorting, skewness and kurtosis values indicate a change in tsunami wave energy which causes a change in grain size. The granulometric analysis shows that the deposition of the youngest paleotsunami deposits candidate was initiated by a very strong current with the greatest energy, thus depositing very coarse sand to gravel, followed by a gradual decrease in energy and the tsunami wave process began to reverse towards the sea, then receded with the lowest energy and deposited finer grains. The sediment sources come from two different places, this shows that the sources come from the sea and the coast around the deposited paleotsunami candidates.

Keywords: paleotsunami deposits, deposition process, granulometric analysis, Ternate, North Maluku

ABSTRAK: *Pulau Ternate merupakan pulau gunung api yang terletak di Laut Maluku. Tsunami pernah melanda Ternate sebelum tahun 1900 atau terjadi sebelum usia penduduk yang tinggal di pulau ini. Kandidat paleotsunami telah ditemukan di pesisir barat Pulau Ternate. Singkapan tersebut memiliki panjang 50 m dan lebar 1 m, ditemukan di bawah produk letusan Gamalama yang terjadi pada tahun 1907. Kandidat paleotsunami terdiri dari paling tidak, lima lapisan yang berasal dari peristiwa tsunami yang berbeda. Analisis granulometri telah dilakukan untuk masing-masing lapisan. Hasil yang diperoleh bahwa endapan paleotsunami memiliki sortasi yang kurang baik yang mengindikasikan bahwa ukuran butir tercampur, hal ini disebabkan energi gelombang tsunami bervariasi terhadap waktu saat mengangkut dan mengendapkan sedimen. Skewness bervariasi dari sangat halus hingga sangat kasar, menunjukkan perubahan energi gelombang tsunami yang berlaku dari sangat tinggi ketika naik ke daratan menurun ketika kembali ke laut. Kurtosis bervariasi dari leptokurtik, platikurtik, dan mesokurtik. Variasi nilai mean, sorting, skewness dan kurtosis menunjukkan adanya perubahan energi gelombang tsunami yang menyebabkan perubahan ukuran butir. Analisis granulometrik menunjukkan bahwa endapan yang diduga produk paleotsunami termuda, proses pengendapannya diawali oleh arus yang sangat kuat dengan energi terbesar, sehingga mengendapkan pasir yang sangat kasar hingga kerikil, diikuti dengan penurunan energi secara bertahap dan proses gelombang tsunami mulai berbalik arah menuju laut, kemudian surut dengan energi terendah dan mengendapkan butir-butir yang lebih halus. Sumber sedimen tersebut berasal dari dua tempat yang berbeda, yaitu berasal dari laut dan pantai di sekitar endapan yang diduga hasil kejadian tsunami masa lalu (paleotsunami).*

Kata Kunci: *endapan paleotsunami, proses pengendapan, analisis granulometri, Ternate, Maluku Utara*

INTRODUCTION

Ternate Island is a volcanic island located in the Maluku Sea. Based on its tectonic conditions, Ternate is an area prone to tsunamis, which caused by earthquakes, volcanic activity or due to underwater landslides. According to the tsunami catalog, tsunami have ever hit Ternate Island in 1608, 1673, 1771, 1840, 1846, 1856, 1857, 1858, 1859, 1871, 1889, 1892, 1900 (Soloviev & Ch.N.Go., 1974), and 1994 (Satake & Imamura, 1995).

The tsunami history in this island was occurred before the age of the people living in this island. Therefore, the tsunami traces findings on this island can be very important as an early warning to the people to face the similar tsunami events that might occur in the future.

The Maluku Sea is an arc-arc collision zone, which is located at the confluence of the Eurasian, Pacific and Philippine plates (Figure 1). This collision forms a double subduction zone in the Maluku Sea known as the Mayu Ridge subduction zone.

The consequences of this subduction zone produce a series of volcanoes along the west in the Sangihe Islands and in the east along Halmahera Island and form volcanic islands, which is Ternate is one of them and Gamalama is the name of the volcano.

In the investigation of tsunami traces in Ternate Island which conducted on November 2022, at least three paleotsunami layers have been found in the western part of the Island, namely the Loto area (Figure 2). The Loto area has characteristics of a straight beach with a wavy morphology, composed of sand, gravels, pebbles to boulder of rocks which are products of the Gamalama volcano.

Based on its position, Loto is located in an estuary, the mouth of the Loto river or also known as Barangka Loto (Barangka means river) which ends into the Maluku Sea. This place relatively natural and undisturbed by human activity.

Based on the Geological Map of Gamalama Volcano, Ternate, North Maluku, surface deposits of Ternate Island are composed by the results of eruptions from the Gamalama Volcano itself (Figure 3). Starting from Prehistoric times (before the 5th century) to the present (Bronto et al., 1982).

The deposits of each generation of the Gamalama volcano, based on the source of the eruption, are divided into three parts, in order from oldest to youngest, as follows: Old Gamalama (Gt) consists of types of lava flows and related rocks (GtLu); Pyroclastic deposits (Gtig); and the lava deposit (GtLa), occurred in Pre-historic times. Mature Gamalama (Gd) consists of types of lava flows and related rocks, namely GdL and GdLu; Pyroclastic deposits consist of Gdpf, Gdpl, Gdp; and the Gdla lava deposits. Happened in pre-historic times.

Young Gamalama (Gm) which is divided into two based on the time it occurred, namely the prehistoric era and the historical era. In prehistoric times, it consisted of related types of lava flows and rocks, namely GmLu, Gm L1, Gm L2, Gm L3, and Gm L5, while those that occurred in historical times were Gm L6, and Gm L7. Whereas pyroclastic deposit products in prehistoric times consisted of Gm pf, and those that occurred in historical times were Gmbv and Gmpm, and Gmpt which lasted from

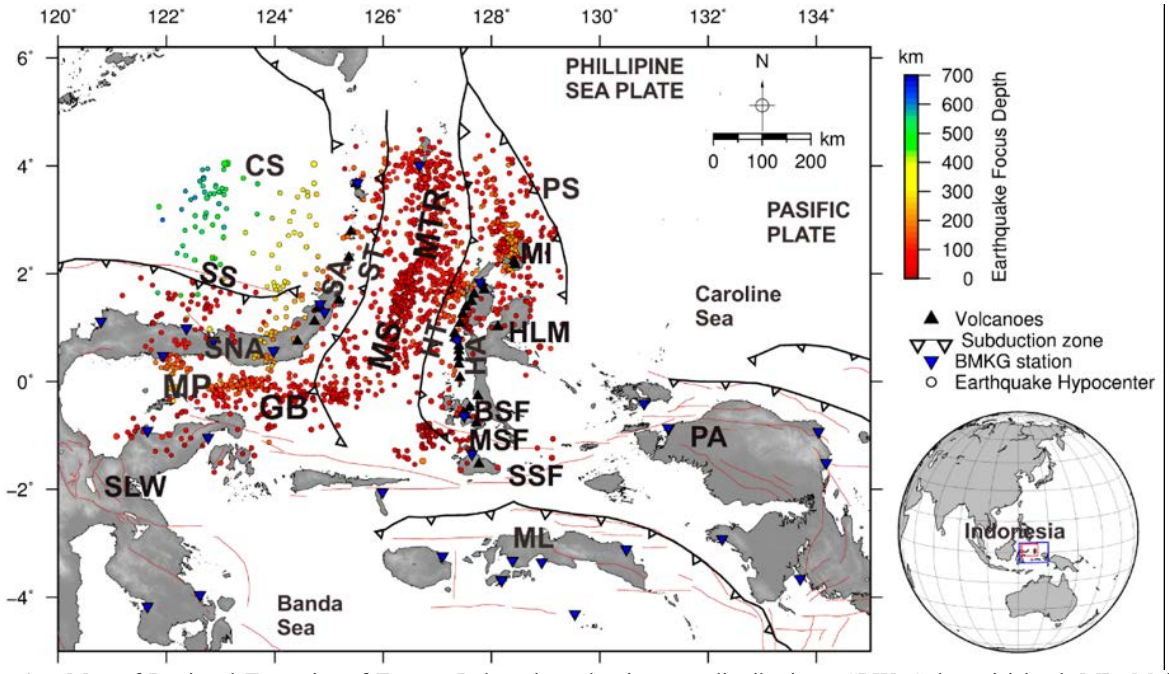

Figure 1. Map of Regional Tectonics of Eastern Indonesia and epicenters distributions; SLW: Sulawesi island; ML: Molucca island; PA: Papua island; HLM: Halmahera island; SNA: Sulawesi's north arm; SS: Sulawesi slab; PS: Philippine slab; HT and ST: Halmahand Sangihe Trench; HA and SA: Halmahera and Sangihe volcanoes arc; CS: Celebes sea; MP: Minahassa peninsula; GB: Gorontalo Basin; MS: Molucca Sea; MTR: Mayu-Talaud Ridge; BSF, MSF, and SSF: Bacan, Molucca, and Sula Sorong Faults, respectively (Rachman et al., 2022).

Figure 2. Area of Interest (left) in the western part of Ternate (right) (Google Earth, 2022)

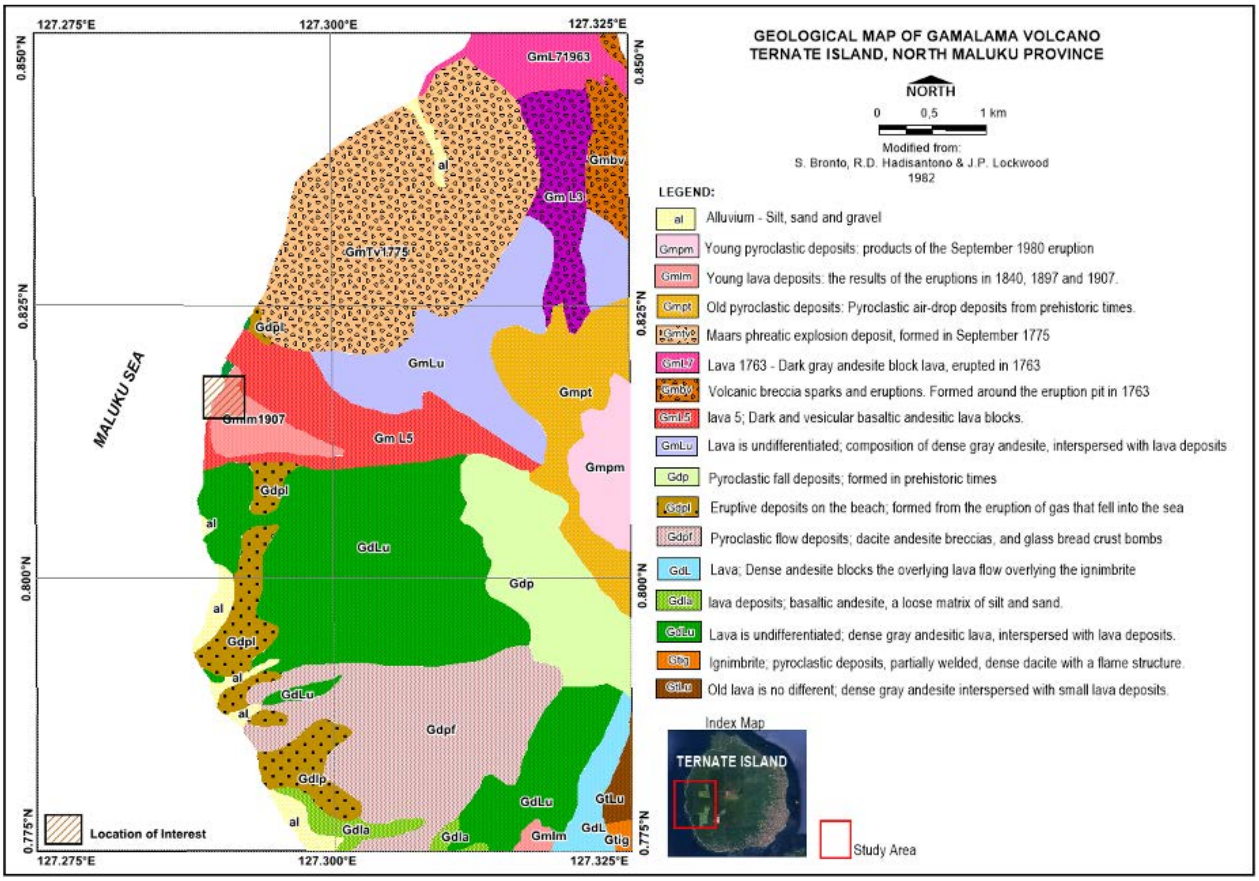

Figure 3. Geological Map of Gamalama Volcano (Bronto et al., 1982)

prehistoric times to historical times; There are Maar deposit products, which occurs as a result of weakly consolidated phreatic eruptions, while on the slopes as layered foundation deposits with bomb, sag and plant lapilli structures; whereas in historical times there were phreatic eruptions accompanied by the formation of the Tolire Jaha and Tolire Kecil maars, which occurred in 1775 (GmTv). Lava deposits occurred in historical times, namely Gmlm, which is a young lava deposit. Surface deposits consist of debris pyroclastic deposits (pr) and alluvium consisting of silt, sand, gravel and lumps (al).

Tsunami deposits are generally preserved in low-lying areas such as estuaries and lagoons and are made up of sediments resulting from the erosion of coastal areas (sand dunes, beach embankments, cliffs) and parts of the seabed that were eroded by the tsunami waves.

The tsunami deposits show a wide variety of bed forms and sedimentary structures; their properties are

highly dependent on the physical setting of the deposition site and on the nature of the events that caused it, such as current strength and surface geology. However, some common features are recognized in most tsunami deposits, reflecting the physical nature of the tsunami waves. Very large wavelength and period compared to storm surge. At the same time, these general features reflecting the shape of a tsunami wave can serve as criteria for distinguishing a tsunami deposit from a storm deposit.

The general characteristics of tsunami deposits are described below based on some examples of ideal environments for deposition and preservation. Refers to tsunami deposits in the coastal lowlands, including shallow bays, lagoons and ponds. These areas, which are separated from the open sea, usually have sufficient water depth and accommodation space for the deposition of tsunami deposits with well-developed sediment structures. The relatively high sediment flux in this shallow water area provides favorable preservation conditions for fast burial of tsunami deposits (Fujiwara, 2008).

Tsunami deposits exhibit a wide spectrum of bed forms and sedimentary structures, which are related to the physical properties of the flow, such as velocity, density, viscosity, and predominant grain size. However, some general characteristics are recognized in the tsunami deposits from various deposition sites. This results from the fact that tsunamis have much longer wavelengths and periods than wind-generated waves, such as storm surges.

These extraordinary physical properties of the tsunami, under ideal conditions of deposition and preservation, are well recorded in the tsunami deposits as a unique arrangement pattern of bed forms and sedimentary structures: (1) alternation of sediment sheets deposited from high-energy sediment flows and silt beds, (2) repeated course reversals and (3) series of thinning and smoothing of sediment sheets.

Thick tsunami deposits sometimes consist of complete four deposition units, Tna to Tnd in ascending order (Figure 4A), which reflect the change in wave amplitude with time (Figure 4B). The Tna unit corresponds to relatively small waves in the early stages of a tsunami. At this stage, the sediment is fine grained with rip up clasts, which are bounded by mud drape. The very coarse-grained TnB unit is evidence of the occurrence of large waves in the middle of a tsunami. At this stage, the deposited sediment is a coarse grained dune with gravel fragments and anti-dune structures. The sequence of decimation and upward decimation from Tnb Unit to Tnc Unit shows the process of tsunami receding with a hummocky structure. The Tnd unit is a muddy layer with plant remains, formed by suspension fallout, indicates a return to a low-energy state after the tsunami (Fujiwara, 2008).

Tsunami deposits usually have a gradual bedding, fining upward and thinning landward sedimentary structure. Meanwhile, coastal sediments are characterized by repeated layers, containing a mixture of fragments originating from various sources, including cliff erosion, rivers, volcanoes, coral reefs, sea shells, sea level rise, and cannibalism of ancient coastal deposits (Trenhaile, 2005).

METHODS

The paleotsunami and paleosoil sediment samples were taken from Ternate Island on November 2022.

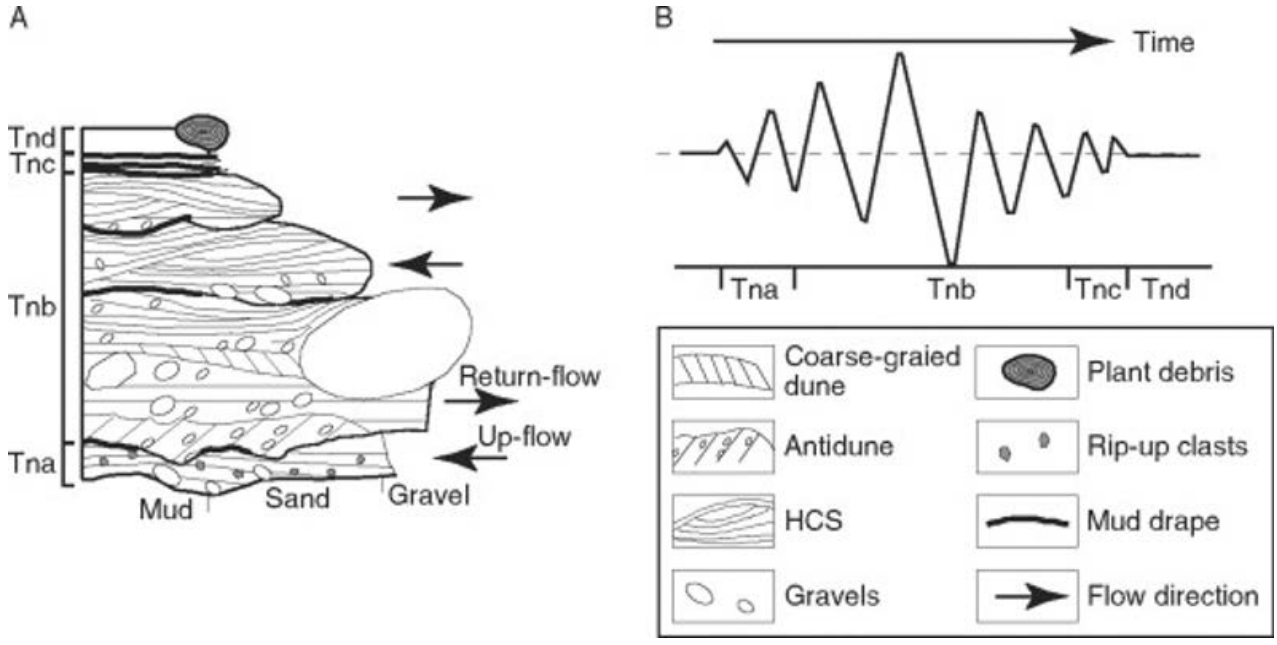

Figure 4. Sequence of tsunami deposits (Fujiwara, 2008)

Laboratory tests have been carried out for each sample, both paleotsunami and ancients coastal deposits, totally 12 samples by using the method grain size analysis.

Distribution of a sediment is the result of processes and infer the energy present (Heinzel, 2016), it can show the sediment transport itself, which can be read based on grain size tests in the laboratory. Grain size testing (granulometric) is carried out in the following stages:

1. Weigh the sample to determine the initial weight (wet condition)
2. Prepare each sample for drying
3. Removing the water content of the sample by drying the sample in the oven
4. Weigh the sample to determine the dry weight (Figure 5)
5. Determine the weight of the sample to be tested (analyzed)
6. Prepare the sieving equipment with the sieve assembly according to the desired opening sequence in phi units (-2.00; -1.00; 0.00; 1.00; 2.00; 3.00; 4.00; 5.00; and 6.00)
7. Sieve each sample so that the number of grains on each sieve size is obtained.
8. Weigh the sieve results with each sieve size (Figure 6).
9. The amount obtained is used as input for calculating and analyzing grain size using a statistical program, to determine its characteristics and deposition process.

After megascopic observations and conducting laboratory tests, the results obtained are used as input in a statistical calculation program. In this case we use the Excel program developed by Balsilllie (2002) and Blott & Pye (2001). As for the identification of grain size textures, we used literature materials obtained from online lectures by Prof. Meor Akif from the University of Malaya (2021), Dr. C.E. Heinzel from University of Northern Iowa (2016), and Mclaren (1980).

Mean

Graphic Mean can be calculated with formula from Folk and Ward, 1957 (Figure 7).

$$M = \frac{\emptyset 16 + \emptyset 50 + \emptyset 84}{3} \quad \ldots\ldots\ldots\ldots\ldots\ldots\ldots\ldots (1)$$

Sorting

Sorting measure of the range grain size present, apart from being visually observe (hand lens, microscope), also can be calculate from the result. Sorting is inclusive graphic standard deviation (σ_i). One standard deviation

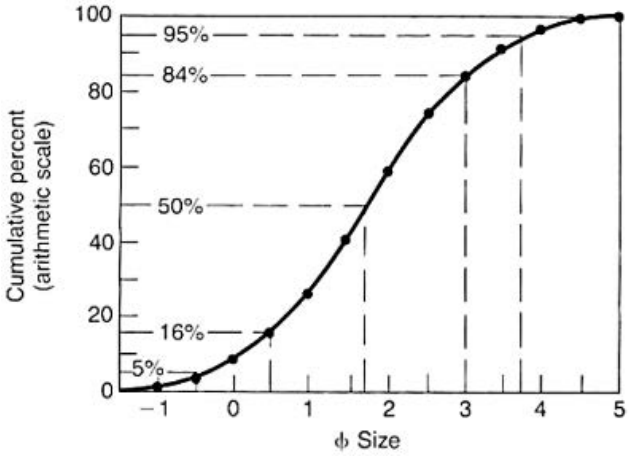

Figure 7. Determining the Graphic Mean Particle Size (Folk and Ward, 1957)

covers approximately the central 68% of area under

Figure 5. Weighing of the sediment samples

Figure 6. Drying (left) and Sieving (right) Machines

frequency curve (Figure 8), and can be calculated from grain size data (e.g. from sieve analysis), using the formula:

$$\sigma i = \frac{\emptyset 84 - \emptyset 16}{4} + \frac{\emptyset 95 - \emptyset 5}{6.6} \quad \ldots\ldots\ldots\ldots\ldots\ldots\ldots\ldots\ldots\ldots (2)$$

Illustration of sorting (Figure 9), corresponding to verbal terms and graphic standard deviation (Jerram, 2001):

Skewness

Skewness is a measure of the amount of deviation from a normal distribution (i.e., an asymmetrical frequency curve). Most of natural sediments do not yield a perfect normal grain size distribution (bell curve). Skewed distribution is asymmetrical distribution. Skewness can be calculated using formula:

Higher deviation from zero is greater skewness

Sorting Description	**Standar Deviation**
Very well sorted	< 0.35Ø
Well sorted	0.35 – 0.50Ø
Moderately well sorted	0.50 – 0.71Ø
Moderately sorted	0.71 – 1.00Ø
Poorly sorted	1.00 – 2.00Ø
Very poorly sorted	2.00 – 4.00Ø
Extremely Poorly Sorted	>4.00Ø

Kurtosis

Kurtosis is sharpness of a grain size frequency curve. Sharp-peaked (leptokurtic) better sorting in central portion

$$S = \frac{\emptyset 84 + \emptyset 16 - 2(\emptyset 50)}{2(\emptyset 84 - \emptyset 16)} + \frac{\emptyset 95 + \emptyset 5 - 2(\emptyset 50)}{2(\emptyset 95 - \emptyset 5)} \quad \ldots\ldots\ldots\ldots\ldots (3)$$

Calculated Skewness	**Verbal Skewness**
> + 0.30	Strongly Fine Skewed
+ 0.30 to + 0.10	Fine Skewed
+ 0.10 to – 0.10	Nearly Symetrical
- 0.10 to – 0.30	Coarse Skewed
<- 0.30	Strongly Coarse Skewed

(Figure 10). Flat-peaked (platycurtic) poorer sorting in central portion. Kurtosis can be calculated with the formula:

$$K = \frac{\emptyset 95 - \emptyset 5}{2.44(\emptyset 75 - \emptyset 25)} \quad \ldots\ldots\ldots\ldots\ldots\ldots\ldots\ldots\ldots\ldots (4)$$

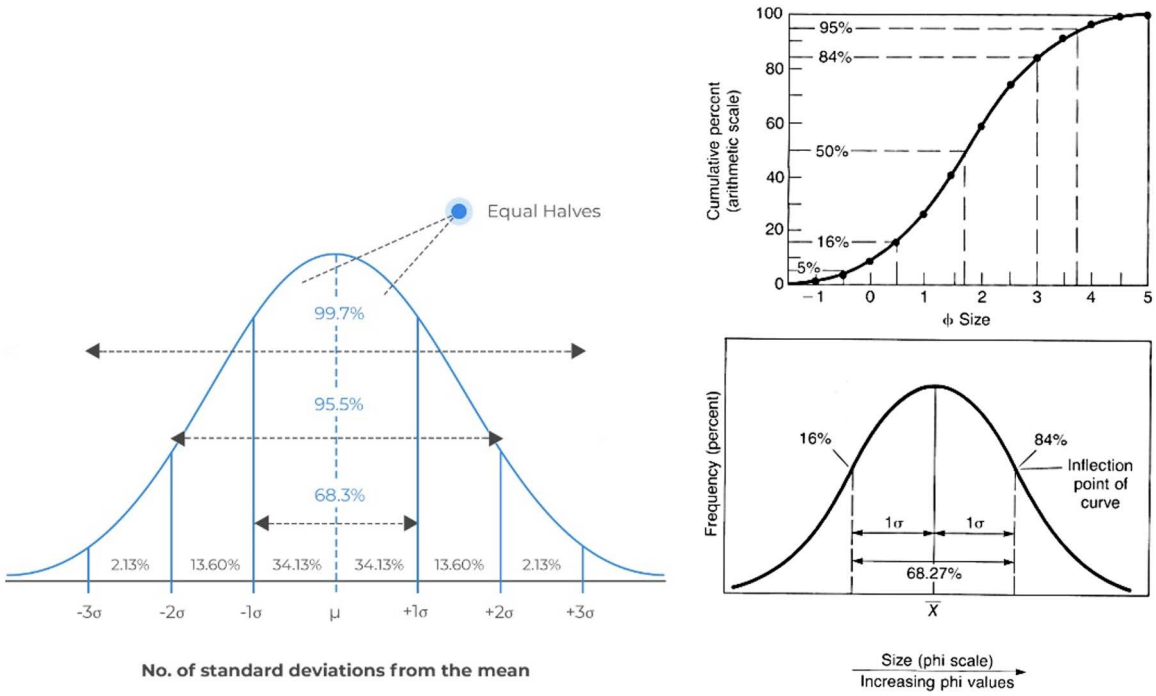

Figure 8. Graphical method of calculating sorting (Folk and Ward, 1957).

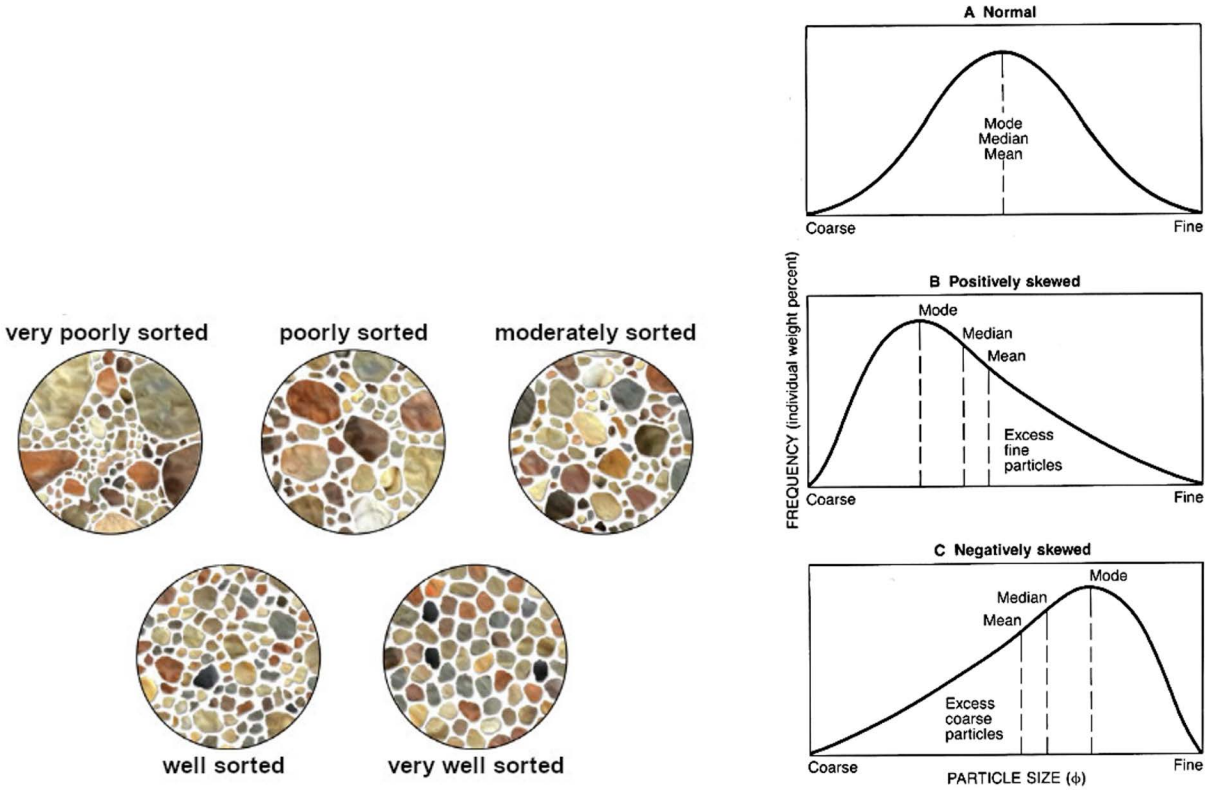

Figure 9. Illustration of Sorting (left) and Graphical Estimation of Skewness (right) (Geocache, 2023)

RESULTS AND DISCUSSION

The paleotsunami candidates were found at location of 127.29488°E – 0.82129°S. The youngest was deposited beneath the Gamalama eruption product which is occurred

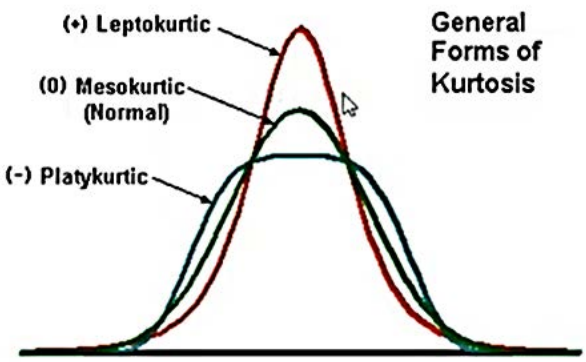

Figure 10. Graphic Estimation of Kurtosis (Akif, 2021)

Calculated Kurtosis	Verbal Kurtosis
< 0.67	Very Platykurtic
0.67 - 0.90	Platykurtic
0.90 - 1.11	Mesokurtic
1.11 - 1.50	Leptokurtic
1.50 - 3.00	Very Leptokurtic
>3.00	Extremely Leptokurtic

in 1907 (Figure 11). The thickness of the product of the Gamalama Volcano eruption reaches 7.3 m, with a distance of approximately 50 m from the coastline.

The first paleotsunami layer (J in Figure 11) is covered unconformably by paleosoil in the form of blackish coarse sand with a thickness of 5 cm, while below the layer it is bounded by paleosoil with a thickness of 15 cm, in the form of blackish gray old beach sand with rock fragments that have oriented nearly north-south or in the direction of the outcrop.

The first layer can be divided into three main layers, but there are very thin layers (mud drape) that separates the second layer from the first and the second to the third layers which has each thickness about 0,5 mm. The three main layers can be named as bottom (Tna) with thickness of 0.5 cm, middle (Tnb) of 2 cm, and top (Tnc) of 0.3 cm. The Tnd unit was very thin, so it can not easy to distinguish (Figure 12).

After excavating vertically downwards, it was found layers presumed to be older paleotsunami deposits with a thickness of 1.8 cm (Figure 11), which based on the difference in color, can be divided into two layers with an upper layer of 1 cm thick in the form of very fine sand with a light greenish gray color and 0.8 cm in the form of very fine brownish-gray sand. The second paleotsunami deposit was found under a 15 cm thick paleosoil. Layers suspected as the third paleotsunami deposit were found 15 cm later, as well as the fourth paleotsunami deposit with a thickness of 1.5 cm each. The layer which is suspected as the fifth or oldest paleotsunami deposit, was found 20 cm after the fourth layer, with a deposit thickness of 5.5 cm.

Let us named the youngest paleotsunami deposit as the first (1st), the next paleotsunami deposit which is older than the first one, we called the second (2^{nd}), the third (3^{rd}), the Forth (4^{th}) and the fifth (5^{th}) paleotsunami deposits. Only three samples of tsunami sediments could analysed in the laboratory, which are the first, the second and the fifth. While the third and the forth could not be taken for analysed because they were too thin, so they were mixed with the paleosoil above and below them. Here is the respective weight for granulometrical analysis (Table 2).

Megascopically, it was observed the physical properties of the sediment grains of the paleotsunami deposits which are then calculated statistically. Below (Figure 13) are the first, second, and the fifth paleotsunami sediment grains. It can be seen here that the grain color is dominated by dark gray and black, and part of it is silicate in the form of transparent quartz, red and yellowish white rocks.

Based on statistics calculation of grain-size distribution, it is obtained values of mean grain size, sorting, skewness and kurtosis (Table 3). The results obtained show that the sorting of all paleotsunamis were poorly sorted, those indicate the sediment size are mixed (large variance), and this is due to the energy of tsunami wave is varies in time when transport and deposits the sediment.

Skewness varied from strongly fine skewness to strongly coarse skewness, indicating of prevailing changing of tsunami wave energy from very high when its run up inland decreasing when it returning into the sea. Negative skewness shown by top layer of the 1^{st} paleotsunami deposits and middle layer of the 5^{th} paleotsunami deposits indicate of finer grain sizes. While positive values show coarser grain.

Kurtosis of the first top layer is leptokurtic, means the frequency distribution or its graphical interpretation having greater kurtosis than normal distribution or fat-tailed, meaning of having many outliers, while middle and bottom are platykurtic distribution which mean thin tailed, or have few outliers. The fifth top and middle layer both have mesokurtic, which mean the outlier characteristic of an extreme event.

Based on the results of granulometric analysis, information was obtained that the first paleotsunami (the youngest) was dominated by coarse silt (fine-sized sediment). In the top of the first paleotsunami, has composition of fine grains dominates over coarse grains

(silt 56.84%; sand 42.8417% and gravel 0.32%) and containing roots remains. The middle part of paleotsunami first layer has the percentage of sand-sized grains is slightly more than fine grains (silt 45.7013%; sand

Figure 11. Left: Paleotsunami deposits found beneath the product of the Gamalama volcano; Right: Outcrop with five layers of suspected paleotsunami deposits (B,D,F,H and J) bounded by paleosoil (A, C, E, G, I and K)

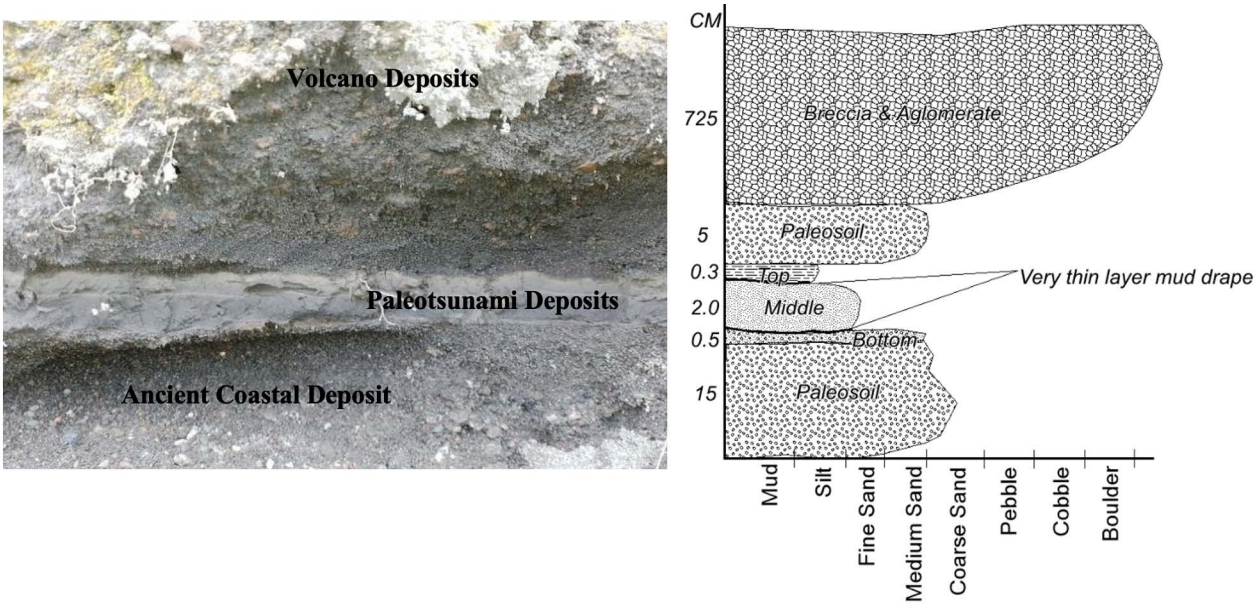

Figure 12. The Youngest First Layer Beneath the Product of the Gamalama Volcano (left) and Its Profil (right)

Table 2. The Analyzed Tsunami Suspects Samples

No.	Name of Samples	Weight (Gram)	
		Wet	Dry
1.	The first Paleotsunami (*top*)	202.32	147.61
2.	The first Paleotsunami (*middle*)	208.73	163.25
3.	The first Paleotsunami (*bottom*)	278.61	237.08
4.	The second Paleotsunami	33.08	29.17
5.	The fifth Paleotsunami (*top*)	24.50	21.26
6.	The fifth Paleotsunami (*middle*)	81.07	67.60
7.	The fifth Paleotsunami (*bottom*)	107.36	90.90

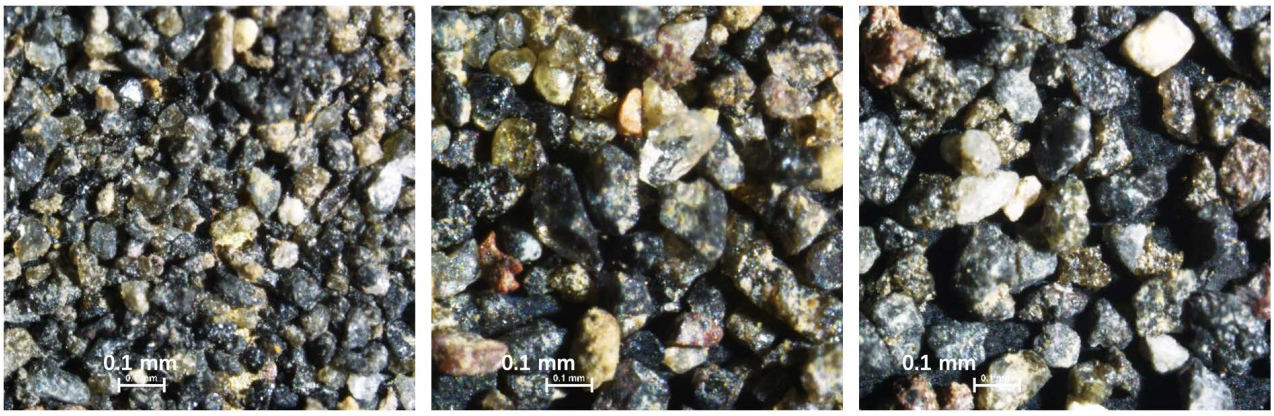

Figure 13. Megascopically of first Paleotsunami (left), the second (middle) and the fifth paleotsunami deposits (right)

Table 3. Sediment Texture of Mean, Sorting, Skewness and Kurtosis

Name of Paleotsunami	Mean	Sorting	Verbal of Sorting	Skewness	Verbal of Skewness	Kurtosis	Verbal of Kurtosis
1st paleotsunami (Top)	3.17	1.10	Poorly Sorted	-0.56	Strongly Coarse Skewed	1.37	Leptokurtic
1st paleotsunami (Middle)	2.58	1.36	Poorly Sorted	0.46	Strongly Fine Skewed	0.78	Platykurtic
1st paleotsunami (Bottom)	0.83	1.28	Poorly Sorted	0.30	Fine Skewed	0.72	Platykurtic
2nd paleotsunami	1.20	1.03	Poorly Sorted	1.33	Strongly Fine Skewed	0.63	Very Platykurtic
5th paleotsunami (Top)	1.43	1.47	Poorly Sorted	0.08	Nearly Symmetrical	0.97	Mesokurtic
5th paleotsunami (Middle)	1.92	1.58	Poorly Sorted	-0.24	Coarse Skewed	0.92	Mesokurtic
5th paleotsunami (Bottom)	1.17	1.63	Poorly Sorted	0.12	Fine Skewed	0.82	Platykurtic

Table 4. Percentage of grain size in paleotsunami and paleosoil deposits

No.	Name of Layers	% Gravel-Pebble	% Sand	% Silt
1.	The 1st Paleotsunami (Top)	0.32	42.84	56.84
2.	The 1st Paleotsunami (Middle)	0.85	53.45	45.70
3.	The 1st Paleotsunami (Bottom)	4.47	52.28	43.26
4.	The 2nd Paleotsunami	0.65	91.70	7.65
5.	The 5th Paleotsunami (Top)	1.98	86.12	11.90
6.	The 5th Paleotsunami (Middle)	2.01	80.16	17.83
7.	The 5th Paleotsunami (Bottom)	3.61	83.63	12.75

53.4512%; gravel 0.8475%). Meanwhile the bottom of first paleotsunami layer, has coarse size grains greater than finer grains and has more gravel (silt 43.26%; sand 52.28%; gravel 4.47%). The results are as listed in Table 4.

The following is a histogram that shown by the first (the youngest) paleotsunami deposits suspect. Figure 14 is the histogram of the bottom layer, shows dominantly percentage of sand, the existence of gravel, and a bimodal curve indicating that the sediment sources come from two different places.

The results of the grain size analysis were entered into the Excel program developed by Basillie et al. (2002), which plotted grain size of phi units in X directions and Cummulative Percent in Y directions, in order to determine the agencies of transportation and depositional process (Figure 15). Below is the guide how to read the curves.

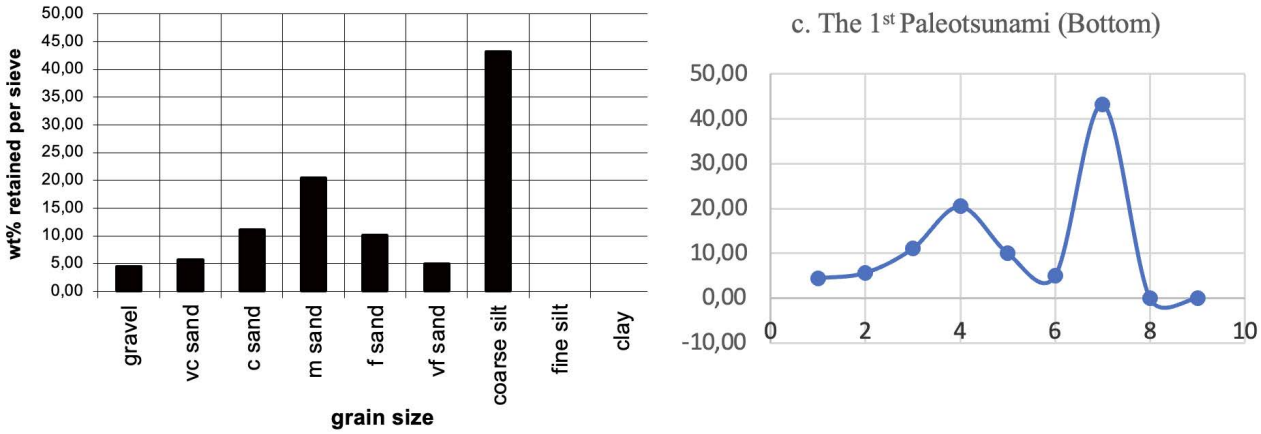

Figure 14. The bottom layer of First Paleotsunami sediment histogram (left) and Grain size curve showing sediment sources two different sources bimodial in the Bottom layer of youngest (the first) paleotsunami deposits (right)

Basic line-segment geometries identifying transportation and depositional signatures forthcoming from the use of aritmethic probability paper. Line-segment geometries were determined by Tanner (1986, 1991) and Balsillie, 1995 (Balsillie, 2002).

Figure 16 is an accumulation plot, shows the deposition process of the bottom layer, which has steep sloping indicates highest energy of the deposition characterized by deposition of pebble and coarse-sized grains (D). The character shown by the bottom layer shows the mechanism of sediment deposition by the tsunami waves when run up inland.

Next is the histogram of middle layer of first paleotsunami deposits (Figure 17), which shows of gradually large numbers from coarser to the finer sediment grains and unimodal curve indicating of single source of sediment.

Figure 18, is the deposition process of the middle layer, which begins with tsunami wave activity, and is deposited by sand by low to moderate wave energy levels and deposits coarse sand-sized material (B). This condition is continued with the fluvial energy phase, with the energy level being higher than before indicating that there are wave currents that will return seaward and deposits finer sized grains (D).

The histogram of the top layer of the first paleotsunami deposits, which shows the predominance of fine grains, indicating that the suspension process played a more important role, this occurred when the tsunami energy was exhausted and receded back towards the sea, while the percentage curve shows unimodal indicating of the single source of sediment (Figure 19).

The deposition process of the top layer of first paleotsunami deposits, beginning with the flow of tsunami waves with moderate to high energy and depositing sand-sized grains (D), followed by the process of decreasing the energy level to be lower, and depositing finer grains (G),

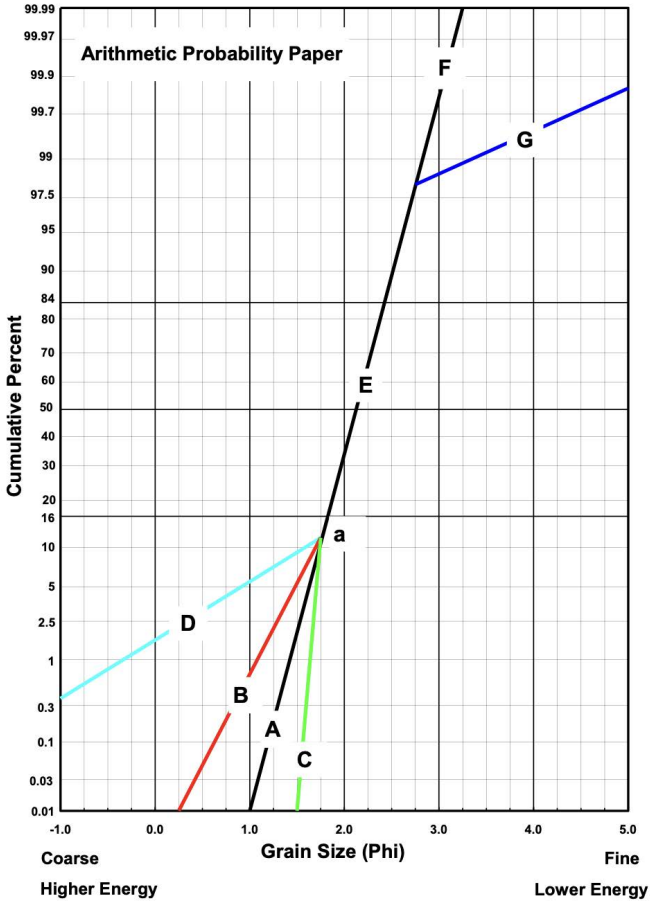

Figure 15. Geometry of the basic line segments that identify trans-deposition processes (Tanner, 1986, 1991; Balsillie, 1995; in Balsillie, 2002)

which signifies settling current from the water, but continue with the moderate energy (D) (Figure 20).

The second paleotsunami deposit or older than the first paleotsunami deposit, showing coarse grains predominate over fine grains (Table 2), with the depositional process showing segment B initiating wave activity with highest energy and depositing very coarse

Table 5. Guide of the Determination of Transpo-Depositional Agencies (Balsillie, 1995)

Segment	Descrition of Granulometric Interpretation
---AEF---	Gaussian distribution. Plot as a straight line on probability paper.
---B---	Shows that the element of the transo-deposition force operating is wave activity; point relative to segment E is termed a surf break. This relatively gentle slope represents beach sand. The higher the slope of segment B, the higher the wave energy. Note that for sand-sized materials, breaking waves usually occur for low to moderate wave energy conditions. For high-energy waves, point a moves from the plot (towards the bottom) and segment B disappears (that is, the energy of the wave exceeds the strength of even the coarsest available sand (Savage, 1958; Balsilie, 1999).
---C---	Shows eolian process; point a is termed, relative to segment B, the eolian hump.
---D---	Represents fluvial energy; has a steep slope. The greater the slope, the higher the energy level. This segment is called the fluvial rough tail. It may also represent a transpo-depositional tidal current process.
---E---	The middle segment of the sample distribution
---G---	Represents a low-energy tail which is called a regulatory tail and, if present, may indicate a decrease in energy for the total distribution or for segments of the distribution containing coarser sediments. This indicates settling from water.

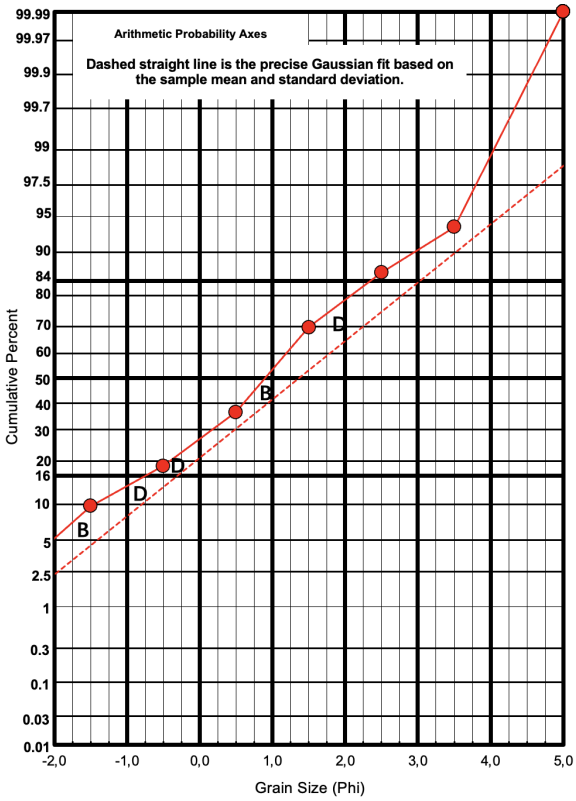

Figure 16. The bottom layer of first paleotsunami deposition process diagram.

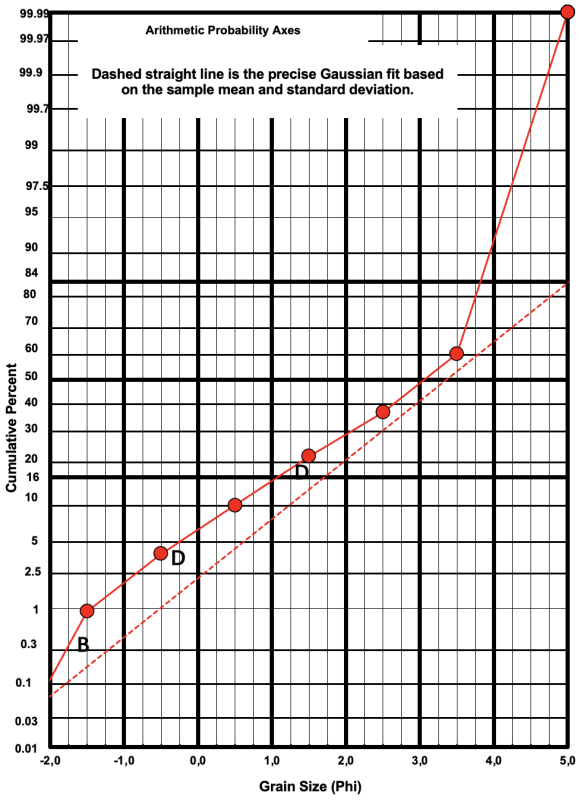

Figure 18. The middle layer of first paleotsunami deposition process diagram

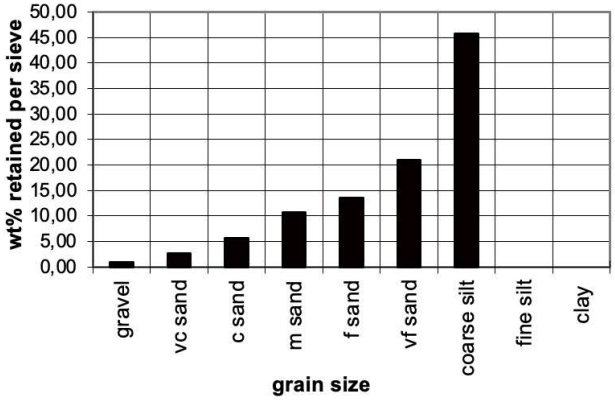

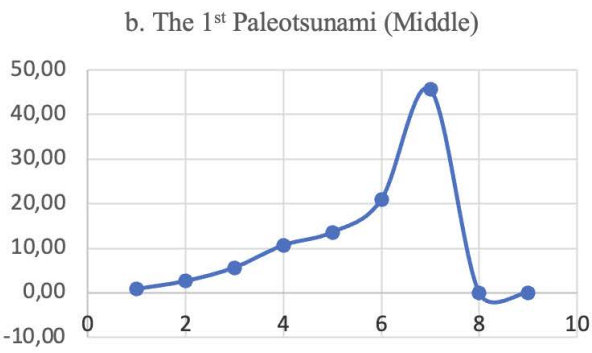

Figure 17. The middle layer of First Paleotsunami sediment histogram (left) and Grain size curve showing unimodal of single sediment source.

sand-sized material, followed by processes transpo-

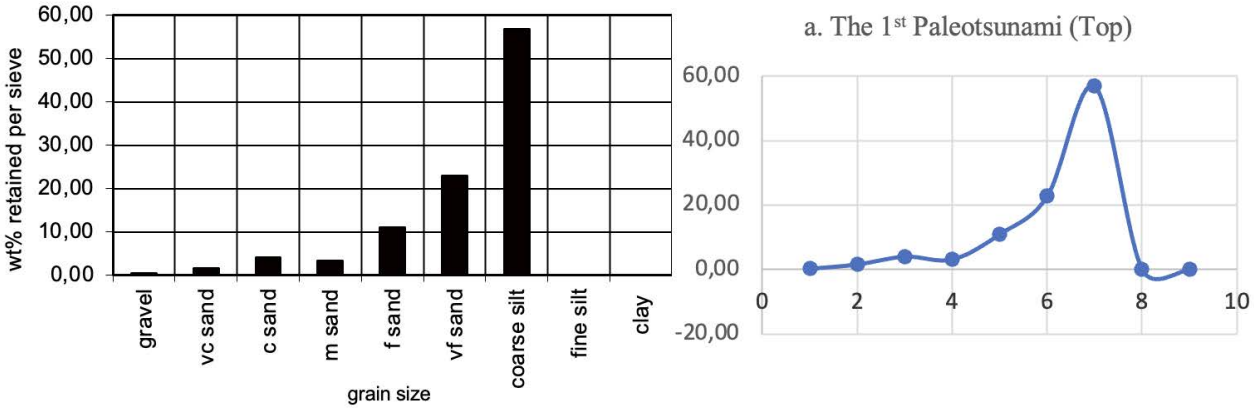

Figure 19. The First Paleotsunami sediment histogram at the top (left) and Grain size curve showing unimodal of single sediment source (right).

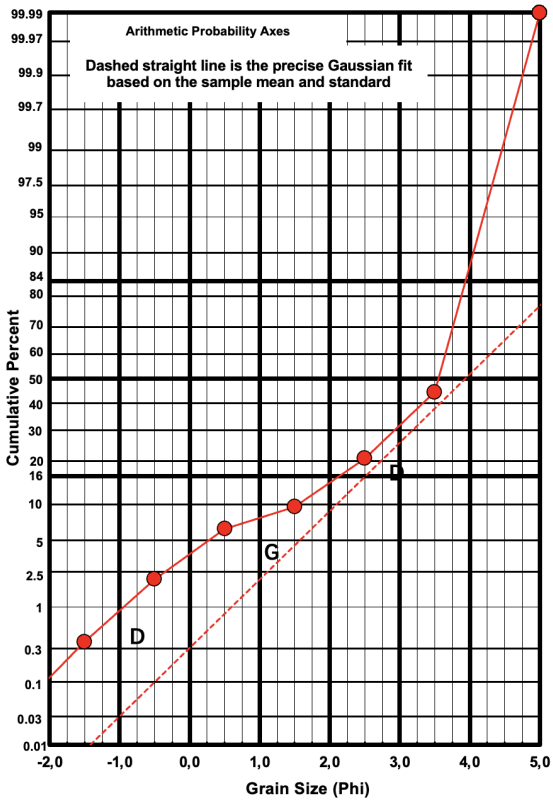

Figure 20. The Top Layer of the first paleotsunami deposition process diagram (Top)

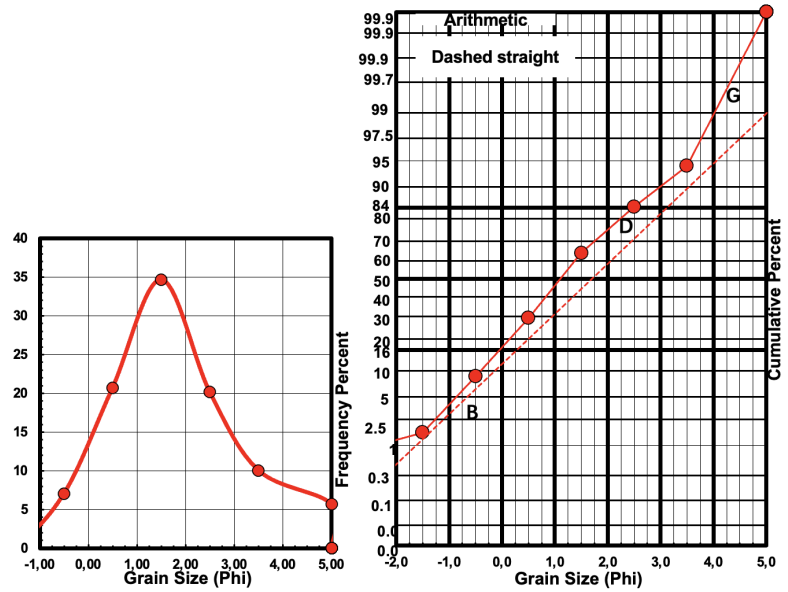

Figure 21. The Top Layer of the second paleotsunami deposition process diagram (Top)

depositional of tidal currents (segment D) with high energy levels and deposits coarse-sized grains (Figure 21).

The fifth paleotsunami deposit has the same characteristics as the second paleotsunami deposit, which begins with segment B followed by segment D which shows high depositional energy and deposits coarse-sized material (Figure 22).

Both the second and fifth paleotsunami deposits do not have fine grain layers, this is probably due to the very thin thickness of the layers so that they were not properly detected during laboratory testing.

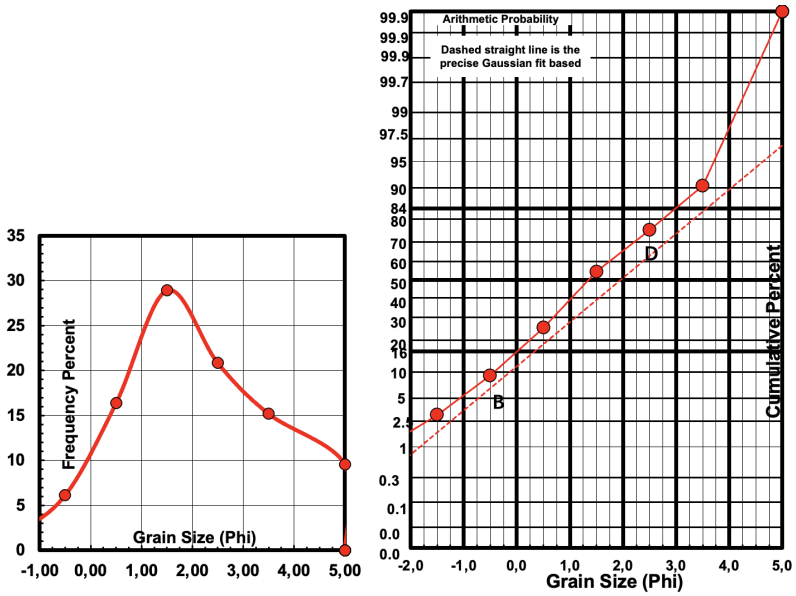

Figure 22. The Top Layer of the fifth paleotsunami deposition process diagram (Top)

CONCLUSSIONS

According to those granulometric analysis, it shows that the deposition of the youngest paleotsunami deposits was initiated by a very strong current with the greatest energy, so that it deposited a very coarse sand grains down to gravel. Followed by a gradual decrease in energy and the process of the tsunami wave starting to reverse direction towards the sea, and then receding with the lowest energy and depositing finer grains. While the sediment sources come from two different places, indicating the source comes from both the sea and the coast around the place where the paleotsunami deposits were deposited.

The vertical changes in the grain size distribution and in the type of sedimentary structures in the youngest paleotsunami deposits are clarified. The paleotsunami deposits are mainly composed of four units (Tna, Tnb, Tnc and Tnd in ascending order). The Tnd unit or the upper part of the youngest paleotsunami deposits contain the remains of plant roots, which shows the characteristics of tsunami deposits.

Variations in the mean, sorting, skewness and kurtosis values indicate a change in the energy of the tsunami wave, causing a change in grain size.

ACKNOWLEDGEMENTS

The author would like to express deep gratitude to the Volcanology and Geological Hazard Mitigation, Geology Agency, Ministry of Energy and Mineral Resources, Ternate Island Tsunami Deposit Investigation Team, all officers at the Gamalama Volcano Observation Post, in Ternate, Indonesian Navy Base in Ternate, STKIP Kie Raha Ternate, and all parties who are very helpful for the smooth running of activities that cannot be mentioned one by one.

REFERENCES

Akif., M., 2021. *Online Lecture of Sedimen Lecture, Texture: Grain Sorting.* Sedimentology Lecture 2, Texture: Grain Sorting - YouTube

Balsillie, J.H., 1995. *William F. Tanner on Evironmental Clastic Granulometry: Florida Geological Survey*, Special Publication No. 40, 144 p.

Balsillie, J.H., Donoghue, J.F., Butler, K.M., and Koch, J.L., 2002. Plotting equation for Gaussian, percentiles and a spreadsheet program for generating probability plots. Journal of Sedimentary Research, 72 (6), p. 929-933.

Blott, S.J. and Pye, K., 2001. *GRADISTAT: a Grain Size Distribution and Statistics Package for the Analysis of Unconsolidated Sediments*. Earth Surface Processes and Landforms 26, 1237-1248.

Bronto, S., Hadisantono, R.D., Lockwood, J.P., 1982. *Peta Geologi Gunung Api Gamalama, Ternate, Maluku Utara*. Direktorat Vulkanologi, Departemen Energi dan Sumber Daya Mineral.

Folk, R.L., and Ward, W.C., 1957. *A Study in the Significance of Grain-Size Parameters. Journal of Sedimentary Petrology,* 27, 3-26. https://doi.org/10.1306/74D70646-2B21-11D7-8648000102C1865D

Fujiwara, O., 2008. *Tsunami Depositional Processes Reflecting the Waveform in a Small Bay Interpretation from the Grain-Size Distribution and Sedimentary Structures*. In Book: Tsunamiites pp. 133-152

Geocache, 2023. Urban earth - *Sediment Sculptor*. https://www.geocaching.com/geocache/GC7Z2X2

Google Earth, 2022. *Ternate Island*. Online Application.

Haris, Ron., dan Major, J., 2016. *Waves of destruction in the East Indies: the Wichmann catalogue of earthquakes and tsunami in the Indonesian region from 1538 to 1877*. Geological Society Publication. https://www.lyellcollection.org/journal/sp

Heinzel, C.E., 2016. *Particle-Size Analysis*. Online Presentation. Dept. of Earth and Environmental Science, University of Iowa.

Jerram, D.A., 2001. *Visual Comparator for Degree of Grain-Size Sorting in Two and Three Dimensions*. Computers and Geosciences 27 (4): 485-492. http://doi.org/10.1016/S0098-3004(00)00077-7

McLaren, P., 1980. *An Interpretation of Trends in Grain Size Measures*. Geological Survey of Canada.

Rachman, G., Santosa, B.J., Nugraha, A.D., Rohadi, S., Rosalia, S., Zulfakriza, Sungkono, Sahara, D.P., Muttaqy, F., Supendi, P., Ramdhan, M., Ardianto, Afif, H., 2002. *Seismic Structure Beneath the Molucca Sea Collision Zone from Travel Time Tomography based on Local and Regional BMKG Networks*. Appl. Sci. 2022, 12(20), 10520; https://doi.org/10.3390/app122010520

Satake, K., and Imamura, F., 1995. *Tsunami in Ternate Island*. In Latief et al., 2000, Tsunami Catalog.

Soloviev, S.L., dan Go., Ch. N., 1974. *Tsunamis on the Western Shore of the Pasific Ocean*. Moscow, "Nauca" Publishing House, 308 Halaman.

Tanner, W.F., 1986. *Inherited and Mixed Traits in The Grain Size Distribution*: In W.F. Tanner (ed.), Modern Coastal Sediments and Processes, Proceedings of the 9th Symposium on Coastal Sedimentology Tallahassee, FL: Department of Geology, Florida State University, p. 41-50.

Tanner, W.F., 1991. *Suite Statistics: the Hydrodynamic Evolution of the Sediment Pool*: In J.P.M. Syvitski (ed.) Principals and Application of Particle Size Analysis, Cambridge: Cambridge University Press, p 225-236.

Trenhaile, A.S., 2005. *Beach Sediment Characteristics*. In Schwartz, M.L., (eds) Encyclopedia of coastal

science. Encyclopedia of Earth Science Series. Springer, Dordrecht. pp 177-179. https://doi.org/10.10071/1-4020-3880-1_41

ASSESSMENT OF THREE-DIMENSIONAL BAROCLINIC CIRCULATION MODEL FOR THE MUSI COASTAL AREA

KAJIAN MODEL SIRKULASI BAROKLINIK TIGA-DIMENSI UNTUK KAWASAN PESISIR MUSI

Septy Heltria[1], Amir Yarkhasy Yuliardi[2*], Gentio Harsono[3], and Marita Ika Joesidawati[2]

[1] Department of Fisheries Resources Utilization, Faculty of Animal Science, Jambi University, Muaro Jambi, 36361, Indonesia

[2] Department of Marine Science, Faculty of Fisheries and Marine, Universitas PGRI Ronggolawe, Tuban, 62381, Indonesia

[3] Faculty of Defence Strategy, Indonesian Defence University, Bogor, Jawa Barat 16810 Indonesia

*Corresponding author: amiryarkhasy@gmail.com

(Received 02 February 2023; in revised from 09 February 2023; accepted 11 July 2023)

DOI : http://dx.doi.org/10.32693/bomg.38.2.2023.811

ABSTRACT: The hydrodynamics of the Musi estuary ecosystem is influenced by the flow of water discharge from the river, tidal circulation within the estuary, and complex bathymetry. Numerical modeling is one of the best ways to explain the characteristics and processes occurring in the estuary. However, the obtained model requires validation to ensure its accuracy despite the complexity added by variability in tidal and bathymetric conditions, making the validation process more challenging. This difficulty can be overcome by using high-resolution data, which provides a refined understanding of the river-to-sea estuary flow and its variability. The validation process involves the use of conductivity-temperature-depth (CTD) instruments and mooring tidal stations. The validated model is considered capable of accurately simulating tidal propagation as it represents the temperature-salinity-density properties within the estuarine environment. The development of this model demonstrates the effective implementation of these parameters within the Musi estuary ecosystem domain. The 3D model simulation is used to consider the vertical discretization in the river-estuary-sea channel, which enhances the representation of temperature-salinity-density in the water column. The obtained results suggest that the 3D-MIKE modeling is well-suited for operational purposes, including the prediction of hydrodynamics and the management of estuarine areas, specifically in the Musi estuary ecosystem.

Keywords: hydrodynamic, validation model, baroclinic circulation, Musi estuary, and coastal area

ABSTRAK: *Hidrodinamika ekosistem muara Musi dipengaruhi oleh aliran debit air sungai, sirkulasi pasang surut di muara, dan batimetri kompleks. Untuk menjelaskan karakteristik dan proses kejadian di muara, salah satu cara terbaik yang dapat dilakukan adalah dengan menggunakan model numerik. Model yang diperoleh perlu divalidasi agar teruji keakuratannya. Variabilitas saat kondisi pasang surut dan batimetri akan meningkatkan kompleksitas aliran yang menyebabkan proses validasi menjadi lebih sulit. Hal ini dapat diatasi dengan menggunakan data resolusi tinggi sehingga aliran dan variabilitas alur sungai-muara laut menjadi lebih jelas. Validasi dilakukan dengan menggunakan instrumen conductivity-temperature-depth (CTD) dan penempatan mooring tidal station. Model yang telah divalidasi dianggap mampu menyimulasikan propagasi pasut secara akurat yang mencerminkan sifat temperatur-salinitas-densitas di muara. Pengembangan model ini menunjukkan bahwa parameter-parameter tersebut telah terimplementasikan dengan baik pada domain ekosistem muara Musi. Hasil simulasi model 3D digunakan dengan mempertimbangkan diskritisasi vertikal pada kanal hulu-muara-lautan untuk memperoleh representasi suhu-salinitas-densitas yang lebih baik dalam kolom air. Hasil yang diperoleh menunjukkan bahwa pemodelan 3D-MIKE cukup baik digunakan pada level operasional, antara lain untuk memprediksi hidrodinamika dan mengelola kawasan estuari, khususnya di ekosistem muara Musi.*

Kata Kunci: *hidrodinamik, validasi model, sirkulasi baroklinik, muara Musi, dan wilayah pesisir*

INTRODUCTION

Estuaries are an important ecosystem that provide breeding, shelter and feeding grounds for numerous species. Gradient distribution in temperature, salinity, vegetation, bathymetry and sediment parameters in these ecosystems create diverse habitats. These parameters can undergo changes as a result of both human activities and natural processes, such as climate change. The influence of these factors on estuary ecosystems has turned them into a research topic that has attracted researchers (Wagner et al., 2011; Brown et al., 2016; Jeffries et al., 2016). Temperature is one of the critical parameters for estuarine ecosystems and directly impacts the habitat, existence and growth rate of species. Various studies have indicated that high temperatures can cause stress and even mortality in a species (Brown et al., 2013; Ralston et al., 2015). Several factors that can affect temperature include river flow, heat exchange by the atmosphere, and flow interaction with the sea or ocean adjacent to the estuary area (Monismith et al., 2006).

The study area is located on the east coast of Sumatra which is directly adjacent to the Bangka Strait (2.1^0S – 2.25^0S and 104.4^0W – 105.6^0W), It was conducted in the Musi-Banyuasin estuary, South Sumatra. The area consists of the ROFI zone (Freshwater Influence Area), including the Banyuasin, Musi and Upang estuaries, which are downstream of the densely populated Palembang city (Figure 1),

The Musi coastal area represents the largest estuary in the South Sumatra province characterized by a central body extending 30 km and connected to the Bangka Strait with a depth range of 0 to 15 m. The lithological units of study area generally consist of quaternary alluvium (gravel, sand, silt and clay) and swamp deposits (mud, silt, and sand) (Gafoer, et al., 1995). This area features a narrow platform heavily influenced by tides. Research conducted by Surbakti (2012) and Nurisman et al., (2012) found that the Musi River estuary shows a single (diurnal) tidal type, with tidal currents dominating at a speed of 10.1 cm/s. Three significant geomorphological features dominate this area, including Payung Island located in the middle of the Musi estuary, the convergence of three estuaries, and the narrow strait linking the Natuna and Java seas. The flow at the study site is related to the tidal amplitude resulting in a mixing process within the estuary. The main driver of circulation at the mouth of the Musi River is tides, with other factors such as river discharge and wind also having an effect (Rodrigues, 2015).

It is important to know the modeling of coastal systems, especially in estuaries, influenced by fresh water, such as in the Musi estuary and its surrounding coastal areas, to understand the unique physical processes that characterize them. Measurement of several in situ environmental variables or time-limited studies is not sufficient to translate coastal processes because coastal systems are complex (Restrepo et al., 2018). The combination of interacting physical factors, such as bathymetry, coastline, outflow of estuaries and distribution of flow fields makes the coastal system a complex hydrodynamic system (Murthy et al., 2008; Iglesias et al., 2020). Therefore, the coastal system must be decomposed into smaller systems and one way to determine the structure of the coastal system is to use a numerical model approach. Models enable a better understanding of the interactions between the various components in the system. They are also needed to define scenarios and answer scientific questions (Petihakis et al., 2012). Therefore, it will result in a precise understanding of coastal processes, including spatiotemporal variations. This is valuable for the development of more comprehensive and integrated coastal management plans. The hydrodynamic model plays a significant role in the formation of current and density patterns as a basis for transport models. Given the importance of advection and/or diffusion in studies closely related to coastal systems.

Several types of numerical models have been used to simulate hydrodynamic processes in coastal systems. MIKE 3D is one of these models, known for its capability to simulate two dimensions in 2D and 3D, in sigma, cartesian or lagrangian vertical coordinates and spatial dimensions. It can also combine formulations in each process. The flexibility possessed by MIKE 3D facilitates its application in various types of systems and for research purposes or undertaken work. Indeed, in the last 10 years the model has been applied in several studies in Musi estuaries; Sari et al., (2013) used the 2D SMS model for distribution of salinity, while Syarifudin et al., (2016) employed the MIKE 21 model to simulate sediment transport. In the coastal system consisting of the Musi estuary, Banyuasin estuary and Upang estuary, the study is focused on the vertical structure of the water masses. In order to apply the model output, the constructed model must be built properly and scientifically. Validation is needed to demonstrate the degree of confidence that can be shown in the model results. Model validation is a process that aims to explain that specific models can be simulated with a considerable degree of accuracy at certain locations (Williams & Esteves, 2017).

The validity of the model is confirmed by comparing the simulation results with in situ observations. The MIKE 3D model is regularly used and validated, but no published work has yet focused specifically on the Musi estuary. As the model application is baroclinic, the validation must also consider the seawater temperature and salinity. This study will provide better insight regarding the validation of model results in the estuary area, especially in the Musi and its surroundings. The objective is to determine the vertical structure within the Musi estuary domain from a vertical-temporal perspective using the 3D MIKE model. The model results will be compared with in situ measurements of the CTD. This study is the first to conduct a validation process using CTD for the Musi estuary domain. The main results of the model are expected to represent the coastal physical processes,

reliable during its use in real-world operational settings, and its forecast ability that will be useful for coastal environmental management.

METHODS AND MATERIALS

Data collection occurred between September 1-10, 2016, and data processing extended from October 2019 to February 2020. It comprises of two cross-sections (red dotted line): cross-section A1-A2 from the mainland to the Upang estuary and longitudinal cross-section B1-B2 from upstream to the sea, passing through the Musi River. The tidal data capture station (BIG) is represented by the black point. The wind data collection station is marked by the black triangle. CTD measurements were taken at two locations, denoted by black pinpoints (St.1 and St.2). The mooring point is the same as that of St.2.

Tidal data used in this study were obtained from three sources with a 1-hour time interval during data processing. The initial tidal data was derived by predicting EMB bathymetry which was processed using MIKE 3D software as the boundary and initial condition hydrodynamic model. Furthermore, tidal data were gathered from the results of mooring measurements at station 2 (St.2) over 3 days, from September 7-9, 2016 with 1-hour intervals and tidal model extraction data at the same time and location, both of which were used for model verification. Wind data retrieved from Copernicus (https://resources.marine.copernicus.eu/products), was employed to understand existing wind patterns in the area, with daily u10 specifications at the surface layer. The u10 wind data represented one month in September 2016 and used to identify dominant pattern and speed at the study site. Discharge data was obtained from field current measurements at three locations: Telang, Musi, and Upang Rivers. Current data was obtained using a current meter with a mooring procedure for 72 hours with 1 hour data interval at each location. This data was then used to calculate the flow rate, determined by the river flow velocity (m/s) and wet cross-sectional area (m2). The wet cross-sectional area was determined using the mid-section model from Chow (1989). The discharge can be obtained through the equation:

$$Qf = v \times A \quad (1)$$

where:
Qf= River discharge (m^3/s)
A= Cross-sectional area (m^2)
v= Flow velocity (m/s)

Bathymetry data in the study area were acquired from the Hydro Oceanographic Service of the Indonesian Navy No. 160 with a scale of 1: 50,000 and BIG in 2015. This data was digitized using Qgis 3.8 software to obtain water depth and coastline with latitude, longitude and depth output. Salinity, temperature, and turbidity data were obtained from measurements, using Conductivity-Temperature-Depth (CTD) instrument that taken at low tide, and from scientific publications. The measurement data consists of two stations to represent the transverse and longitudinal cross-sections taken during and at low tide (Figure 2).

The created model consists of a baroclinic 3D hydrodynamic model. Its initial are based on the average input of tidal values from 5 sources, including the Musi, Telang, Upang, and Banyuasin rivers, and the Bangka

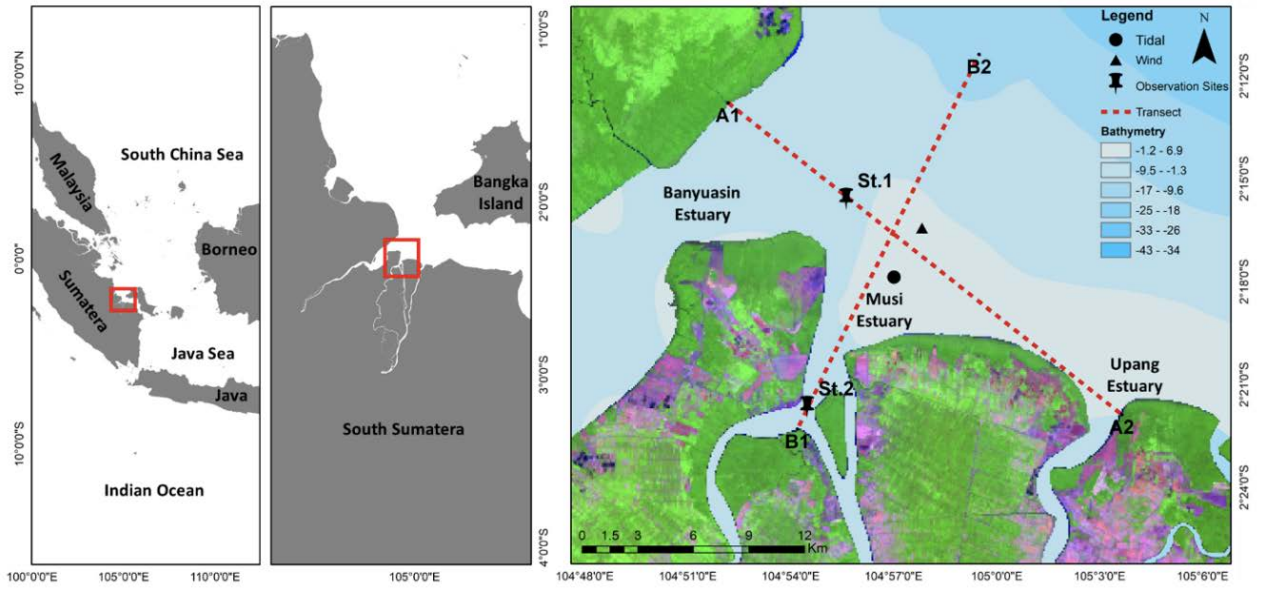

Figure 1. Research Location Map with two cross-sections (red dotted line): cross-section A1-A2 from the mainland to the Upang estuary, and longitudinal cross-section B1-B2 from upstream passing through Musi River to the sea. Black circle denotes the tidal data capture station owned by Geospatial Information Agency (Badan Informasi Geospasial (BIG), black triangle is wind data collection station, black pinpoints (St.1 and St.2) at two locations marked the decreasing CTD, and mooring point is at the same location as St.2.

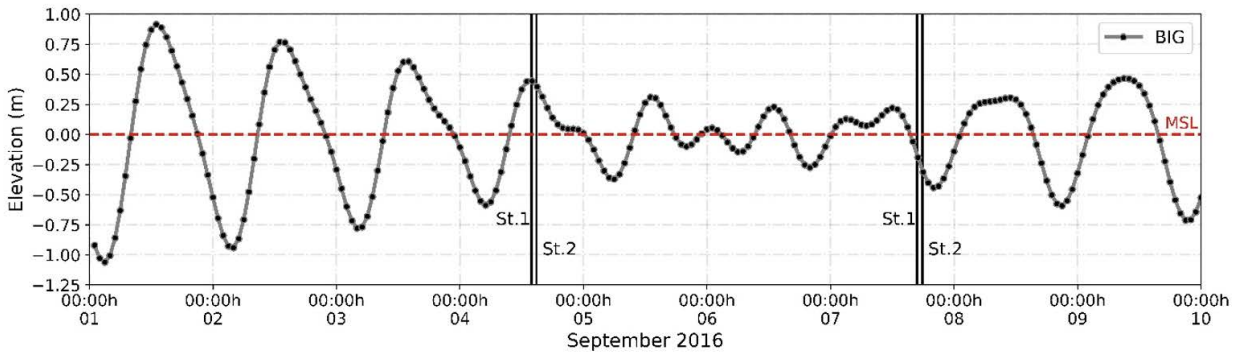

Figure 2. Water level elevation during CTD data collection and tidal mooring based on calibrated BIG data. CTD data at each station is taken twice during flood and ebb.

Strait. Tidal values are predicted using on the MIKE 3D device based on the bathymetry conditions of the waters. The model domain is illustrated in Figure 3. In the baroclinic 3D model, the initial conditions are made based on the minimum, maximum and average values of temperature and salinity. Furthermore, boundary values are set using source data of temperature and salinity with a constant value. The hydrodynamic model describes the flow conditions at the study site which are simulated using tides, discharge and bathymetry. The model is simulated for 21 days to describe flood and ebb tide conditions. The model configurations used are listed in Table 1.

The hydrodynamic model provides the basis for simulating movements in the waters. It formulates the movement of currents, tides over time intervals. The momentum and continuity equations are used to determine the motion of water influenced by various forces. The following describes the equations used, based on the MIKE module of DHI (2012).

Continuity equation:

$$\frac{\partial u}{\partial x} + \frac{\partial v}{\partial y} + \frac{\partial w}{\partial z} = S \quad (2)$$

Momentum equation:

$$\frac{\partial u}{\partial t} + \frac{\partial u^2}{\partial x} + \frac{\partial vu}{\partial y} + \frac{\partial wu}{\partial z} = fu + g\frac{\partial \eta}{\partial x} - \frac{1}{\rho_0}\frac{\partial \rho_a}{\partial x} - \frac{g}{\rho_0}\int_z^n \frac{\partial \rho}{\partial x}dz + F_u + \frac{\partial}{\partial z}\left(v_t\frac{\partial u}{\partial z}\right) + u_s S \quad (3)$$

$$\frac{\partial v}{\partial t} + \frac{\partial v^2}{\partial y} + \frac{\partial uv}{\partial x} + \frac{\partial wv}{\partial z} = -fv + g\frac{\partial \eta}{\partial y} - \frac{1}{\rho_0}\frac{\partial \rho_a}{\partial y} - \frac{g}{\rho_0}\int_z^n \frac{\partial \rho}{\partial y}dz + F_v + \frac{\partial}{\partial z}\left(v_t\frac{\partial v}{\partial z}\right) + v_s S \quad (4)$$

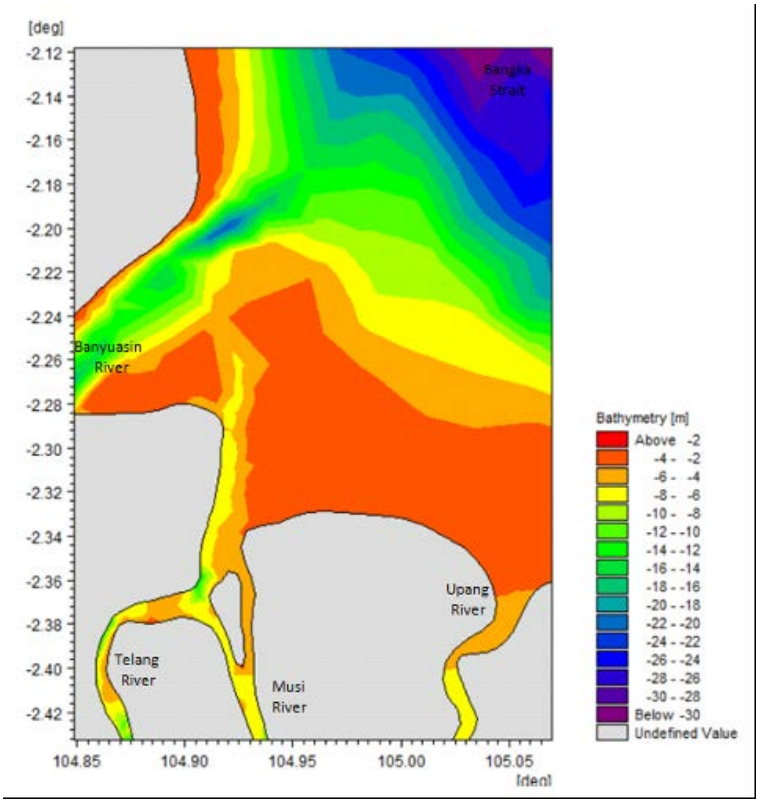

Figure 3. The bathymetry of the Musi estuary as a model domain

Table 1. Musi coastal area model configuration.

Parameter	Application of Simulation	
Model Characteristics		= 3D-Baroclinic
Simulation Time	Number of step	= 6048
	Time step interval	= 300
	Simulation period	= 01/09/2016 01:00:00 – 22/09/2016 23:00:00
Area	Maximum Element Area	= 0.0005 $(deg)^2$
	Angle Mesh	= 26 (deg)
Grid	Origin	= 105.081E -2.105S
Mesh Boundary	1. PUSHIDROSAL bathymetry data (2015) 2. BIG bathymetry data (2015) 3. Field tide data (2016)	
Discharge	Telang River	= 142.6 m^3/s
	Musi River	= 202.15 m^3/s
	Upang River	= 211.7 m^3/s

$$\frac{\partial v}{\partial t}+\frac{\partial w^2}{\partial z}+\frac{\partial uw}{\partial x}+\frac{\partial wv}{\partial y}=-fw+g\frac{\partial \eta}{\partial z}-\frac{1}{\rho_0}\frac{\partial \rho_a}{\partial z}-\frac{g}{\rho_0}\int_z^n\frac{\partial \rho}{\partial z}dz+F_w+\frac{\partial}{\partial z}\left(v_t\frac{\partial v}{\partial z}\right)+w_sS \quad (5)$$

$$\rho_a = \rho_0 g\eta + \rho_0 \int_{-z}^{0} Bdz \quad (6)$$

$$B = B=\frac{\rho-\rho_0}{\rho_0}\,g \quad (7)$$

The horizontal stress section is described using the stress-gradient relationship, which is simplified to:

$$F_u = \frac{\partial}{\partial x}\left(2A\frac{\partial u}{\partial x}\right)+\frac{\partial}{\partial y}\left(A\left(\frac{\partial u}{\partial y}+\frac{\partial v}{\partial x}\right)\right) \quad (8)$$

$$F_v = \frac{\partial}{\partial y}\left(A\left(\frac{\partial u}{\partial y}+\frac{\partial v}{\partial x}\right)\right)+\frac{\partial}{\partial y}\left(2A\frac{\partial u}{\partial y}\right) \quad (9)$$

Temperature Function:

$$\frac{\partial T}{\partial t}+u\frac{\partial T}{\partial x}+v\frac{\partial T}{\partial y}+w\frac{\partial T}{\partial z}=\frac{\partial}{\partial z}\left(K_v\frac{\partial T}{\partial z}\right)+\frac{\partial}{\partial x}\left(A_H\frac{\partial T}{\partial x}\right)+\frac{\partial}{\partial y}\left(A_H\frac{\partial T}{dy}\right) \quad (10)$$

Salinity Function:

$$\frac{\partial s}{\partial t}+u\frac{\partial s}{\partial x}+v\frac{\partial s}{\partial y}+w\frac{\partial s}{\partial z}=\frac{\partial}{\partial z}\left(K_v\frac{\partial s}{\partial z}\right)+\frac{\partial}{\partial x}\left(A_H\frac{\partial s}{\partial x}\right)+\frac{\partial}{\partial y}\left(A_H\frac{\partial s}{dy}\right) \quad (11)$$

where:
t = time
x,y,z = cartesian coordinates
u,v,w = flow velocity components
g = gravitational acceleration (m^2/s)
ρ = density
ρ_0 = reference density (1024.78 kg m^{-3})
η = elevation
f = *coriolis* parameters
S = amount of discharge from the source
A_V *dan* K_V = vertical eddy viscosity and vertical diffusion coefficient (*log law formulation* ($1.8e^{-6}$ m^2/s))
A *dan* A_H = vertical eddy viscosity and horizontal diffusion coefficient (*smagorinsky formulation* (0.28 m^2/s))
B= buoyancy
T= temperature
s= salinity

Model verification was carried out to determine the accuracy of the data by comparing field tide data and statistical simulation results (Zaman & Syafrudin, 2007). The verification method used is the average relative error (MRE < 50%: Accepted, MRE > 50%: Re-simulation) with the following equation:

Relative Error (*RE*) $\frac{|X-C|}{X}\ x\ 100\ \%$ (12)

Mean Relative Error (*MRE*) $\sum_0^n \frac{RE}{n}$ x 100% (13)

where:
c = simulation results data
x = field data
n = amount of data

RESULTS

The Musi-Banyuasin estuary is the place where four rivers are located, namely the Upang River, Musi River, Telang River, and Banyuasin River, which directly face the Bangka Strait. The flow in the estuary originates from the dynamics of tides and river discharge. The tides enter through propagation from the South China Sea to the north of Bangka and the Java Sea, which enters through the south of the Bangka Strait. The tides in the Musi-Banyuasin estuary are of the diurnal type, occurring once a

day, with a Formzhal number of 3.06, in accordance with the results of previous studies (Surbakti et al., 2022; Radjwane et al., 2018). During high tide, water from the sea enters the estuary, while during low tide, the water flows out of the estuary. The river discharge flow comes from the Banyuasin River and the Musi River, which have three branches: the Telang River, the Musi River, and the Upang River. Heltria et al. (2021) has calculated the flow rate for each river. The Musi River discharge is known to be 202.15 m^3/s, the Upang River discharge is 211.7 m^3/s, and the Telang River flow rate is lower than that of the Musi River, at 142.6 m^3/s. The Musi River and Upang River originate from the same stream, which then separate due to a delta. Although the current velocity is assumed to be the same in both rivers, the flow rate is calculated based on the cross-sectional area of each river. The Banyuasin River estuary has a large cross-sectional length of approximately 6 km, making tides play an important role in the flow at this location. The visualization of the direction of movement of the dominant wind in the waters of the Musi estuary is shown by the wind rose diagram. The dominant wind direction moves from south to north with a speed ranging from 1.3 to 5.2 m/s, as shown in Figure 4.

The 3D bathymetry obtained from the PUSHIDROSAL and BIG data in Figure 5 shows the seabed morphology of the Musi-Banyuasin estuary waters. The Banyuasin estuary, with a larger cross-section, has a varying depth range of 0.2 m - 22 m, which is deeper than the Musi estuary. The depth range of the Musi estuary, where the Musi and Telang rivers originate, is 0.2 m - 12.9 m. The morphology of the waters is formed by sediment deposits from rivers that flow into this estuary. As the water reaches the Bangka Strait, the water depth increases to 38 m, which is considered shallow water.

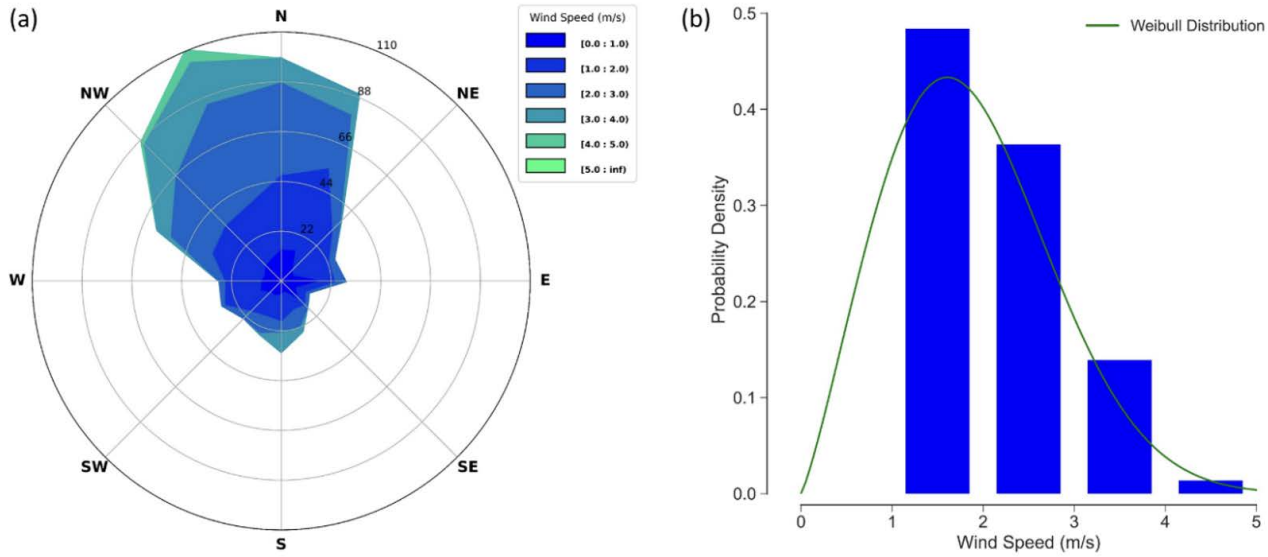

Figure 4. Wind distribution with respect to (a) direction and (b) speed on the Musi coast. Blue to green in (a) indicates low to high speed.

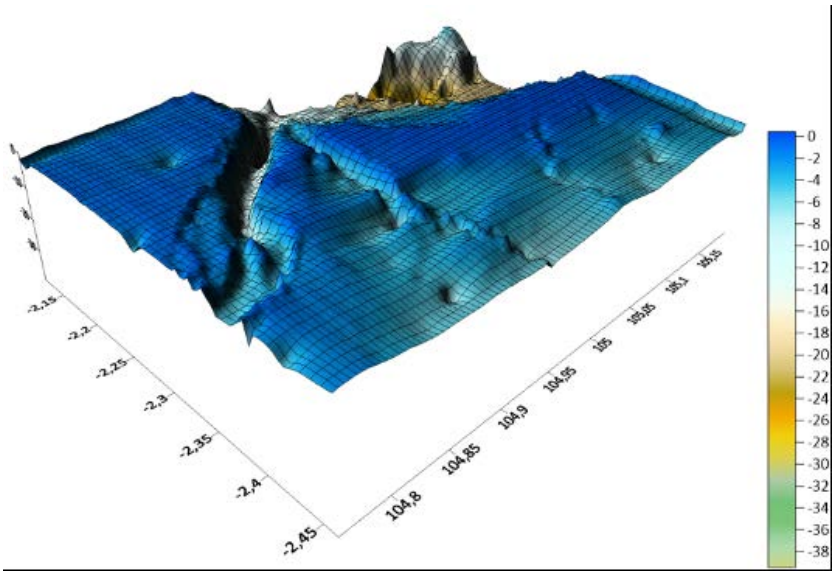

Figure 5. 3D Bathymetry of the Musi-Banyuasin estuary. Colors represent depth in meters (m). Color scale with 2m intervals.

The validation of the hydrodynamic and salinity models is known through the verification value of the mean relative error (MRE). The verification value of the hydrodynamic model uses tidal data, namely tides at the same point in the model and measurement results in the study area (Figure 6). The resulting model MRE value is 30.74%, which means that the model results adequately represent the hydrodynamic conditions in the study area. The verification method used is the verification of the average relative error (MRE < 50%: Accepted; MRE > 50%: Re-simulated). Sugianto (2012) in his model verification obtained a value of <35% and was still acceptable for further analysis. Insitu data collection right at the mouth of the estuary shows the formation of two peaks at high tide. The mass of sea water and riverine inflow towards upstream causes the buildup, indicating an increase in water mass during high tide. As the tide recedes, the sea water continues to enter, maintaining the formation of peaks. The mass of sea water entering the estuary weakens at the lowest tide. The error value obtained may be influenced by other factors, such as tidal currents and water conditions during field measurements. Adding more to the complexity of bathymetry in the field, there are differences in tides between model simulation and field results, which is smoother for model simulation result.

Figure 7 presents a comparison between temperature and salinity values obtained from observation data and model data during high and low tide. The data from station-1 was collected at the estuary's mouth, which is directly connected to the Bangka Strait. Here, water masses receive direct input from the Musi and Banyuasin estuaries. On the other hand, the data from station-2 was acquired at the confluence of the Telang and Musi rivers, near Payung Island.

The range of station-1 temperature values at high tide in the observation data is 29.36℃ – 29.93℃, and for the model data, it is 29.65℃ – 29.97℃. The correlation between the two datasets shows a good value, namely R2 = 0.97 at high tide. The biggest difference is at a depth of 3.34 m, which is 0.31℃, with a maximum depth of 6.64 m. At low tide, the temperature value range for the

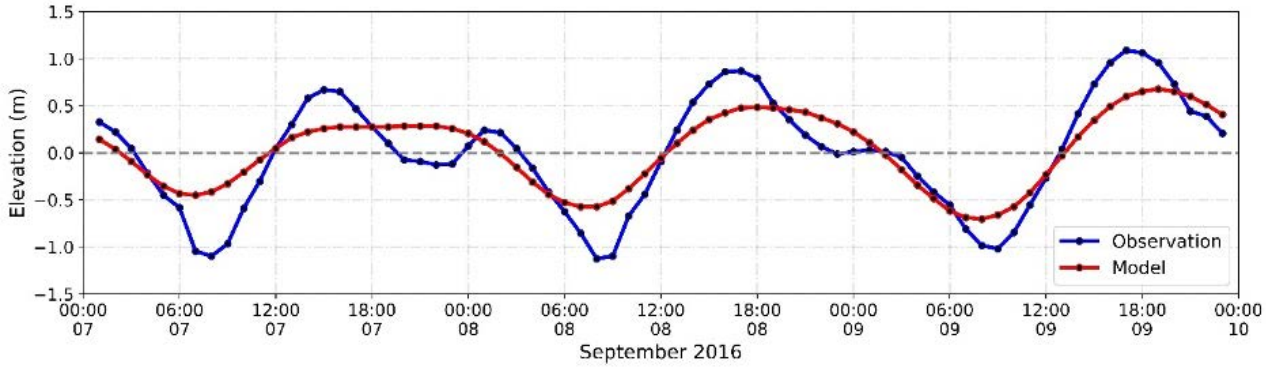

Figure 6. Data validation using tidal mooring data (observation) with the results of the hydrodynamic model running.

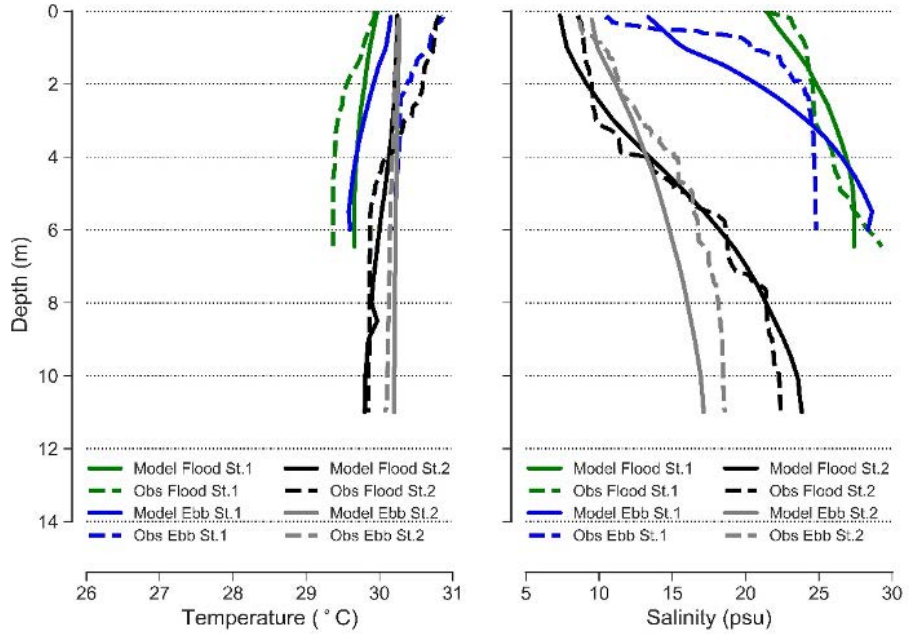

Figure 7. Data validation using observational data (CTD) with model data sampled at station 1 and station 2 (according to CTD location).

observation data is 30.20℃ – 30.26℃, and for the model data, it is 29.58℃ – 30.15℃. The correlation between the two datasets at low tide is smaller than at high tide, namely R2 = 0.91, with a maximum difference of 0.70℃ at a depth of 0.17 m. At station-2, the range of temperature values for the observation data at high tide is 29.85℃ – 30.81℃, and for the model data, it is 29.80℃ – 30.24℃. The correlation between the two datasets is smaller than that of station-1, namely R2 = 0.77, with a maximum difference of 0.57℃ at a depth of 0.12 m and a maximum depth of 11 m. At low tide, the temperature range for the observation data is 30.08℃ – 30.26℃, and for the model data, it is 30.20℃ – 30.27℃. The correlation between the two datasets is R2 = 0.97, with a maximum difference of 0.11℃ at the maximum depth of data collection.

At station 1, the range of observed salinity data values is greater than the model data, explicitly 23.07 Psu – 29.30 Psu compared to 21.75 Psu – 27.40 Psu, respectively. Station-1 is located in zone 1, which is classified as the polyhaline zone with a salinity range of > 18 Psu – 30 Psu, according to Heltria et al. (2022). The correlation between the two datasets is R2 = 0.77, with a maximum difference of 1.91 Psu at the maximum depth of data collection. During low tide, the range of observed data values is 10.41 Psu – 24.82, while the model data is 13.35 Psu – 28.62 Psu. The data correlation is smaller, specifically R2 = 0.67, with a maximum difference of 5.13 Psu at a depth of 1.25 m. The salinity value at station-2, during high tide, shows a correlation value of R2 = 0.98, with a maximum difference of 1.64 Psu at a depth of 3.87 m. The salinity range is lower than at station-1, as the mass flow of fresh water dominates and falls within the mesohaline zone (Heltria et al., 2022). The range of observed salinity data is 8.55 Psu – 22.36 Psu, while the model data is 7.33 Psu – 23.83 Psu. During low tide, the range of observed salinity data values is 8.64 Psu – 18.57 Psu, while the model data is 9.50 Psu – 17.12 Psu. The correlation between the two datasets is R2 = 0.97, with a maximum difference of 2.28 Psu at a depth of 4.94 m.

DISCUSSIONS

Modeling is capable of reproducing several temperature-salinity-density stratifications. Stratification in the estuary area occurs due to variations in the input of freshwater from upstream and seawater in the estuary. The surface layer typically has lower salinity than the layer beneath it due to its lighter mass. This finding is supported by Surbakti et al. (2022). Patty (2013) also suggests that depth and shape of the bottom topography of the waters are internal factors that influence the distribution of temperature, salinity, and density.

Figure 8 depicts the vertical pattern of temperature, salinity, and density during the ebb tide. Specifically, Figure 8.a-b-c represents a cross-section across A1-A2 (Banyuasin estuary – Musi estuary – Upang estuary). On the other hand, Figures 8.d-e-f represents a cross-section on B1-B2 (upstream – ocean). In the cross-sections A1-A2 and B1-B2, the modeling results clearly show the presence of temperature-salinity-density stratification at the study site.

From cross-section A1-A2, the Banyuasin estuary exhibits the strongest stratification. This estuary has a deeper depth compared to the other estuaries. Meanwhile, the Musi and Upang estuaries show more homogeneous temperature-salinity and density simulations, indicating less stratification. The Banyuasin estuary, which is adjacent to the Musi estuary, is situated in a relatively deep section of the Banyuasin River. The model results reliably demonstrate that temperature-salinity and density stratification in this area is the strongest compared to other estuaries. During low tide, when the intrusion of seawater is minimal and the majority of water outflows from rivers into the sea, the model successfully reproduces the temperature-salinity-density stratification. The temperature-salinity-density model in the Musi and Upang estuaries clearly differs, which is characterized by warm temperatures, as well as low salinity and density.

Stratification of temperature-salinity-density was revealed in cross-section B1-B2, as shown by the model results (Figure 8.d-e-f). This stratification can also be seen both in the model and at the time of measurement during data verification. During periods of high and low tides, stratification can be captured by the model. Stratification occurs on a small and sometimes a large scale depending on the period of occurrence and location. The highest temperature observed in the surface layer is located in the middle of the Musi River, close to the mainland, and is complemented by low salinity. The surface temperature is higher, especially in shallow waters because solar energy is more effective in increasing seawater temperature (Maharani et al., 2014). The salinity on the surface has a smaller value due to the input of fresh water from upstream towards the sea, while seawater infiltrates the estuary through the bottom layer. The model shows a gradient of temperature-salinity from the upstream region to the ocean region. The temperature seems to gradate smaller as it heads towards the ocean, while the salinity and density increase as it heads towards the ocean. In the estuary stratification area, the dominance is influenced by salinity, which also causes differences in density (Beer, 1997).

In cross-section B1-B2, intrusion from the sea is stuck in the middle of the cross-section with a distance of 0.1 deg from point B1, specified by the temperature 29.88-29.94℃ (light green in Figure 8.d), salinity 27-28 Psu (brick red in Figure 8.e), and density 12.5-14 (brownish yellow in Figure 8.f). This intrusion from the sea spreads through the bottom of the waters, although in the upper section, it is still dominated by water from the mainland (rivers). This happens because during low tide, sea water heads to the ocean so that water from the mainland with a large discharge goes to the sea. Meanwhile, there is no visible intrusion of sea water masses can be seen in cross-section A1-A2, in which the model looks homogeneous.

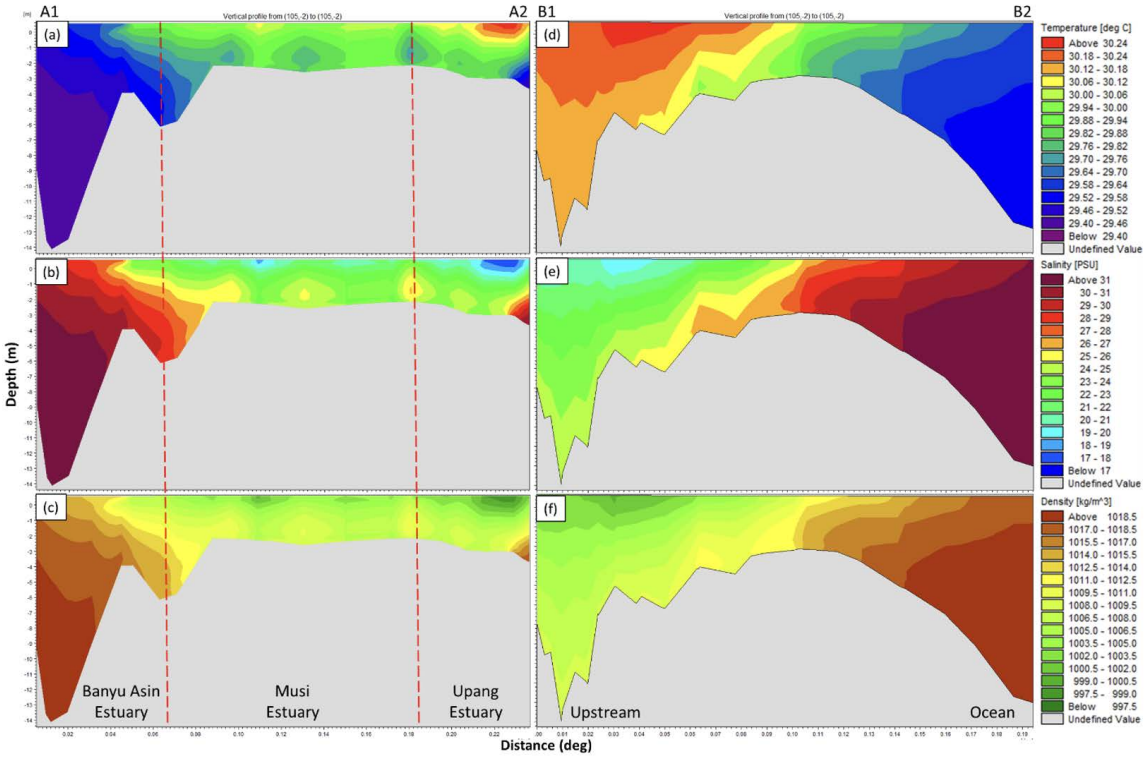

Figure 8. Vertical distribution of (a) temperature (b) salinity (c) density of cross-section A1-A2 (divided into the Banyuasin estuary-Musi estuary-Upang estuary); and (d) temperature (e) salinity (f) density of cross-section B1-B2 during low tide.

Vertical salinity stratification can signify the type of estuary in the Musi-Banyuasin estuary, that is, there is a strong push by the mass of seawater which pushes the mass of freshwater so that high salinity is in the bottom layer and lower salinity is in the upper layer. Having the mixing, the estuary can fall into the type of partially mixed estuary. This is in line with research conducted by Heltria et al. (2022) at the same location and Duxbury (2002), which stated that the partially mixed estuary type is characterized by a strong mass flow of seawater, horizontal mixing at the bottom of the waters, and a combination of vertical mixing.

Figure 9 shows the vertical pattern of temperature, salinity, and density during the flood tide. Specifically, Figure 9.a-b-c is a cross-section across A1-A2 (Banyuasin estuary - Musi estuary - Upang estuary), while Figure 9.d-e-f represents transverse cross-section on B1-B2 (upstream – ocean). The flow of water in the river is observed to be in one direction, flowing from upstream to downstream until it reaches the estuary and then flows into the sea. This flow appears to form two types of flow sources, namely surface water flow (from the river) and underwater flow (from the sea), which converge in the estuary area. The magnitude of this flow varies depending on the area of the watershed, geomorphology, and the amount of rainfall, subsequently affecting the river discharge. The modeling results reveal a significant stratification of temperature-salinity-density parameters during high tide. In cross-section A1-A2, the weakest stratification is observed in the Banyuasin estuary, which tends to be homogeneous and persistent, and consistent with conditions during low tide, particularly in the deeper layers. This is influenced by the depth of the Banyuasin estuary, which is deeper than the Musi estuary, resulting in a dominance of high salinity from seawater in the bottom layer. The Musi and Upang estuaries exhibit well-stratified model results from temperature-salinity-density simulations. It is evident from the model results that the temperature-salinity-density stratification in this area is fairly uniform, with a gradation observed in each parameter from the surface layer to the bottom layer of the water. The model accurately reproduces the temperature-salinity-density stratification during the tides, particularly when the tides intrude from the ocean, bringing in a massive water mass. In the Banyuasin estuary, a clearer stratification pattern depicting the layers of water mass, was formed due to the mixing at high tide, compared to at low tide.

In cross-section B1-B2, results from modeling during high tide show stratification of temperature-salinity-density (Figure 9.d-e-f). At high tide, stratification occurs both towards the sea in the surface layer and towards the land in the bottom layer of the water. The highest temperature is found in the surface layer, which is located in the middle of the Musi River close to the mainland. Its area is wider during low tide. Low salinity was also observed in the surface layer, indicating fresh water mass. The model results during the high tide period

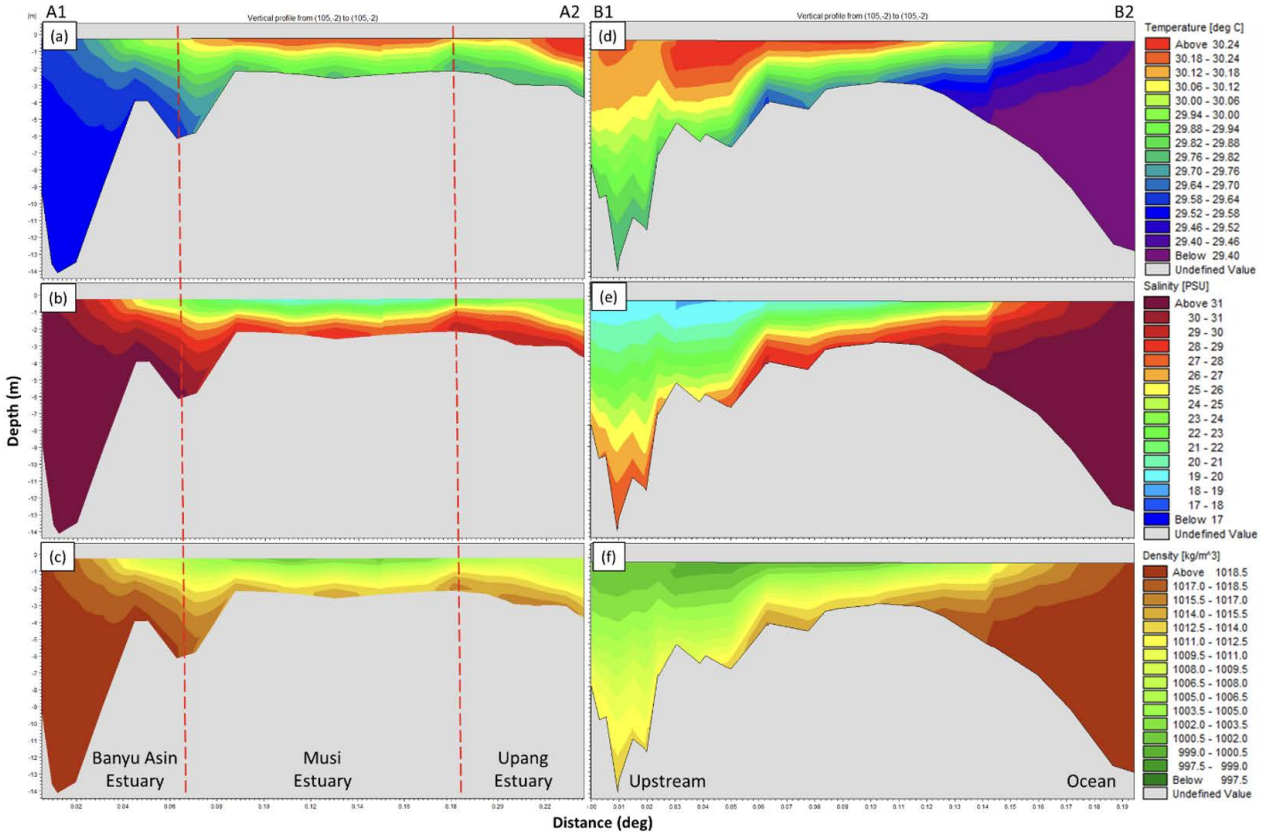

Figure 9. Vertical distribution of (a) temperature (b) salinity (c) density of cross-section A1-A2 (divided into the Banyu Asin estuary-Musi estuary-Upang estuary); and (d) temperature (e) salinity (f) density of cross-section B1-B2 at flood time.

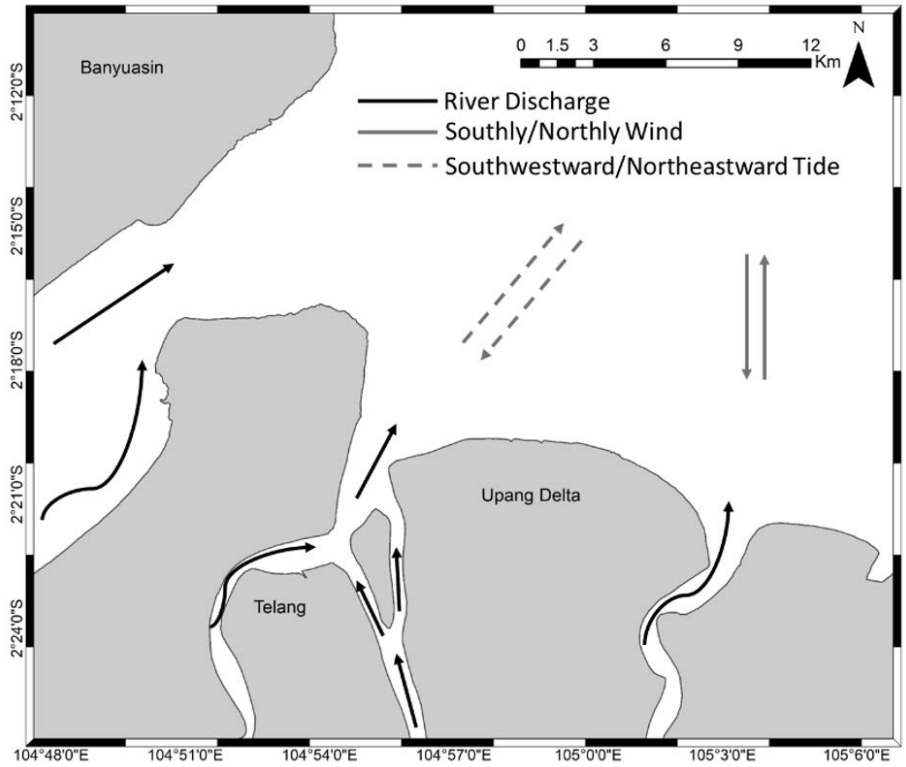

Figure 10. Schematic of stream transportation routes in estuaries: the black solid line represents the river discharge flowing to the sea, the gray solid line represents the to-and-fro path of wind flow in September, and the gray dashed line represents the direction of in-and-out tidal circulation at the study site.

imply a gradient of the temperature-salinity-density layer

that protrudes from the upstream area to the ocean. The surface layer is dominated by water masses from rivers, flowing from the mainland towards the ocean. Whereas,

the bottom layer consists of water masses from the ocean. The intrusion of the incoming waters from the sea spreads through the bottom to the very back of the basin, close to the land. This intrusion, characterized by a temperature of 29.88-29.94°C (light green in Figure 9.d), salinity of 27-28 Psu (brick red in Figure 9.e), and density of 12.5-14 (brownish yellow in Figure 9.f), enters the mainland quite far, almost reaching point B1. This occurs because during high tide, sea water moves onto the land with significant pressure, pushing water from the ocean to flow towards the land. there is an. The intrusion of water masses that spreads through the bottom of the water also can be observed in cross-section A1-A2, which appear stratified. Based on the model results obtained in cross-section B1-B2, the salinity gradient increases due to the intrusion of salty and low-temperature water mass into the estuary, which is the characteristic of seawater.

Circulating water flow can be controlled by complex interactions between tides, wind pressure, and fresh water discharge from rivers (Vaz et al., 2009). Winds are likely to contribute to the circulation of water flows and vertical stratification. The process relies on heat exchange when water interact with the atmosphere, as well as advection of salinity in the water. At this location, the wind predominantly blows towards the north, added as a significant influence along with the effects of tides and river flow. Estuaries are often considered an area that all the processes mentioned above can mix well, and this well-stratified area can be observed at different time periods during the high and low tide cycles (Rodrigues & Fortunato, 2017).

Currents from rivers to estuaries induce flow paths, which are mainly controlled by fresh water discharge (Vaz & Dias, 2014). The flow path of the Banyuasin, Musi, and Upang Rivers is mentioned as the main driving force behind the flow. This flow controls the outflow in various areas of the estuary (Figure 10). River discharges from the land to the sea can spread and transport property through river canals. The outflow of the Banyuasin, Musi, and Upang Rivers carries properties, especially on the surface, which is seen in the middle area of the Musi-Upang estuary as a significant area to be traversed due to the shallow bathymetry. The tides that enter and exit in the estuary mouth make this area very influenced by tides, as seen clearly from the pattern derived in the model.

CONCLUSSIONS

Coastal areas and estuaries are areas where freshwater sources from land and sea meet. Here, the characteristics of physical processes often overlap with water masses, resulting in a complex ecosystem. This ecosystem is influenced by factors such as river water discharge, tides, and bathymetry. Due to its broad and complex nature in spatiotemporal scale, relying solely on in situ and/or spatial data is insufficient to explain the processes occurring in this area. To address this limitation, a numerical model can be used to estimate and approximate the reality on the ground. This model helps in understanding the properties of water masses in terms of space and time, as well as the interactions between different components of the system. It is also valuable for monitoring and managing related resources. The model's accuracy is validated through field measurements at various points, yielding reliable values for further analysis. Overall, during low tide, the salt intrusion from the sea is confined in the middle of the cross-section. Conversely, during high tide, salt intrusion can enter the mainland at a secure location near the island.

ACKNOWLEDGEMENTS

Special thanks are extended to Denny Alberto Satrya Gumay and Lerma Yuni Siagian for their invaluable contribution in providing field data. We would also like to express our gratitude to PUSHIDROSAL and BIG for generously providing us with the necessary data for this research and for letting us use the Python program for the analysis and graphing conducted in this paper. Finally, we would like to thank all those who provided valuable input and suggestions during the writing process.

REFERENCES

Beer, M., 1997. *Plasma Physics Princeton Laboratory*. Princeton University, New Jersey.

Brown, L.R., Bennett, W.A., Wagner, R.W., Morgan-King, T., Knowles, N., Feyrer, F., Schoellhamer, D.H., Stacey, M.T., and Dettinger, M., 2013. Implications for future survival of Delta Smelt from four climate change scenarios for the Sacramento–San Joaquin Delta, California. *Estuaries and Coasts*, 36(4): 754–774. DOI: 10.1007/s12237-013-9585-4

Brown, L.R., Komoroske, L.M., Wagner, R.W., Morgan-King, T., May, J.T., Connon, R.E., and Fangue, N.A., 2016. Coupled downscaled climate models and ecophysiological metrics forecast habitat compression for an endangered estuarine fish. *PLOS ONE*, 11(1). DOI: 10.1371/journal.pone.0146724

Chow, V.T., 1989. *Hidrolika Saluran Terbuka*. Penerbit Erlangga, Jakarta. 609pp.

DHI, 2012. MIKE 21 & MIKE 3 FLOW MODEL FM, *Hydrodynamic and Transport Module Scientific Documentation*.

Duxbury, A.B, 2002. *Fundamentals of Oceanography*. 4th Ed., McGraw Hill, San Francisco. 344pp. ISBN: 0-07-242790-6

Heltria, S., Nurjaya, I.W., and Lumban-Gaol, J., 2021. Turbidity front dynamics of the Musi Banyuasin

Estuary using numerical model and Landsat 8 satellite. *AACL Bioflux*. 14(1) 1-13.

Heltria, S., Yuliardi, A.Y., Kismawardhani, R.A., Nurjaya, I.W., Siagian, L.Y., and Gumay, D.A.S., 2022. Distribution of salinity and temperature in Musi estuary: Using vertical salinity gradient for Estuary Classification Zone. *Jurnal Ilmu Dan Teknologi Kelautan Tropis*, 14(2): 217–231. DOI: 10.29244/jitkt.v14i2.40222

Iglesias, I., Avilez-Valente, P., Luís Pinho, J., Bio, A., Manuel Vieira, J., Bastos, L., and Veloso-Gomes, F., 2020. Numerical modeling tools applied to estuarine and coastal hydrodynamics: A user perspective. *Coastal and Marine Environments - Physical Processes and Numerical Modelling*. 20pp. DOI: 10.5772/intechopen.85521

Jeffries, K.M., Connon, R.E., Davis, B.E., Komoroske, L.M., Britton, M.T., Sommer, T., Todgham, A.E., and Fangue, N.A., 2016. Effects of high temperatures on threatened estuarine fishes during periods of extreme drought. *Journal of Experimental Biology*, 219(11): 1705–1716. DOI: 10.1242/jeb.134528

Maharani, W.R., Setiyono, H., and Setyawan, W.B., 2014. Studi distribusi suhu, salinitas dan densitas secara vertikal dan horizontal di perairan pesisir, Probolinggo, Jawa Timur. *Journal of Oceanography*, 3(2):151–160

Monismith, S.G., Genin, A., Reidenbach, M.A., Yahel, G., and Koseff, J.R., 2006. Thermally driven exchanges between a coral reef and the adjoining ocean. *Journal of Physical Oceanography*, 36(7): 1332–1347. DOI: 10.1175/jpo2916.1

Murthy, C.R., Sinha, P.C., and Rao, Y.R., 2008. *Modelling and monitoring of coastal marine processes*. Springer. 246pp.

Nurisman, N, Fauziah, and Surbakti, H., 2012. Karakteristik pasang surut di alur pelayaran Sungai Musi menggunakan metode admiralty. *Jurnal Maspari*, 4(1): 110–115. ISSN: 2087-0558

Patty, S.I., 2013. Distribution temperature, salinity and dissolved oxygen in Waters Kema, North Sulawesi. *Jurnal Ilmiah Platax*, 1(3): 148–157. DOI: 10.35800/jip.1.3.2013.2580

Petihakis, G., Triantafyllou, G., Korres, G., Tsiaras, K., and Theodorou, A., 2012. Ecosystem modelling: Towards the development of a management tool for a marine coastal system part-II, ecosystem processes and biogeochemical fluxes. *Journal of Marine Systems*, 94: S49–S64. DOI: 10.1016/j.jmarsys.2011.11.006

Ralston, D.K., Brosnahan, M.L., Fox, S.E., Lee, K.D., and Anderson, D.M., 2015. Temperature and residence time controls on an estuarine harmful algal bloom: Modeling hydrodynamics and alexandrium fundyense in Nauset Estuary. *Estuaries and Coasts*, 38(6): 2240–2258. DOI: 10.1007/s12237-015-9949-z

Restrepo, J.C., Ospino, S., Otero, L., Pierini, J., and Alvarez-Silva, O., 2018. Saltwater intrusion into a river with high fluvial discharge: A microtidal estuary of the Magdalena River, Colombia. *Journal of Coastal Research*, 34(6): 1273–1288. DOI: 10.2112/jcoastres-d-17-00144.1

Rodrigues, J.G.R., 2015. The Tagus estuarine plume variability: impact in coastal circulation and hydrography. *Master's thesis*. University of Aveiro, Aveiro, Portugal. 70pp.

Rodrigues, M., and Fortunato, A.B., 2017. Assessment of a three-dimensional baroclinic circulation model of the Tagus estuary (Portugal). *AIMS Environmental Science*, 4(6): 763–787. DOI: 10.3934/environsci.2017.6.763

Radjawane, I.M., Saputro, B.S.C., and Egon, A., 2018. Model Hidrodinamika Pasang Surut di Perairan Kepulauan Bangka Belitung. *Jurnal Teknik Sipil*, 25(2): 121–128. DOI: 10.5614/jts.2018.25.2.5

Sari, C.I, Surbakti, H., and Fauziyah, 2013. Pola sebaran salinitas dengan model numerik dua dimensi di muara Sungai Musi. *Maspari Journal*, 5(2): 104-110

Sugianto, D.N., 2012. Model Distribusi Data Kecepatan Angin dan Pemanfaatannya dalam Peramalan Gelombang di Perairan Laut Pacitan, Jawa Timur. *Indonesian Journal of Marine Scinces*, 15(3): 143–152. DOI: 10.14710/ik.ijms.15.3.143-152

Surbakti, H., 2012. Karakteristik pasang surut dan pola arus di muara Sungai Musi, Sumatera Selatan. *Jurnal Penelitian Sains*. 15(1) 15108: 35-39. ISSN: 1410-7058

Surbakti, H., Nurjaya, I.W., Bengen, D.G., and Prartono, T., 2022. Kontribusi massa air tawar dari estuari Banyuasin ke perairan Selat Bangka pada musim peralihan II. *POSITRON*, 12(1): 29–38. DOI: 10.26418/positron.v12i1.53035

Syarifudin, A., Imanuddin, M.S, and Simanjuntak, B., 2016. Model hidrodinamika dan sediment transport pada muara Sungai Musi Palembang, Sumatera Selatan. *Bina Darma e-Journal*. [as accessed from http://eprints.binadarma.ac.id/id/eprint/2344]

Vaz, N., Fernandes, L., Leitão, P.C., Dias, J.M., and Neves, R., 2009. The Tagus Estuarine Plume Induced by Wind and River Runoff: Winter 2007 Case Study. *Journal of Coastal Research*, Special Issue 56(II): 1090–1094.

Vaz, N., and Dias, J.M., 2014. Residual currents and transport pathways in the Tagus estuary, Portugal: The role of freshwater discharge and wind.

Journal of Coastal Research, 70: 610–615. DOI: 10.2112/si70-103.1

Wagner, R.W., Stacey, M., Brown, L.R., and Dettinger, M., 2011. Statistical models of temperature in the Sacramento–San Joaquin Delta under climate-change scenarios and ecological implications. *Estuaries and Coasts*, 34(3): 544–556. DOI: 10.1007/s12237-010-9369-z

Williams, J.J., and Esteves, L.S., 2017. Guidance on setup, calibration, and validation of hydrodynamic, wave, and sediment models for shelf seas and estuaries. *Advances in Civil Engineering*, 1–25. DOI: 10.1155/2017/5251902

Zaman, B., and Syafrudin, S., 2007. Model Numerik 2-D (Lateral & Longitudinal) Sebaran Polutan Cadmium (Cd) Di Estuari Sungai (Studi Kasus: Estuari Sungai Babon, Semarang). *Jurnal Presipitasi: Media Komunikasi dan Pengembangan Teknik Lingkungan,* 3(2): 1–8. DOI: 10.14710/presipitasi.v3i2.1-8

PROVENANCE AND DISTRIBUTION OF MIDDLE BAONG SAND IN THE MALACCA STRAIT AND ITS SURROUNDING

PROVENANS DAN SEBARAN BATUPASIR BAONG TENGAH DI SELAT MALAKA DAN SEKITARNYA

Totong Koesnadi Usman[1,2*], Yoga Andriana Sendjaja[3], and Nurdrajat[3]

[1] Postgraduate Study Program, Geological Engineering Faculty, Padjadjaran University, Jl. Dipati Ukur No. 35, Bandung, 40132

[2] PT. Pertamina (Persero), Jalan Mega Kuningan Barat III Jakarta 12950

[3] Geological Engineering Faculty, Padjadjaran University, Jl. Dipati Ukur No. 35, Bandung, 40132

*Corresponding author: t.usman@pertamina.com

(Received 23 May 2023; in revised from 1 June 2023; accepted 19 November 2023)

DOI : http://dx.doi.org/10.32693/bomg.38.2.2023.832

ABSTRACT: The Middle Baong Sand Formation has long been ascribed to the Malay Peninsula. However, this contradicts the results of chronostratigraphic correlation and rare earth element (REE) analysis, which indicate another source from the south. This research was conducted in North Sumatra, especially in Pertamina's onshore and offshore work areas. The comparison area is located in Kutacane-Karo and the Malay Peninsula. The objective of the study is to understand the provenance of the Middle Baong Sand Formation in North Sumatra. Data from four wells and 32 outcrops are used to evaluate the provenance and distribution of Middle Baong Sand in the study area. Besides that, secondary data from three outcrops are also used to support the analysis. The methods used in this study are chronostratigraphic correlation and REE analysis. The results showed that the provenance of the Middle Baong Sand onshore is estimated to originate from southwest Sumatra, contrary to general assumptions. Validation was carried out by comparing Malay Peninsula data with Kutacane research data and wells using REE analysis. The analysis results showed that the Middle Baong Sand Formation in the onshore area has a different provenance from the Middle Baong Sand Formation in the offshore area, which contradicts other research conducted so far. Based on this study, it is concluded that the paleogeography of the North Sumatra basin undergoes deepening symmetrically in the central basin since 10.46 million years ago (Mya).

Keywords: Middle Baong Sand, rare earth element (REE), provenance, paleogeography, North Sumatra Basin

ABSTRAK: *Formasi Pasir Baong Tengah telah lama dianggap berasal dari Semenanjung Melayu. Namun hal ini bertentangan dengan hasil korelasi kronostratigrafi dan analisis unsur tanah jarang (UTJ) yang menunjukkan adanya sumber lain dari arah selatan. Penelitian ini dilakukan di Sumatra Utara khususnya di wilayah kerja Pertamina darat (onshore) dan lepas pantai (offshore). Daerah pembanding terletak di Kutacane-Karo dan Semenanjung Melayu. Tujuan penelitian adalah untuk mengetahui asal usul Formasi Pasir Baong Tengah di Sumatra Utara. Empat data sumur dan 32 data singkapan digunakan untuk mengevaluasi sumber dan penyebaran Pasir Baong Tengah di daerah penelitian. Selain itu, tiga data singkapan sebagai data sekunder juga digunakan untuk mendukung analisis. Metode yang digunakan dalam penelitian ini adalah korelasi kronostratigrafi dan analisis UTJ. Hasil penelitian menunjukkan bahwa provenans Pasir Baong Tengah yang berada di darat diperkirakan berasal dari barat daya Sumatra. Hal ini bertentangan dengan asumsi umum. Validasi kemudian dilakukan dengan membandingkan data dari Semenanjung Melayu dengan data penelitian Kutacane dan data sumur menggunakan analisis UTJ. Hasil analisis menunjukkan bahwa Formasi Pasir Baong Tengah di area darat memiliki provenans yang berbeda dengan Formasi Pasir Baong Tengah di area lepas pantai. Hasil ini bertentangan dengan penelitian-penelitian lain yang telah dilakukan selama ini. Pemetaan dan analisis data yang komprehensif menyimpulkan bahwa paleogeografi Cekungan Sumatra Utara pada 10,46 juta tahun lalu (jtl) menunjukkan pendalaman di sekitar Selat Malaka.*

Kata Kunci: *Pasir Baong Tengah, unsur tanah jarang (UTJ), provenans, paleogeografi, Cekungan Sumatra Utara*

INTRODUCTION

The research area is located in the North Sumatra Basin (NSB), as shown in Figure 1, with the main focus in the Pertamina onshore and offshore work areas. The outcrop as comparative data is in the Kutacane-Karo area and its surroundings, as primary data, and the Malay Peninsula area, as secondary data.

The Middle Baong Sand (onshore) Formation (MBS) is assumed to have been originally deposited from the Malay Peninsula and later shifted from the south during the Bukit Barisan uplifting period. This assumption is supported by the absence of volcanic fragments (tuffaceous) found in the sediments from the Paleogene and Neogene ages. Consequently, the direction of currents and paleogeography in the basin are described towards the south, with sediment sources originating from the north. In lithostratigraphic correlation, this understanding is readily accepted since the age is of less importance or not considered.

Nowadays, with an increasing amount of drilling in North Sumatra, wells containing hydrocarbons reveal the pattern and spread of the MBS section. The pattern extends along the direction of Sumatra, specifically in the southern part of the North Sumatra coastline. However, in the northern region, sandstone sediments do not develop, even with a four-way dip closure trap. Usman et al. (2023) explained that, based on borehole image data describing several results of the current direction, it was discovered that this sediment was deposited from the east and south to the north (Figure 2). This finding contradicts previous research, which generally suggested that the sediment's provenance originated from the Malay Peninsula.

Therefore, this research is important to define the provenance and distribution of the MBS, both onshore and offshore. So far, Neogene deep sedimentary rocks in NSB, both onshore and offshore, have been widely discussed. These rocks consist of formations, including the Yetai Formation, the Baong Formation with the MBS Unit inside it, and the Keutapang Formation. Researchers such as Kamili et al. (1973), Mulhadiono et al. (1978), Cameron et al. (1980), Mulhadiono et al. (1982), Davies (1984), Anderson et al. (1993), Syafrin (1995), Fuse et al. (1996), Daly et al. (1987), Panguriseng et al. (2011), Bahesti et al., Banukarso et al. (2013, 2014), Ambarwati et al. (2017), and Syarifudin et al. (2018) have extensively discussed both the sedimentology and stratigraphic arrangement of these formations. However, the provenance of these formations, especially when using the rare earth element (REE) approach, has rarely been explored.

In particular, the MBS turbidite marine formation has been widely discussed by Riadhy et al. (1998). They confirmed that the source of the MBS is from the Malay

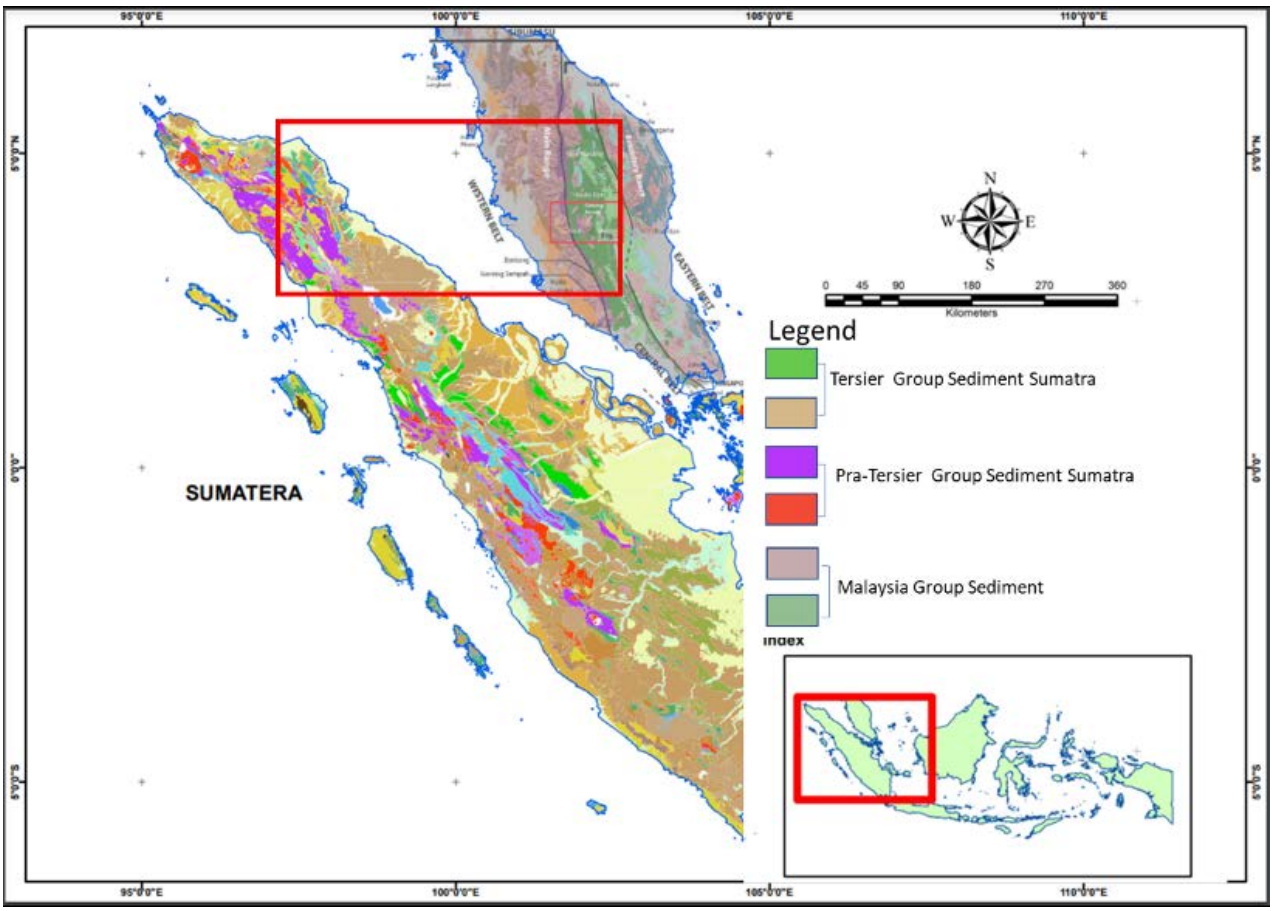

Figure 1. Study area and regional geology map, after Cameron et al. (1981a, 1981b), Keats et al. (1981), and Cameron et al. (1982)

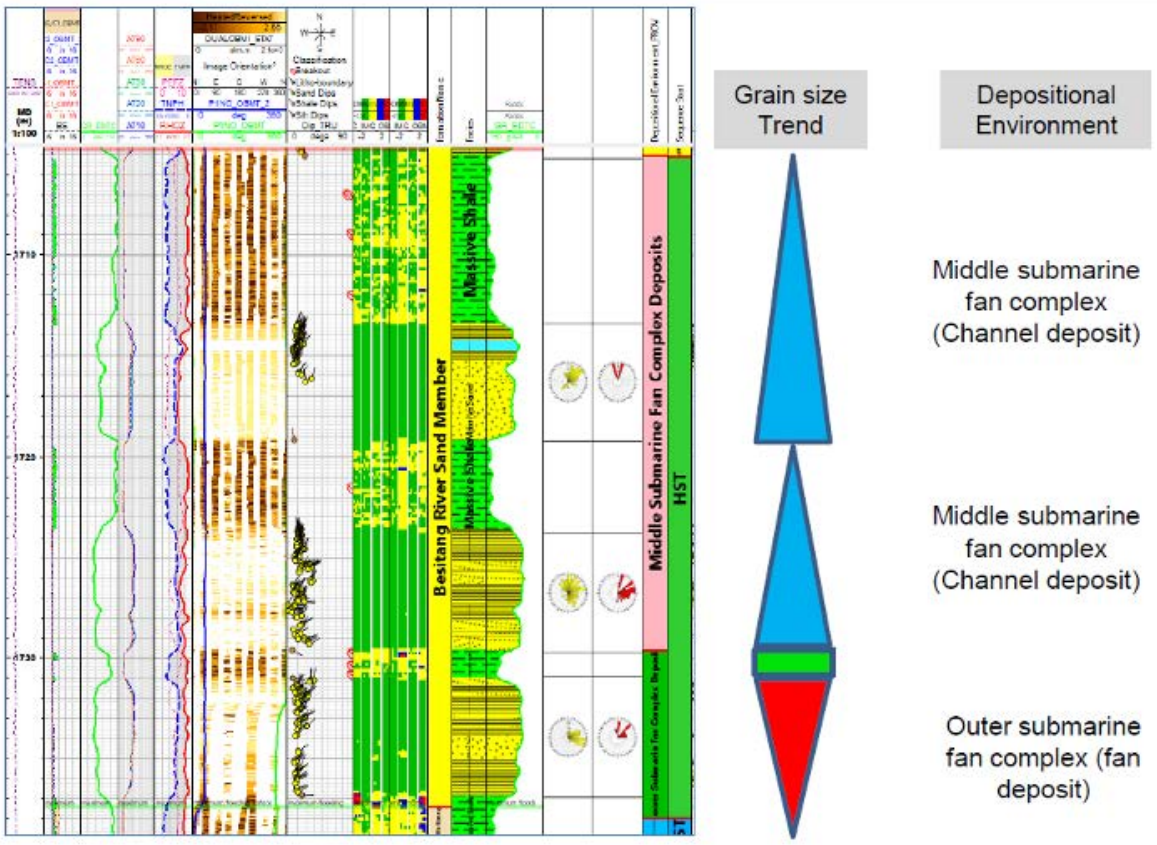

Figure 2. Borehole imaging well data at NSB (Usman et al., 2023)

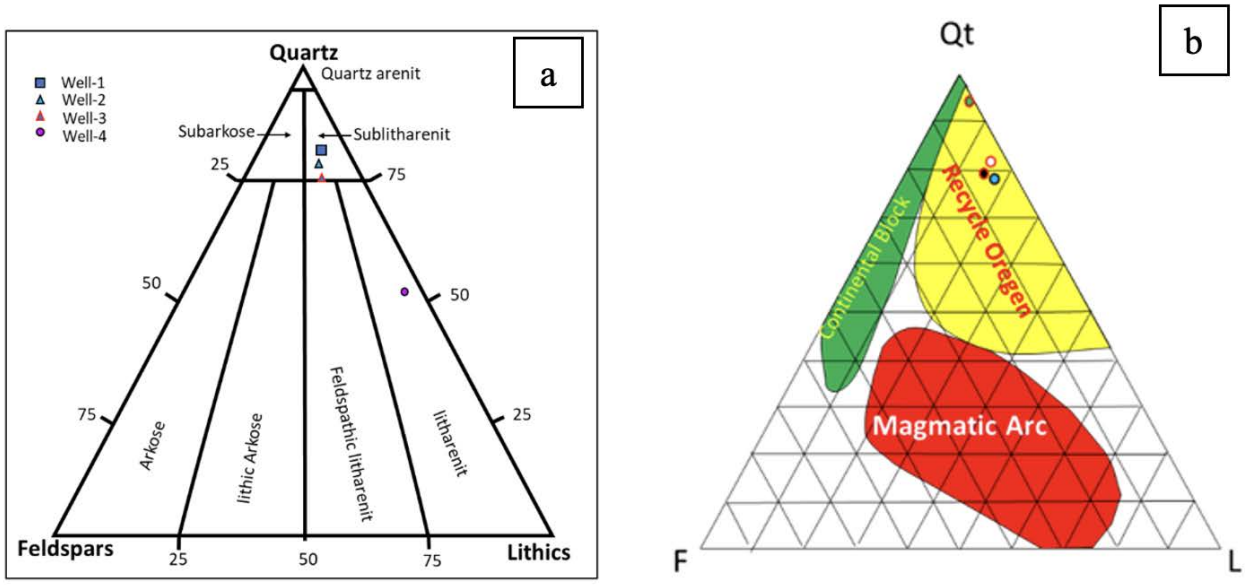

Figure 3. (a) The MBS mineralogical data based on Folks (1974) and (b) Dickinson (1979) diagram (Usman et al., 2023)

Peninsula, which changed from the south during the Bukit Barisan uplifting. This understanding is supported by the fact that sediments in the Paleogene and Neogene ages do not contain volcanic sediments (tuffaceous).

The current direction and paleogeography in the basin are described as moving towards the south, with sedimentary origins from the north. Based on petrology and mineralogy data analysis, Usman et al. (2023) explained that the MBS includes feldspathic litharenite sandstone (Figure 3.a), whose associated petrographic image is as shown in Attachment 3. Furthermore, Qt-F-L diagram after Dickinson's (1979) suggests that the MBS was formed from recycled orogen, meaning it was derived from existing sedimentary rocks (Figure 3.b).

Based on chronostratigraphic data and REE analysis from previous research (Usman et al., 2023), it is necessary to comprehensively map and analyze the existing data. This will facilitate the determination of the sediment origin of the MBS, assuming that clastic sediments came from igneous rocks, sedimentary rocks, or metamorphic rocks that undergo weathering and were transported into the basin.

METHODS

In this study, we used four wells and 32 outcrops of data to evaluate the provenance and distribution of the MBS. Besides that, three outcrops used as secondary data are also utilized to support the analysis. Based on the hypothesis that sediments came from sedimentary rocks, igneous rocks, or metamorphic rocks, it is important to consider that the further the sediments are away from their source of origin, the finer they will become as energy and deposition decrease. Hence, understanding the provenance of sediment is crucial.

To determine the rock origins, several methods can be employed, depending on the availability of data. In this study, the following methods are applied:

a. The chronostratigraphic correlation method is used to find out where the basin center is and where the landward direction is.

b. The REE method is employed to establish the correlation of rock origins using the comparison method with discrimination diagrams from Pearce et al. (1984).

The REE analysis method, supported by the chronostratigraphic correlation method, was used to observe and verify the direction of sedimentation in the study area, both onshore and offshore. Based on the results, the author can determine where the land location was and predict where the sediment originated from. This data will compare the REE of the MBS obtained from well data (below sea level), current surface outcrop data, and previous research data on the Malay Peninsula.

The discrimination diagram (Pearce et al., 1984) will assist in grouping igneous rocks into four categories based on their genesis: volcanic-arc granite (VAG), collision granite (COLG), within-plate granite (WPG), and ocean-ridge granite (ORG). VAG is typically found in the active continental margins and oceanic arcs (Pearce et al., 1984). By determining which group the MBS belongs to, comparisons can be made with the rock group assumed to be the original source. Based on these analyses, a conclusion can be drawn and the origin of the MBS and its paleogeographic form can be determined.

RESULTS

Based on the hypothesis, the MBS on the onshore is predicted from the southwest of the wells. This interpretation is based on the results of borehole image measurements from wells in the onshore NSB, which show sedimentation came from the southwest direction of the well area (Figure 2). In addition, the existence of *Globigerina Siakenesis (T)* at 10.46 Mya within the MBS on BTR, WP, and KB wells shows that sediments deepened towards the northeast, namely from neritic to bathyal (Figure 4).

Based on this data, it is described that the source of the MBS came from the southwest of Bukit Barisan. However, this assumption contradicts other research that mentioned the source of the sediments coming from the Malay Peninsula. On the other hand, the offshore well data show that the provenance rock came from the north to the south.

For offshore data, it is already established that the source provenance was from the Malayan Peninsula.

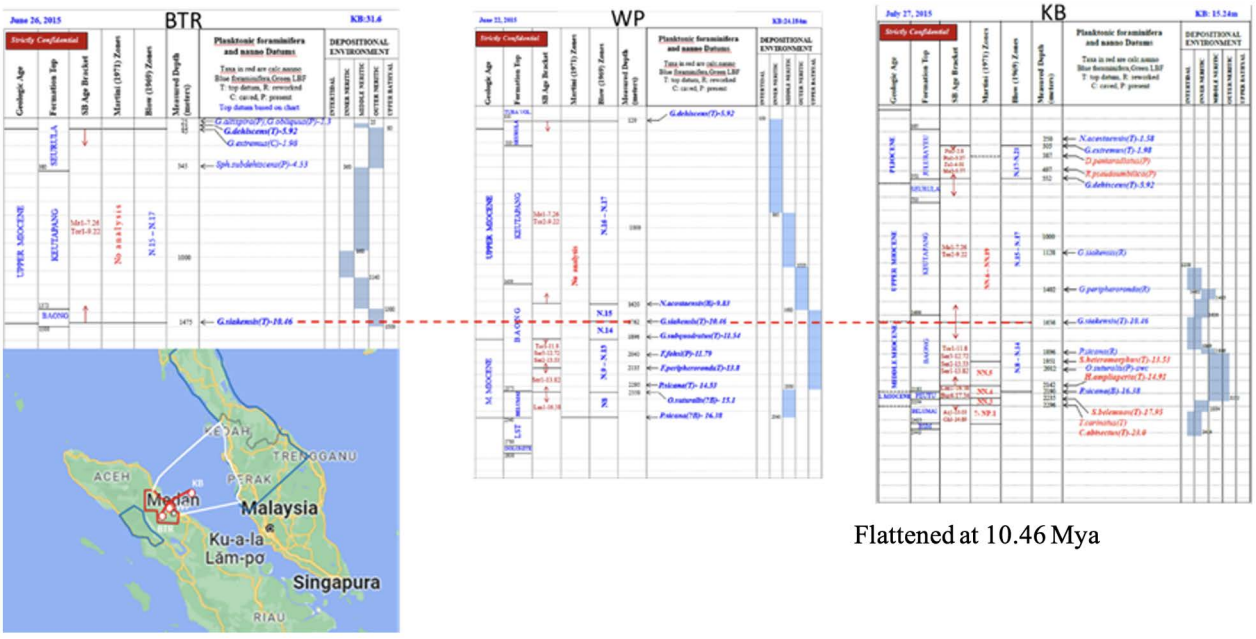

Figure 4. Paleoecological well correlation with Globigerina Siakensis (T) as the marker. (data attached: Attachment 1a-1c)

However, to strengthen the prediction of onshore wells originating from the south, validation was conducted using the comparison method with REE. For this purpose, well data from the onshore area and the Malay Peninsula were compared with well and outcrop data from the southern part of the well area, specifically the region around Kutacane. These comparisons were adjusted based on the prediction results from well borehole image data, as well as rare trace element data from the Malay Peninsula (Pertamina, 2016). The comparison method involves using a graph chart of elements Y vs. Nb (Figure 5).

Based on the data above, it is estimated that the MBS onshore originates from a VAG system. This is consistent with the samples from the southwest Sumatra region in the NSB. In contrast, the data from the Malay Peninsula indicates a WPG system. These findings show that there are two provenances in the NSB area. The data is more likely to be closer to coming from the southwest, represented by samples from the southwest Sumatra region (the NSB, or Kutacane Area), while the data from the Malay Peninsula is believed to be from a different source.

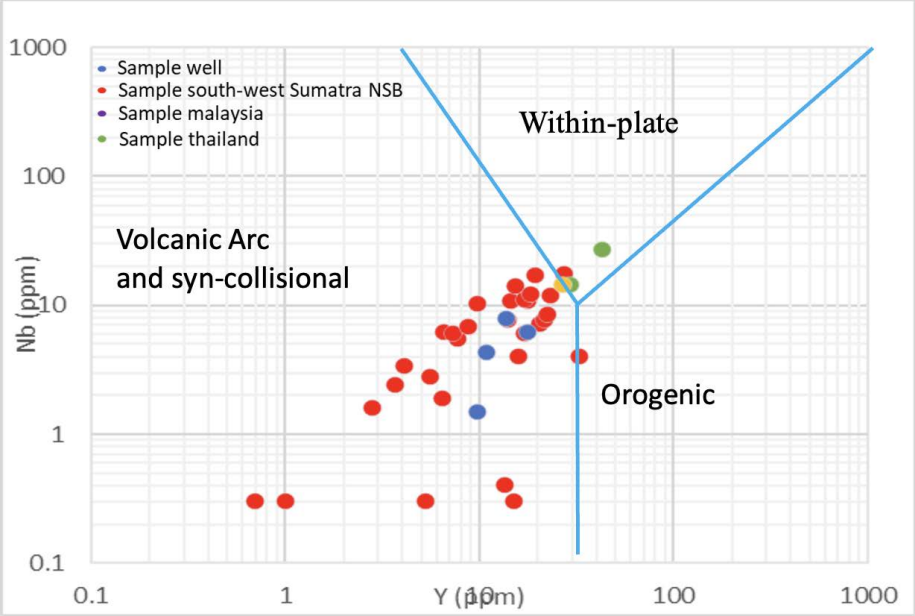

Figure 5. Elements Y vs. Nb discrimination diagram in North Sumatra and surroundings area (data attached: Attachment 2)

DISCUSSIONS

Based on this evaluation, it can be interpreted that as we move offshore in the north of Belawan, the sedimentary deposit tends to be shaly, indicating a deep sea environment. Similarly, as we move from the north offshore to the south towards the coast, the depth increases. Therefore, it can be predicted that Belawan Beach, located in the northern terrain, was the deepest basin where the MBS sediment was deposited, specifically in the bathyal environment (Figure 6).

The condition is almost similar to the present condition, except that during the time of *Globigerina Siakensis (T)* at 10.46 Mya, the environment along the Belawan coast was outer neritic, as was the area of the Strait of Malacca. It can be estimated that the southern onshore area at the time of the Plio-Pleistocene experienced a very strong uplift compared to the Strait of Malacca. As a result, the current onshore area, which was once outer neritic, became land, while the Strait of Malacca remained as sea.

This result is almost similar to the present-day paleogeographic conditions, where the position of the basin is in the Strait of Malacca. However, during the time of *Globigerina Siakensis (T)* at 10.46 Mya, the internal position was on the border of the area around the current coast, with a deeper depth of bathyal compared to the internal present-day position, which is east of the Strait of Malacca.

Thus, it shows that the position in the NSB was around the Strait of Malacca during the formation of the MBS, which has been in existence since 10.46 Mya. This contradicts the results of research from Riady et al. (1998) and Ambarwati et al. (2017), which stated that the source provenance onshore was the same as that offshore, i.e., originating from the Malay Peninsula. Therefore, it can be concluded that the opening of the NSB to the south occurred at the age of 10.46 Mya and the new Strait of Malacca was formed during the Bukit Barisan uplifting, specifically during the Plio-Pleistocene, when the Idi Formation was deposited.

CONCLUSSIONS

The MBS is described based on petrological and mineralogical data as feldspathic litharenite-

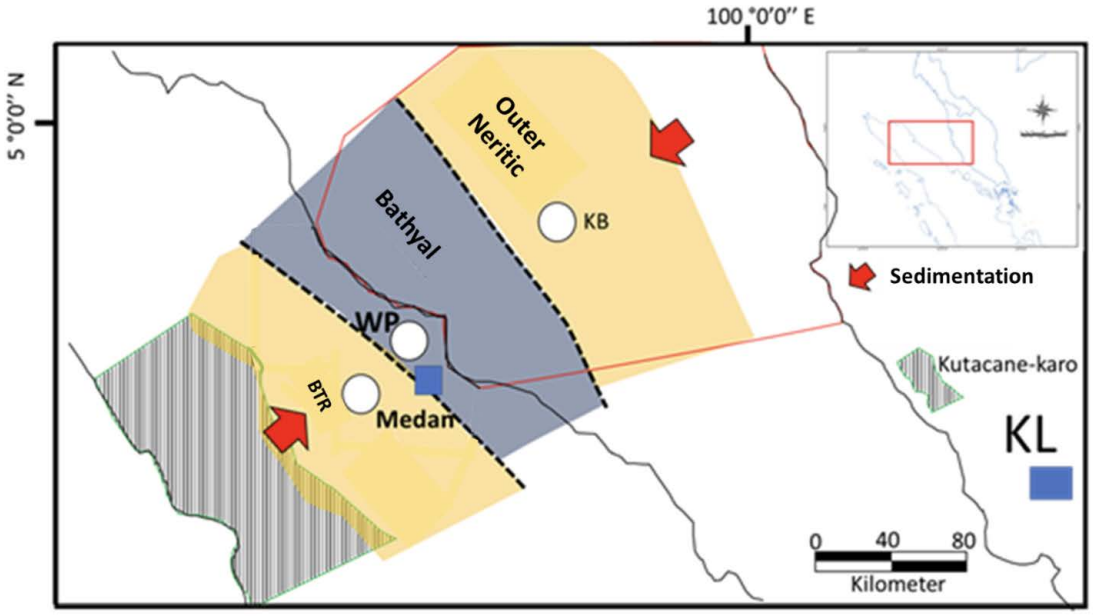

Figure 6. Paleogeography area research based on borehole image data chronostratigraphy and REE comparison (Y vs. Nb): WP= West Pakam, BTR= Batara, KB=Kambuna, KL=Kuala Lumpur

sublitharenite. In contrast, the MBS offshore can be distinguished based on REE data and benthos foram data. It shows that from south to north, the MBS is deeper towards the coast, transitioning from outer neritic to bathyal; while towards the Malay Peninsula, from the coast to the north, it becomes shallower.

Based on the analysis result, there are two sources of the formation. The MBS onshore comes from the south. On the other hand, the MBS offshore comes from the Malay Peninsula. The Strait of Malacca has existed since 10.46 Mya as an interior. However, during the deposition of the MBS (10.46 Mya), this strait took the form of a bathyal interior with a central interior around the Belawan Coast. Currently, it is in the form of a shallow strait.

ACKNOWLEDGEMENTS

Special thanks are extended to Denny Alberto Satrya Gumay and Lerma Yuni Siagian for their invaluable contribution in providing field data. We would also like to express our gratitude to PUSHIDROSAL and BIG for generously providing us with the necessary data for this research and for letting us use the Python program for the analysis and graphing conducted in this paper. Finally, we would like to thank all those who provided valuable input and suggestions during the writing process.

REFERENCES

Ambarwati, W.L., Idris, R., Nurjadi, E., and Mardianza, A., 2017. Provenance discrimination of Lower Baong Interval, Baong Formation, North Sumatra Basin: Constraints from petrografphy and Geochemistry, FSTH. Unpublished.

Anderson, B.L., Bon, J., and Wahono, H.E., 1993. Reassessment of the Miocene Stratigraphy, Paleogeography and Petroleum Geochemistry of the Langsa Block in the Offshore North Sumatra Basin. *Proc. Indonesia Petroleum Association*, 22nd Ann. Conv., 1: 169-190.

Bahesti, F., Subroto, E.A., Manaf, N.A., and Sadirsan, W., 2014. Integrated Basin Analysis and Geomechanic Study of Lower Baong Shale for Preliminary Shale Gas Prospectivity in The North Sumatra Basin. *Proc. Indonesia Petroleum Association*, 38th Ann. Conv.

Banukarso, M., Meckel, L.D., Citrajaya, N., and Raharjo, S., 2013. An Inverted Syn-Rift Play in the Offshore North Sumatra Basin. *Proc. Indonesia Association of Geologist*, 37th Ann. Conv.

Cameron, N.R., Clarke, M.C.G., Aldiss, D.T., Aspden, J.A., and Djunuddin, A., 1980. The geological evolution of Northern Sumatra. Proc. Indonesia Petroleum Association, 9th Ann. Conv., pp.149-187.

Cameron, N.R., Djunuddin, A., Ghazali, S.A., Harahap, H., Keats, W., Kartawa, W., Miswar, Ngabito, H., Rock, N.M.S., and Whandoyo, R., 1981a. Geology of Langsa, Sumatera. Unpublished.

Cameron, N.R., Aspden, J.A., Miswar, and Syah, H.H., 1981b. Geology of Tebingtinggi, Sumatera. Unpublished.

Cameron, N.R., Aspden, J.A., Bridge, D.McC., Djunuddin, A., Ghazali, S.A., Harahap, H., Hariwidjaja, S., Kartawa, W., Keats, W., Ngabito,

H., Rock, N.M.S., and Whandoyo, R., 1982. Geology of Medan, Sumatera. Unpublished.

Daly, M.C., Hooper, B.G.D., and Smith, D.G., 1987. Tertiary Plate Tectonics and Basin Evolution in Indonesia, *Proc. Indonesia Petroleum Association*, 16th Annual Convention, pp. 399-428.

Davies, P.R., 1984. Tertiary Structural Evolution and Related Hydrocarbon Occurrences, North Sumatra Basin. *Proc. Indonesia Petroleum Association*, 13th Ann. Conv., 1: 19-50.

Dickinson, W.R., and Suczek, C.A., 1979. Plate Tectonics and Sandstone Composition, *American Association of Petroleum Geologists Bulletin*, 63: 2164–2182.

Folk, R.L., 1974. *Petrology of Sedimentary Rocks*. Hemphill Publishing Company, United States of America, pp. 1-190.

Fuse, A., Tsukada, K., Kato. W., Honda, H. Selaeman, A., Troyer, S., Wamsteeker, L., Abdullah, M., Davies, R.C., and Lunt, P., 1996. Hydrocarbon Kitchen and Migration Assessment of North Aceh Offshore Basin, North Sumatra, Indonesia from views of Sequence Stratigraphy and Organic Geochemistry, *Proc. Indonesia Petroleum Association*, 25th Ann. Conv., 1: 15-28.

Kamili, Z.A., and Naim, A.M., 1973. Stratigraphy of Lower and Middle Miocene Sediment in North Sumatra Basin. *Proc. Indonesia Petroleum Association*, 2nd Ann. Conv., pp. 53-72.

Keats, W., Cameron, N.R., Djunuddin, A., Ghazali, S.A., Harahap, H., Kartawa, W., Ngabito, H., Rock, N.M.S., Thompson, S.J., and Whandoyo, R., 1981. Geology of Lhokseumawe, Sumatera.

Mulhadiono, Hartoyo, P., and Soedaldjo, P.A., 1978. The Middle Baong Sandstone Unit as One of The Most Prospective Units in The Aru Area, North Sumatra. *Proc. Indonesia Petroleum Association*, 7th Ann. Conv., 1: 107-132.

Mulhadiono, Koesoemadinata, R.P., and Rusnandar, 1982. Besitang River Sand as The First Turbidite reservoir in Indonesia. *Proc. Indonesia Petroleum Association*, 11th Ann. Conv., pp. 265-298.

Panguriseng, M.J., Nurjadi, E., Sadirsan, W.S., Adibrata, B.W.H., and Priambodo, D., 2011. *Proc. JCM Makassar*, 36th HAGI and 40th IAGI Ann. Conv. and Exhibition, Makassar.

Pearce, J.A., Harris, N.B.W., and Tindle, A.G., 1984. Trace Element Discrimination Diagrams for The Tectonic Interpretation of Granitic Rocks. *J. Petrol*. 25: 956–983.

Pertamina, 2015. Biostratigraphic Report on North Sumatra Area. Unpublished.

Pertamina, 2016. "Studi Geologi Mesozoikum Area Sumatera Bagian Utara Propinsi Aceh dan Sumatera Utara". Unpublished.

Riadhy, S., Ismi, C., and Iriani, S., 1998. North Sumatra's Middle Reservoir Prediction and Characterization Using Sequence Stratigraphy 2D Seismic Inversion and 3D Seismic Data, *Proc. Indonesia Petroleum Association*, Jakarta.

Syarifudin, I.Y., and Ariyanto, P., 2018. Tectonostratigraphy of Block A Area, North Sumatra Basin: The Impact of Local Tectonics and Eustasy to Accommodation Space of The Tertiary Interval. Indonesia *Proc. Indonesia Petroleum Association*, 42nd Annual Convention & Exhibition, Jakarta. DOI: 10.29118/IPA18.586.G.

Syafrin, K.N., 1995. Deposition of Middle Baong Sandstone as Post-Rift Incised Valley Fill Sequence, Aru Onshore Area, North Sumatra. *Proc. Indonesia Petroleum Association*, 24th Ann. Conv., 1: 131-146.

Usman, T.K., Sendjaja, Y.A., Nurdrajat, Septama, E., Wardaya, P., Pratama, R., and Rossa, V., 2023. Determination of Sediment Provenance of Onshore Middle Baong Formation Using Rare Earth Element Trace in North Sumatra Basin, *Proc. Joint Convex IAGI-IAFMI-HAGI-IATMI-PERHAPI*, Pangkalpinang.

Attachment 1a (Pertamina, 2015)

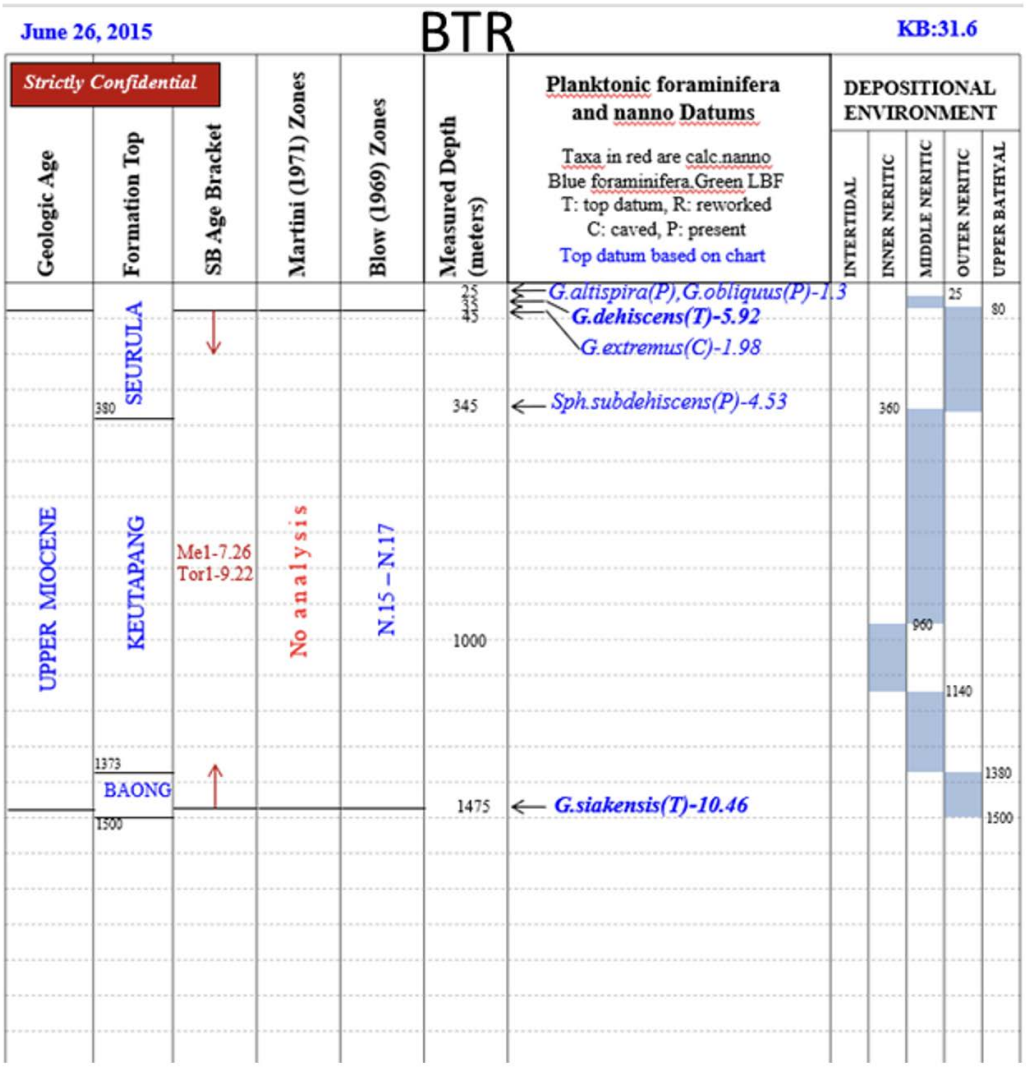

Attachment 1b (Pertamina, 2015)

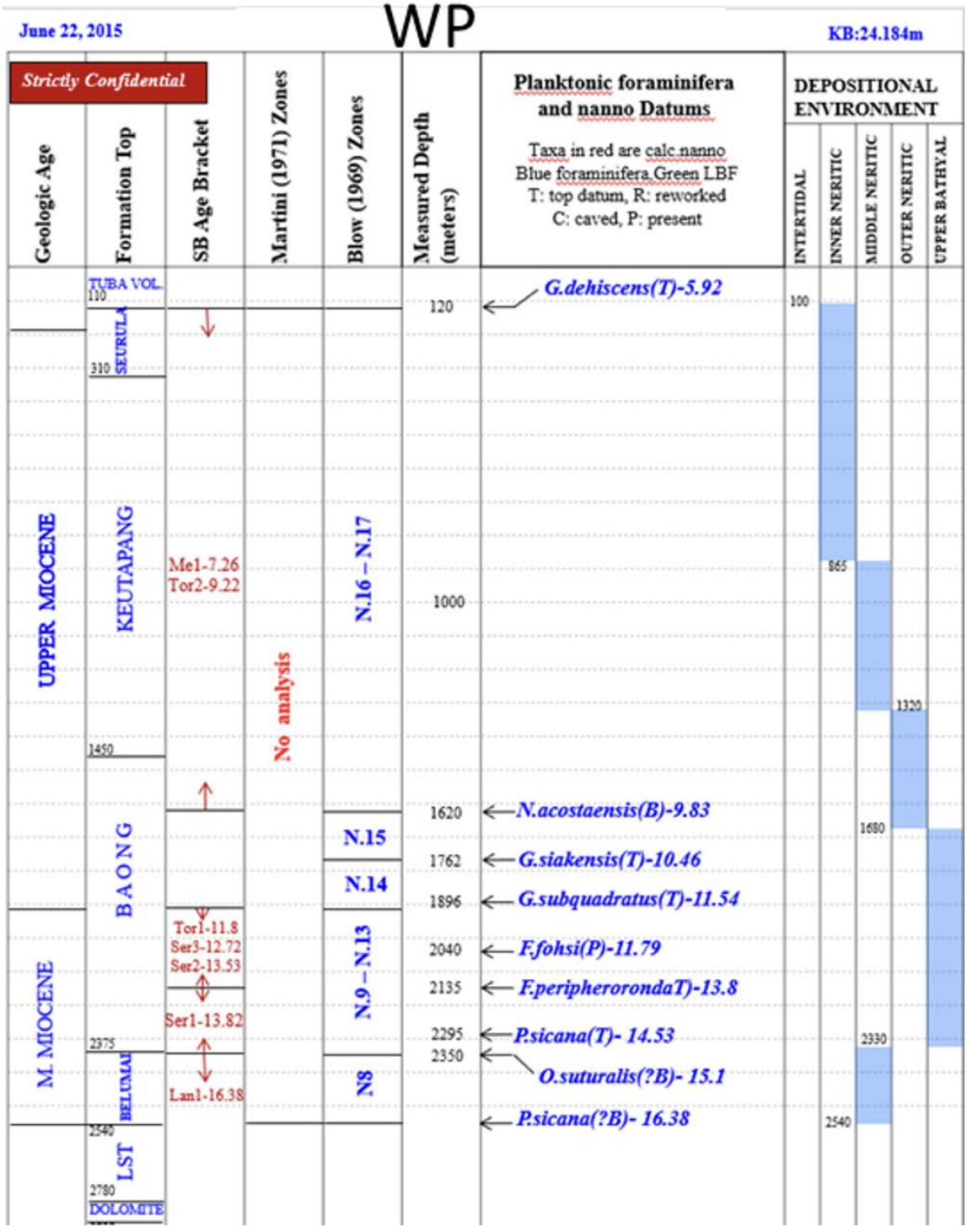

Attachment 1c (Pertamina, 2015)

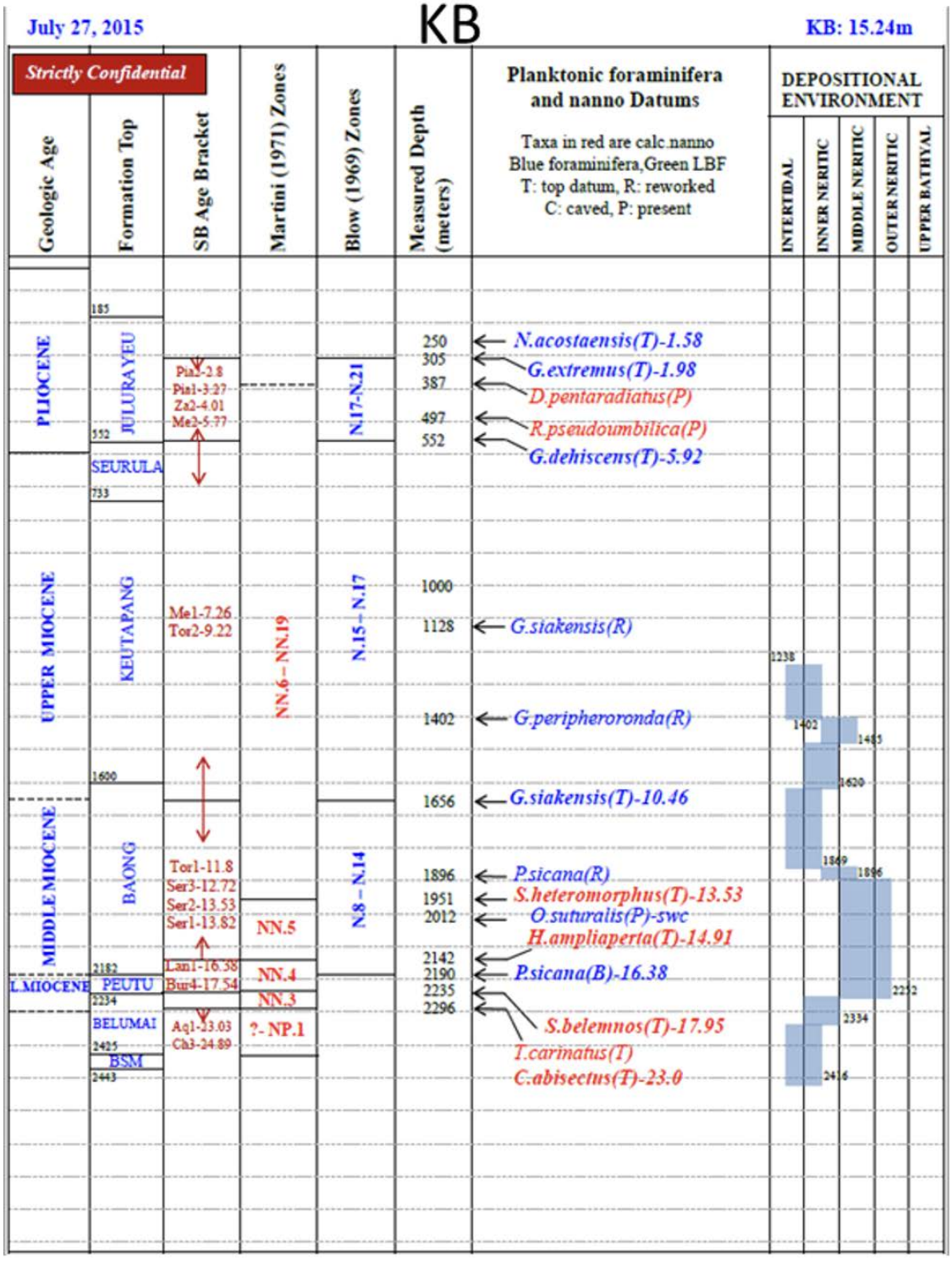

Attachment 2

	Y	Nb
	PPM	PPM
	0.1	0.1
	4A/MS	4A/MS
well-1	10.8	4.3
well-2	13.8	7.9
well-3	9.8	1.5
well-4	17.8	6.2
SW-NSB-1	7.7	5.5
SW-NSB-2	14.1	7.7
SW-NSB-3	14.6	10.9
SW-NSB-4	17.6	10.7
SW-NSB-5	6.5	6.2
SW-NSB-6	13.4	0.4
SW-NSB-7	2.8	1.6
SW-NSB-8	9.8	10.2
SW-NSB-9	15.2	14.2
SW-NSB-1	17	11.1
SW-NSB-1	23	11.8
SW-NSB-1	1	0.3
SW-NSB-1	7.3	6.1
SW-NSB-1	3.7	2.4
SW-NSB-1	18.2	12.3
SW-NSB-1	4.1	3.4
SW-NSB-1	17	6.1
SW-NSB-1	0.7	0.3
SW-NSB-1	15.9	4
SW-NSB-2	19.2	17.2
SW-NSB-2	20.4	7.1
SW-NSB-2	5.3	0.3
SW-NSB-2	32.5	4
SW-NSB-2	6.4	1.9
SW-NSB-2	27.5	17.7
SW-NSB-2	8.7	6.9
SW-NSB-2	21.7	7.7
SW-NSB-2	15.1	0.3
SW-NSB-2	22.5	8.4
SW-NSB-3	5.6	2.8
mly-1	29.5	14.6
mly-2	43	27
tha-01	27	14.6
	1000	1000

Attachment 3. Calcareous sandstone, feldspathic litharenite

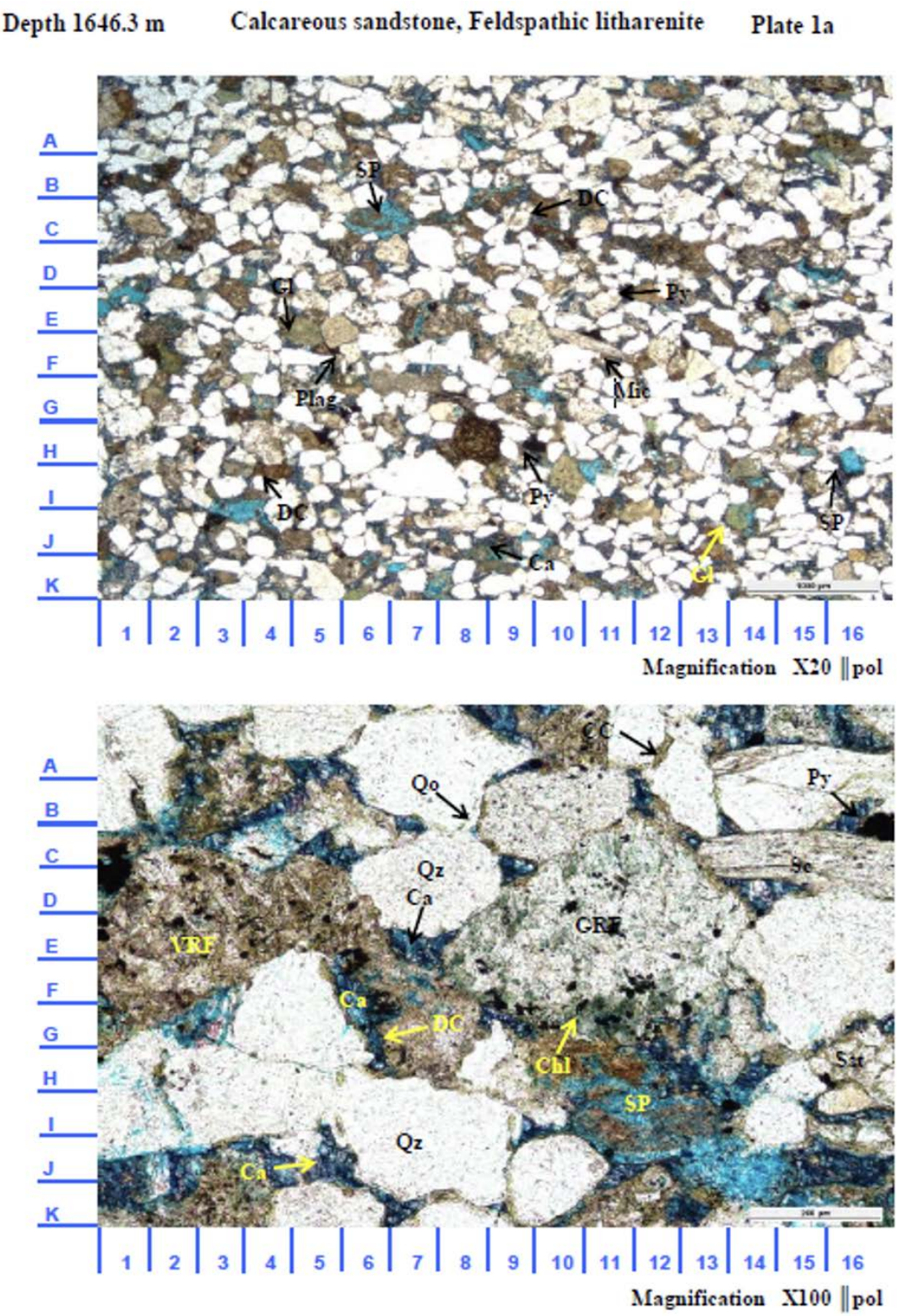

A low magnification image shows ~~that~~ moderately sorted sandstone composed of angular to rounded particles, identified as quartz (Qz), feldspar (F) and rock fragments (RFs). Unstable grain has partially dissolved and results in secondary pore (SP), and also partially replaced by calcite (Ca). Some grain is locally coated with clay (CC). Primary pores are occasionally filled by detrital clay (DC) and Ca. Visible porosity is moderate and the dissolution pore types are dominant. Restricted primary intergranular (IP) type is also recognized.

EXPLORING MARINE GEOLOGY AND OCEANOGRAPHY IN MANGGAR WATERS: A PRELUDE TO THE BURGEONING BELITONG GEOPARK

PENYELIDIKAN GEOLOGI KELAUTAN DAN OSEANOGRAFI DI PERAIRAN MANGGAR: SEBUAH LANGKAH AWAL PADA UPAYA PENGEMBANGAN GEOPARK BELITONG

F.X. Harkin H. Prabowo[1], Luli Gustiantini[1], Marina I. Siti[1], Nur Adi Kristanto[1], Fauzi Budi Prasetio[1], Imelda R. Silalahi[1], Yuli Yulianah[1], Aldi Rahmayadi[1], Catur Purwanto[1], Yusuf Adam Priyohandono[1], Sonny Mawardi[1], Godwin Latuputty[1], Prisca Ayu Wastuwidyarani[1], Adi C. Sinaga[1], Swasti Aninda Piranti[1], Ferry Siboro[1], Agus Subekti[1], Sahudin[1]

[1] Marine Geological Institute (Balai Besar Survei dan Pemetaan Geologi Kelautan), Geological Agency - Ministry of Energy and Mineral Resources, Jl. Dr. Junjunan No. 236, Bandung 40174

*Corresponding author: gustiantini@gmail.com

(Received 10 November 2023; in revised from 20 November 2023; accepted 27 December 2023)

DOI : http://dx.doi.org/10.32693/bomg.38.2.2023.859

ABSTRACT: A survey on marine geology and oceanography was conducted in Manggar Waters, East Belitung, in order to protect the geological heritage of the newly inaugurated Belitong UNESCO Global Geopark (UGGp) in 2021. This study is aimed at understanding the characteristics of the seabed, marine sediments, currents, and coastal features in the area. A bathymetrical survey was done using an Echotrac echosounder to measure water depths, and current measurements were taken with an Infinity device. Forty sediment samples were collected and analyzed for their characteristics. The coastal features were examined through direct observation, and an unmanned aerial vehicle (UAV) drone was used to investigate the morphology of small islands. The results showed that the seabed was mainly composed of coarse sediments, such as sand and clayey sand, with some areas containing gravel near Buku Limau Island. The microfauna foraminifera analysis indicated a relatively low diversity, with *Operculina* and *Amphistegina* being the dominant species. Two types of beaches were recognized: the northern part, consisting of rocky beaches made of igneous rocks, and the southern part, which has flat beaches made of beach alluvium deposits. Abrasion was found to be dominant in the southern part, particularly at Tambak Beach. The study provides valuable information for the planning and management of marine areas in the Belitong Geopark. It also highlights the importance of preserving and protecting the geological heritage of the region. With this newfound knowledge, stakeholders can make cognizant decisions to ensure the conservation of the Belitong Geopark and its unique geological features.

Keywords: Belitong UGGp, marine geopark, marine sediment characteristic, coastal characteristic

ABSTRAK: *Dalam rangka melindungi dan menjaga warisan geologi di Belitong UNESCO Global Geopark (UGGp) yang baru diresmikan pada tahun 2021, maka telah dilakukan survei geologi kelautan dan oseanografi di Perairan Manggar, Belitung Timur. Penyelidikan ini bertujuan untuk memahami karakteristik dasar laut, sedimen permukaan dasar laut, sifat arus, dan karakteristik pantai di daerah tersebut. Survei batimetri dilakukan dengan menggunakan echosounder Echotrac untuk mengukur kedalaman air; sedangkan arus diukur dengan menggunakan alat Infinity. Empat puluh sampel sedimen diambil untuk dianalisis sifat dan kandungan di dalam sedimen. Tipe pantai dianalisis berdasarkan hasil observasi langsung; dan drone kamera tanpa awak digunakan untuk mengamati morfologi di pulau-pulau kecil. Hasil penyelidikan menunjukkan bahwa dasar laut Perairan Manggar sebagian besar terdiri dari sedimen kasar, seperti pasir dan pasir lempungan, sedangkan kerikil hanya dijumpai di beberapa lokasi di dekat Pulau Buku Limau. Analisis mikrofauna foraminifera menunjukkan keanekaragaman yang relatif rendah, dengan Operculina dan Amphistegina sebagai spesies yang dominan. Terdapat dua jenis pantai,*

yaitu di bagian utara yang merupakan pantai berbatu tersusun oleh batuan beku, dan di bagian selatan yang berupa pantai datar dengan endapan aluvium pantai. Abrasi dominan terjadi di bagian selatan, khususnya di Pantai Tambak. Diharapkan hasil survei dan penyelidikan ini dapat memberikan informasi berharga bagi perencanaan dan pengelolaan kawasan laut di Geopark Belitong dengan menitikberatkan pada pentingnya melestarikan dan melindungi warisan geologi di wilayah tersebut. Berdasarkan informasi ini, diharapkan pihak-pihak yang berkepentingan dapat mengambil keputusan yang tepat dalam menjamin keberlangsungan upaya konservasi Geopark Belitong dan keunikan fitur-fitur geologinya.

Kata Kunci: *Geopark Belitong, marine geopark, karakteristik sedimen laut, karakteristik pantai*

INTRODUCTION

Geoparks are geographical areas that are differentiated based on geodiversity, biodiversity, and cultural diversity (Hutabarat, 2023). Geological heritage is managed through the concepts of conservation, education, and sustainable development. Geological heritage containing geological history is the main subject of a geopark area, which can show a unique geological story. Therefore, to build the geological story is not only by observing existing geosites but also by completing and comprehending geological data both on land and at sea.

As one of the ten UNESCO Global Geoparks (UGGp) in Indonesia, the Belitong UGGp, also known as Belitong Geopark, has gained global recognition since 2021. Belitong Geopark is located off the eastern coast of Sumatra in the Bangka Belitung province, Indonesia. The geopark occupies the entire Belitung Island (Belitong UGGp, 2021). It is renowned for its geological heritage, exceptional landscapes and beaches, rich biodiversity, and cultural significance that has noteworthy scientific, educational, and cultural values, undeniably. Zukhri et al. (2021) implied that it is seen as a fresh and compelling magnet for both domestic and foreign visitors. In order to protect the geosites, especially the ones located on the beaches, it is crucial to enhance marine geological and oceanographic information as part of an ongoing effort to conserve and promote the natural and cultural features of the region.

Belitong Geopark is surrounded by the Karimata Strait to the north, the Java Sea to the east and south, and the Gaspar Strait to the west. Being a part of the Karimata Strait, the waters of Bangka Belitung are heavily influenced by tides. According to Wei et al. (2015), tidal

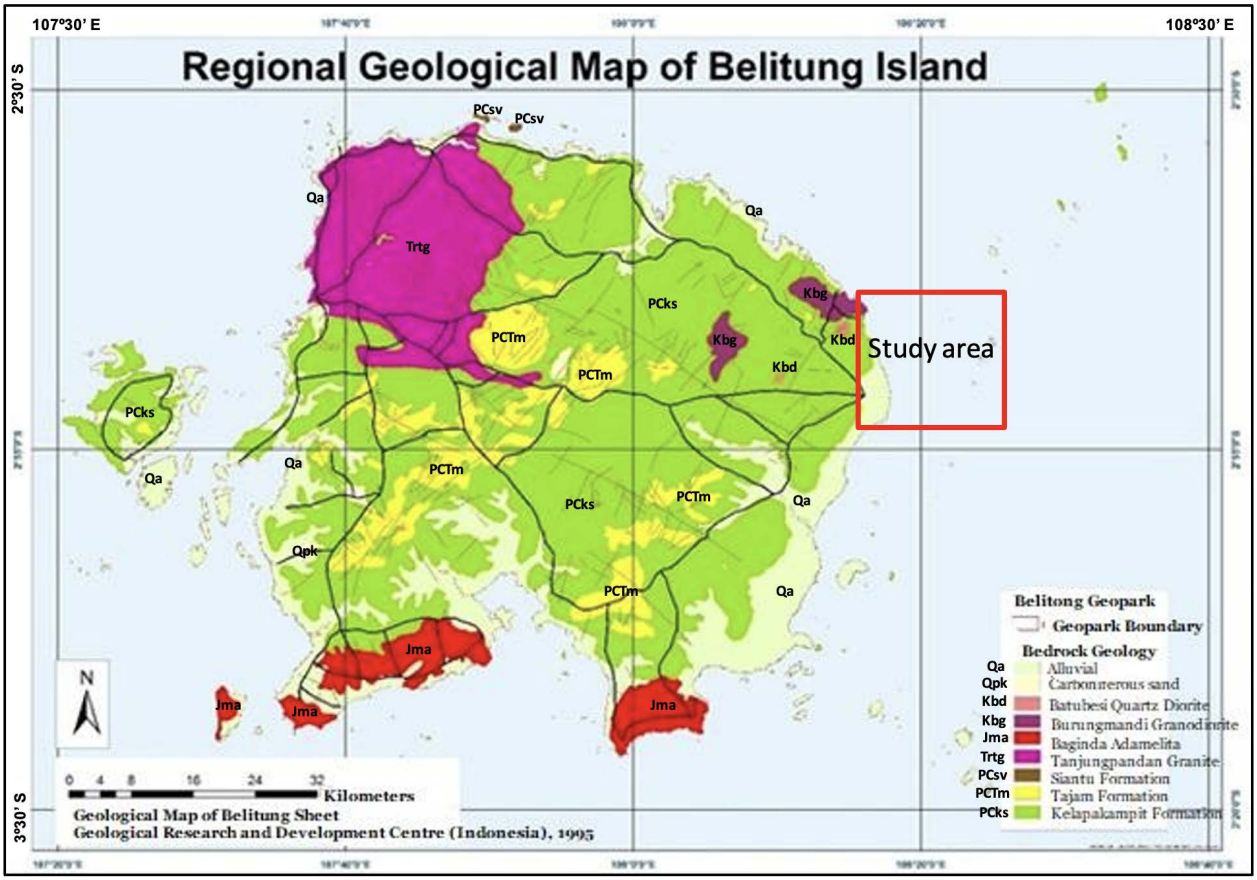

Figure 1. Geological map of Belitung Island surrounding Belitong Geopark (modified from Baharuddin & Sidarto, 1995; Bhinekawati et al., 2020); and the study area of Manggar Waters, off east Belitung Island (red square).

patterns in the Karimata Strait are predominantly diurnal type. These diurnal tides coincide the location of the anti-nodal band of the diurnal tidal waves, where diurnal (daily) tidal waves exhibit looping patterns, as opposed to the nodal band of the semi-diurnal tidal waves, where semi-diurnal (twice-daily) tidal waves exhibit nodal, or stationary, behavior. This distinction is supported by the greater amplitudes and smaller spatial phase-lag changes observed in the diurnal tides compared to the semi-diurnal tides. Wicaksana et al. (2015) argued that the Karimata Strait is greatly impacted by the South China Sea, especially in terms of wind movements and their effects on wave characteristics. The authors reported that significant wave characteristics are observed during the peak of the west monsoon (January) and the east monsoon (August) each year. In January, significant waves in the Karimata Strait reach heights of 1.5–3 m and may continue into February, albeit with a slight decline. In the Java Sea, significant waves can reach heights of 0.5–2.5 m.

Belitong Geopark has a total area of about 4,800 km^2 of land and 13,000 km^2 of sea, with 241 small islands within its boundaries, exposing various geological features (UNESCO, 2021). Among them, there are 27 small islands in the west of Belitung Island (Gaspar Strait) (Hartoko, 2019). Different rock formations can be found in different areas of the geopark, including sedimentary rocks and plutonic rocks (Figure 1). Tin mining has also been a significant contributor to the local economy.

As described by Baharuddin & Sidarto (1995), there are nine lithologies occupy Belitung Island (Figure 1), from youngest to oldest in age formation, namely: alluvial (Qa), carbonaceous sand (Qpk), both are agded Quaternary; Batubesi Quartz Diorite (Kbd) and Burungmandi Granodiorite (Kbg), as stated by Priem et al. (1975) that both having similar age range between 115 – 160 million years ago (Mya), or Cretaceous period; Baginda Adamellite (Jma), aged ranging from 160 – 208 Mya (Priem et al., 1975), or Jurassic period; and Tanjungpandan Granite (Trtg) as Priem et al. (1975) stated as of 208 – 245 Mya, or Triassic period; as the oldest formations in the area, the three interfingering rock formations of Siantu Formation (PCsv), Tajam Formation (PCTm), and Kelapakampit Formation (PCks), dated as of Permo-Carboniferous age, about 250 million years ago.

Quaternary alluvial and beach deposits (Qa) is composed of gravel, pebble-cobble, sand, silt, clay, and coral fragments. Quaternary carbonaceous sand (Qpk) consists of black carbonaceous sand intercalated with clay, with fine to medium grain size, containing heavy minerals, lignite fragments, and occasional cassiterite (tin oxide) layers. Batubesi Quartz Diorite (Kbd) is composed of quartz diorite with a green to light grey color, enclosing minerals such as quartz, K-feldspar, plagioclase, biotite, hornblende, chlorite, and iron oxide. Burungmandi Granodiorite (Kbg) of I-type granite (Pitfield, 1987) consists of granodiorite with a light grey-greenish color and is composed of minerals such as quartz, feldspar, plagioclase, biotite, and hornblende with secondary minerals like chlorite, carbonate, and iron oxide but devoid of cassiterite minerals. Baginda Adamellite (Jma) of I-type granite (Pitfield, 1987) is grey to greyish coarse-grained adamellite, composed of quartz, feldspar, plagioclase, biotite, and hornblende with secondary minerals like chlorite, carbonate, limonite, and iron oxide but lacking cassiterite minerals. Tanjungpandan Granite (Trtg) of S-type granite (Pitfield, 1987) is composed of foliated granite with a light grey color, containing minerals such as quartz, plagioclase, feldspar, biotite, and hornblende. Siantu Formation (PCsv) is only exposed on small islands to the north, deposited in a marine environment, and consists of dark green, massive, and aphanitic lava basalt and volcanic breccia containing subangular-subrounded basalts. Tajam Formation (PCTm) comprises white to green quartz sandstone intercalated with green to brownish siltstone, with both sandstone and siltstone being slightly metamorphosed. Quartz-associated primary tin is found in stockwork veins and fissures found in this rock formation. Kelapakampit Formation (PCks), which is the dominant lithology on Belitung Island, comprises flysch-type sediments indicating marine environment. This formation consists of metasandstone, slate, mudstone, shale, tuffaceous siltstone, and chert. Metasandstone and other sedimentary rocks appear in alternating layers, up to 500 m thick.

Coastal area spatial planning involves the study and analysis of the physical, geological, and oceanographic processes, i.e., wave action, tides, and currents, that shape coastal areas. It helps in understanding the dynamics of coastlines, the interaction between land and sea, and the potential risks and vulnerabilities associated with coastal zones. According to Clark (1996), coastal and marine spatial planning intends to manage and coordinate different uses and activities more efficiently and sustainably. Meanwhile, Suparno et al. (2022) proposed the Marine Spatial Allocations of the Coastal and Small Islands Zoning Plan, emphasizing the significance of marine spatial planning in balancing economic development and environmental conservation, thereby promoting the sustainability of marine resources. All the knowledge will be used to determine suitable locations for various coastal development activities, such as ports and areas for coastal tourism or aquaculture. This study aimed to gather scientific information on the marine geology and oceanography surrounding Manggar Waters to the east of Belitung. Hence, a wide-ranging marine geological survey was conducted to collect data and enrich insights into not only the overall geological knowledge that form the geopark's landscape but also the potential risk of marine hazards related to the region. Potentially, the preliminary findings can be used as a scientific basis for the sustainable management and development of Belitong Geopark.

METHODS

The Marine Geological Institute (MGI, or BBSPGL in Bahasa) entirely ran and provided all the equipment deployed in the survey. Datasets were acquired by employing various methods. This study sought to identify and map the geological features, surface sediment distribution, and sedimentary deposits of the Manggar Waters through a combination of sediment sampling, tidal and current data collecting, bathymetric surveys and coastal observation.

The marine survey was carried out on a fishing boat. The bathymetrical survey involved using an echosounder called Echotrac E20 Teledyne to measure the depth of the water and the morphology of the seabed. This was done along a distance of 390.6 nautical km. On the other hand, LWS, also known as Lowest Water Spring, which represents the lowest tidal level that occurs during the year, is an essential parameter in bathymetric mapping. LWS serves as a consistent reference point for measuring and representing water depths accurately, disregarding varied water levels due to tides, seasonal changes, or other factors. The water depth consistency and accuracy help providing information for the safety of vessel navigation and underwater infrastructure development. Tidal measurements were taken in 15 days on the north coast of Buku Limau Island to validate the results of the bathymetrical survey and comprehend the water conditions.

Current velocity was measured by Infinity AEM Current Meter and is used to serve as data sources for modeling the current in the area to better understand its patterns and intensity. In order to create the current model, Flow Model Flexible Mesh from DHI Mike21 software was used (Danish Hydraulic Institute, 2007). This software includes modules for hydrodynamics (HD) and mud transport (MT). The input data included for generating the model were bathymetry that was collected during the survey, tidal predictions from Globaltide, measurements of total suspended solids (TSS), and discharge measurement rate of the Manggar River from research by Sabri et al. (2017).

Forty marine sediment samples, as shown in Figure 2, were collected along the seabed surface by using grab samplers to study sediment characteristics and composition, including microfauna composition. Mapping work was done on the eastern side of Belitung Island, covering the coast of Manggar and the coasts of small islands (Buku Limau and Siadung Islands), to identify coastal characteristics by using an unmanned aerial vehicle (UAV) drone. It is important to understand sediment properties and composition, as well as coastal characteristics, as is crucial for coastal development and spatial planning.

The environmental condition of the seawater could be recognized by studying various parameters. About twenty seawater samples were collected and analyzed using a multiparameter Milwaukee instrument. This instrument measured temperature, salinity, and turbidity, which are key parameters in assessing the current condition of seawater. Furthermore, to gain a more

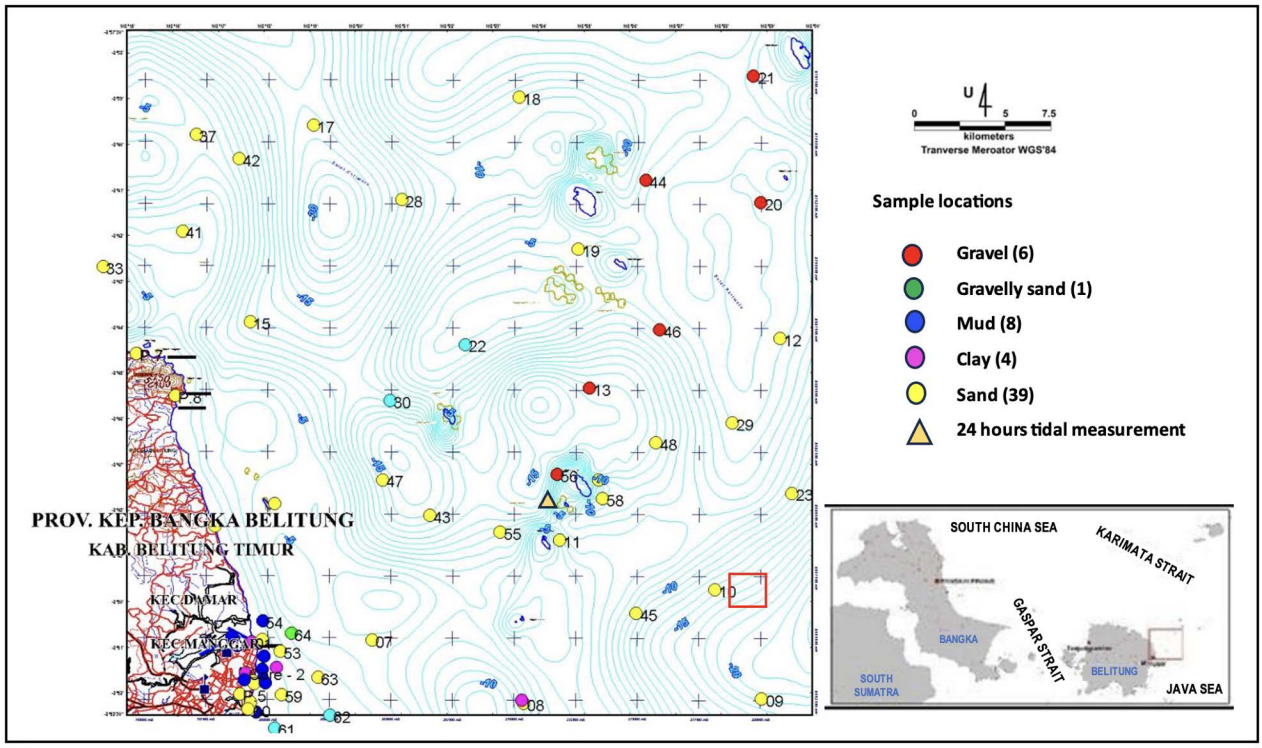

Figure 2. Survey area and sampling locations, shown by sampling number (see map with number attached to each site) and type of sediment samples represented by color, comprises: gravel (red) in 6 locations, gravelly sand (green) in 1 location, mud (blue) in 8 locations, clay (magenta) in 4 locations, and sand (yellow) in 39 locations (see map legend for color and total numbers of each sediment type).

comprehensive understanding of the seawater quality, the collected samples were sent to the Sucofindo Laboratory for additional analysis. In this laboratory, various environmental parameters were analyzed, including biological oxygen demand (BOD), chemical oxygen demand (COD), total suspended solids (TSS), and heavy metal levels. These parameters are essential in evaluating the level of organic pollution, nutrient availability, and the presence of toxic substances in the seawater.

Along with the study of water column, sediment samples were also subjected to analysis. The sediment samples were analyzed for grain size distribution in the Marine Sedimentology Laboratory at MGI. Measuring the particle grain size helps determine the sediment composition and transport processes during deposition. For further analysis of sediment sample composition and micropaleontological studies, the Petrology and Micropaleontology Laboratory at MGI was utilized. The laboratory is specialized in studying mineral composition and microfossils. The identification and examination of sediment composition and microfossils support comprehending the geological processes and paleoenvironmental conditions of the area being studied.

RESULTS AND DISCUSSIONS

LWS was used as a reference point for bathymetric analysis, resulting in varied bathymetry from 0 to over 45 m. Within 5 km of the coast, the water depths ranged from 0 to 10 m. Beyond that distance, the water depths become deeper, ranging between 25 and 45 m (Figure 3). Near the coast, the southern part of the Manggar Waters area is shallower compared to the northern part. However, the deepest water depths are observed further to the eastern part of the area toward the open sea. Several high areas composed of coral reefs were also observed, particularly nearby small islands such as Buku Limau, Siadung, Memperak, and others.

There are two dominant currents in the northern part of Manggar Waters, which are flowing westward and eastward. In the deeper section of the water, specifically at 16 m water depth, the mean (average) of the strongest current speeds is measured to be 0.671 m/s. This indicates that the deep currents in the north part, either in westward or eastward direction, have a speed close to 0.671 m/s on average. On the other hand, at a slightly shallower location with a water depth of 12 m, the maximum (highest) speed of the strongest currents is measured to be 0.764 m/s. This implies that the middle currents reach higher speeds compared to the deeper part, with a maximum speed of 0.764 m/s.

Figure 5 shows the concentrate pattern of current distribution, revealing a correlation between the movement of the concentrates and the direction of the seawater current in different tide phases. During low tide, the concentrate pattern shows a movement towards the north, suggesting that the seawater current moves northward along the coast. On the other hand, during high tide, the distribution of the concentrates is less prominent, signifying that the seawater current is likely being blocked by the high tide, which restricts their movement. Nonetheless, the pattern of concentrate during high tide still shows a relatively southward movement, which implies that the seawater current is moving southward during this time.

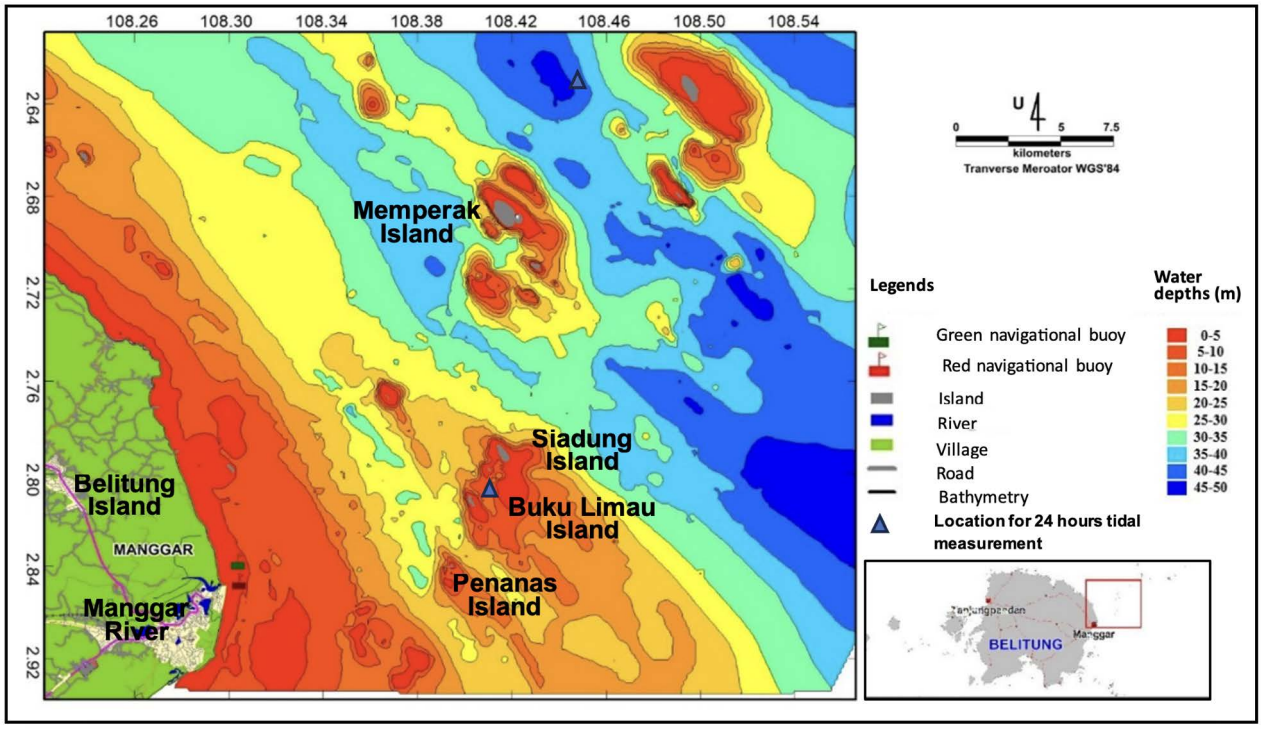

Figure 3. Bathymetry of Manggar Waters, using LWS as the reference point

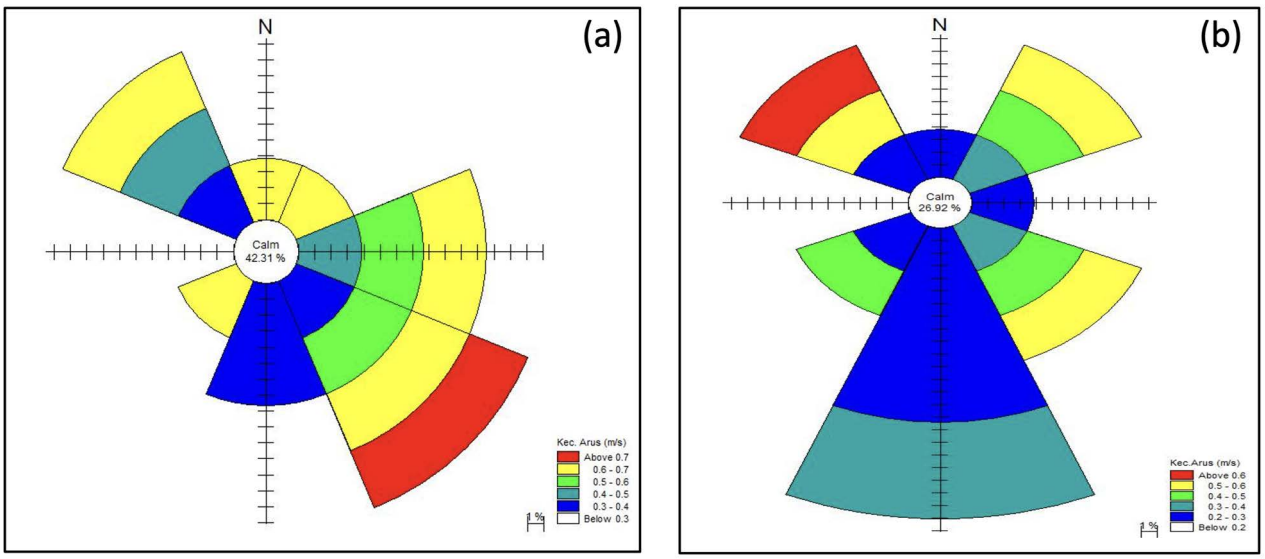

Figure 4. Rose diagrams showing current speed and direction in the north part of Manggar Waters, i.e., (a) the maximum current at 12 m depth (measured at 0.6d, meaning 0.6 X water depth at the location), and (b) the mean current at 16 m depth (measured at 0.8d, meaning 0.8 X water depth at the location).

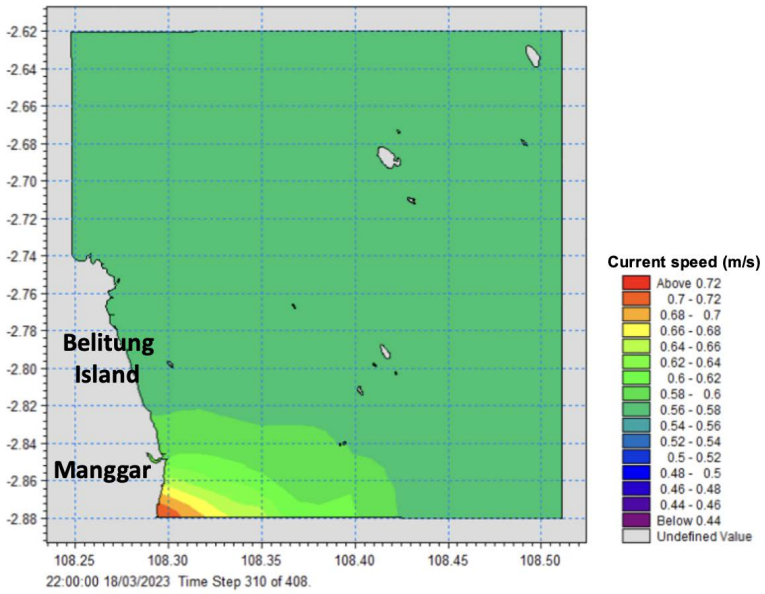

Figure 5. Current model of Manggar Waters, derived from MIKE21 modeling

Based on megascopic identification, the surface sediments of Manggar Waters seabed are predominantly composed of sand, which is distributed around Belitung Island (Figure 6). Sand-sized coral fragments are particularly found around the coral reefs of small islands such as Buku Limau, Siadung, Memperak, and Penanas. Towards the eastern part of the survey area, muddy sand and sandy mud occupy most of this part, i.e., along the Manggar coast and nearby Penanas Island. As identified by Baharuddin & Sidarto (1995), Quaternary alluvium (Qa) predominates beaches in the study area, with revealed rock formations being mostly Kelapakampit (PCks) and occurrences of Burungmandi Granodiorite (Kbg) and Batubesi Quartz Diorite (Kbd) in scarce locations.

Microfauna observation in five samples has shown that the foraminifera diversity in Manggar Waters appears to be relatively low, comprising only twelve genera. This is in contrast to a previous study by Irlani et al. (2013) conducted in the nearby location in Karimata Strait, which revealed 50 genera consisting of 85 species of benthic foraminifera. However, similar to that study, broken benthic foraminiferal tests were found abundantly in the surveyed area. The dominant foraminiferal genera within the sediments are *Amphistegina* and *Operculina* (Figure 7). Other abundant genera include *Quinqueloculina*, particularly *Q. philippinensis*, *Textularia*, and *Calcarina* in some of the samples. These genera are typically associated with coral reef habitats within middle to coarse

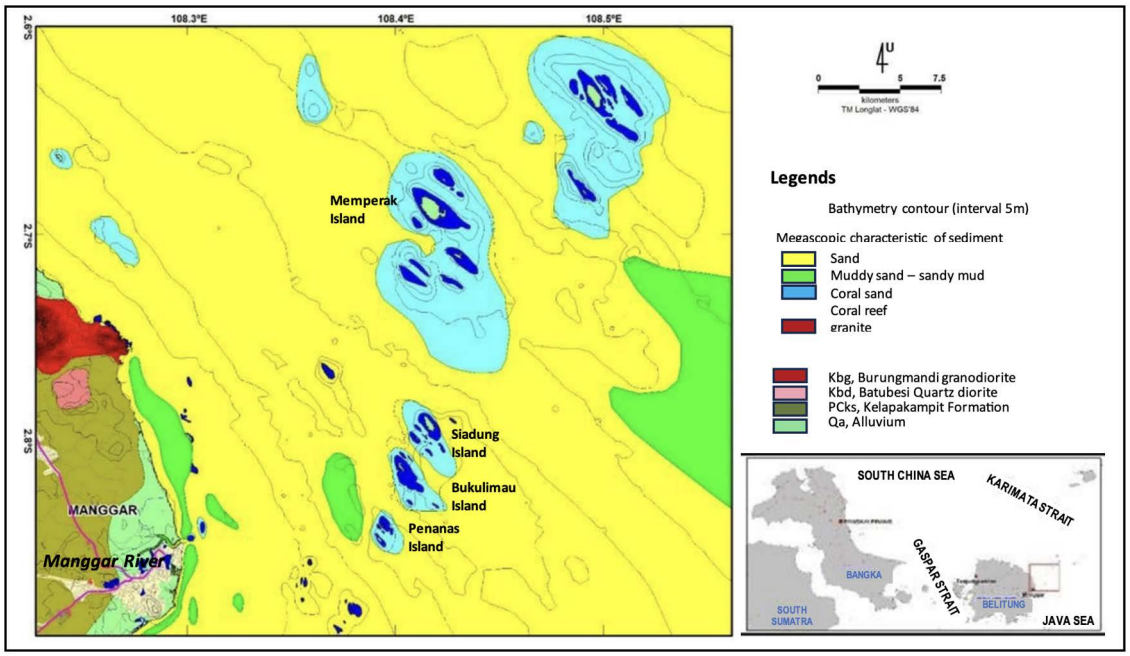

Figure 6. Map of seabed surface sediment distribution around Manggar Waters based on megascopic identification

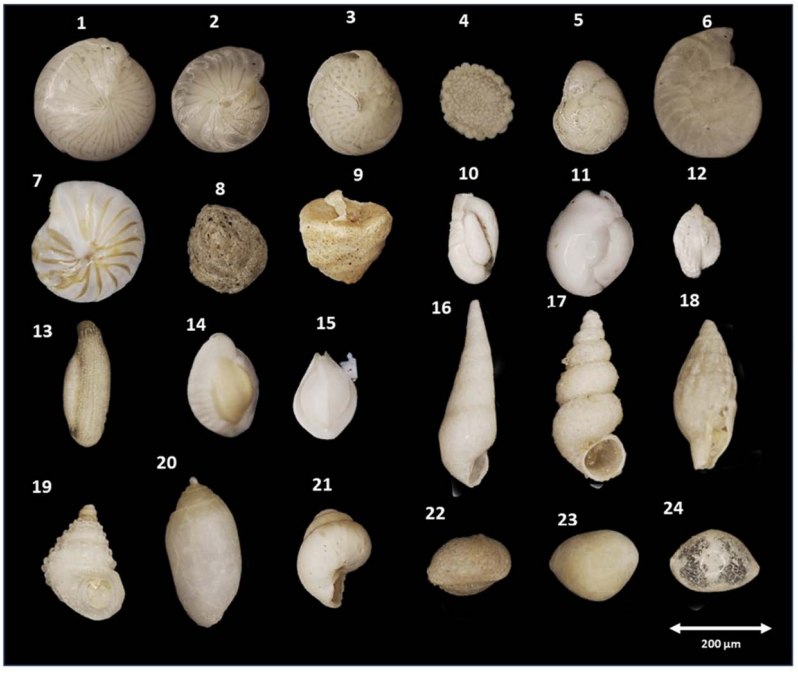

Figure 7. Dominant genera of foraminifera, and other microfauna found in sediment samples of Manggar Waters (1-15. Foraminifera: 1-3. *Amphistegina,* 4. *Planorbulinella,* 5. *Eponides,* 6. *Operculina,* 7. *Peneroplis,* 8-9. *Textularia,* 10-14. *Quinqueloculina,* 15. *Triloloculina;* 16-21: Micro-molluscs; 22-24: Ostracod

sediments (Hallock et al., 2003; Javaux & Scott, 2003). *Operculina* is a larger symbiont-bearing foraminifer that thrives in shallow oligotrophic waters and plays a significant role in calcium carbonate ($CaCO_3$) production (Oron et al., 2018). *Amphistegina*, on the other hand, prefers high-quality reef environments, so a decrease in its abundance suggests environmental quality degradation (Hallock et al., 2003). Notably, in the southern part of the survey area, MGR-10 exhibits a decline in *Amphistegina* abundance.

The levels of heavy metals are relatively low and below the detection limit of the equipment used, based on the analysis of twenty seawater samples. This indicates that the seawater environment is in good condition. However, in certain locations, Zn levels were found to be above the detection limit (Table 1, see numbers in red color), although still below the threshold value for marine

Table 1. Seawater parameter analysis

Samples	Hg (mg/L)	Cr (mg/L)	As (mg/L)	Cd (mg/L)	Cu (mg/L)	Pb (mg/L)	Zn (mg/L)	Ni (mg/L)
MGR-0	< 0.0008	<0.001	<0.001	<0.0008	<0.006	<0.003	0.03	<0.02
MGR-1	< 0.0008	<0.001	<0.001	<0.0008	<0.006	<0.003	<0.01	<0.02
MGR-2	< 0.0008	<0.001	<0.001	<0.0008	<0.006	<0.003	0.02	<0.02
MGR-3	< 0.0008	<0.001	<0.001	<0.0008	<0.006	<0.003	<0.01	<0.02
MGR-4	< 0.0008	<0.001	<0.001	<0.0008	<0.006	<0.003	<0.01	<0.02
MGR-5	< 0.0008	<0.001	<0.001	<0.0008	<0.006	<0.003	0.06	<0.02
MGR-6	< 0.0008	<0.001	<0.001	<0.0008	<0.006	<0.003	<0.01	<0.02
MGR-9 D1	< 0.0008	<0.001	<0.001	<0.0008	<0.006	<0.003	0.01	<0.02
MGR-9 D2	< 0.0008	<0.001	<0.001	<0.0008	<0.006	<0.003	<0.01	<0.02
MGR-9 D3	< 0.0008	<0.001	<0.001	<0.0008	<0.006	<0.003	<0.01	<0.02
MGR-11 D1	< 0.0008	<0.001	<0.001	<0.0008	<0.006	<0.003	<0.01	<0.02
MGR-11 D2	< 0.0008	<0.001	<0.001	<0.0008	<0.006	<0.003	0.07	<0.02
MGR-11 D3	< 0.0008	<0.001	<0.001	<0.0008	<0.006	<0.003	<0.01	<0.02
MGR -12 D1	< 0.0008	<0.001	<0.001	<0.0008	<0.006	<0.003	0.01	<0.02
MGR-12 D2	< 0.0008	<0.001	<0.001	<0.0008	<0.006	<0.003	<0.01	<0.02
MGR-12 D3	< 0.0008	<0.001	<0.001	<0.0008	<0.006	<0.003	0.01	<0.02
MGR-15 D1	< 0.0008	<0.001	<0.001	<0.0008	<0.006	<0.003	<0.01	<0.02
MGR-15 D2	< 0.0008	<0.001	<0.001	<0.0008	<0.006	<0.003	<0.01	<0.02
MGR-15 D3	< 0.0008	<0.001	<0.001	<0.0008	<0.006	<0.003	<0.01	<0.02
MGR-17 D1	< 0.0008	<0.001	<0.001	<0.0008	<0.006	<0.003	<0.01	<0.02
MGR-17 D2	< 0.0008	<0.001	<0.001	<0.0008	<0.006	<0.003	<0.01	<0.02
MGR-17 D3	< 0.0008	<0.001	<0.001	<0.0008	<0.006	<0.003	<0.01	<0.02
MGR-18 D1	< 0.0008	<0.001	<0.001	<0.0008	<0.006	<0.003	<0.01	<0.02
MGR-18 D2	< 0.0008	<0.001	<0.001	<0.0008	<0.006	<0.003	<0.01	<0.02
MGR-18 D3	< 0.0008	<0.001	<0.001	<0.0008	<0.006	<0.003	<0.01	<0.02
MGR-19 D1	< 0.0008	<0.001	<0.001	<0.0008	<0.006	<0.003	<0.01	<0.02
MGR-19 D2	< 0.0008	<0.001	<0.001	<0.0008	<0.006	<0.003	<0.01	<0.02
MGR-19 D3	< 0.0008	<0.001	<0.001	<0.0008	<0.006	<0.003	<0.01	<0.02
Threshold value for marine tourism	0.002	0.002	0.025	0.002	0.05	0.008	0.095	0.075
Threshold value for marine biota	0.001	0.005	0.012	0.001	0.008	0.008	0.05	0.05

Notes: D1: surface water, D2: 0.6 x water depth, D3: 0.8 x water depth
Threshold value: according to KEP-51/MENLH/2004

tourism (0.095 mg/L according to KEP-51/MENLH/2004). Specifically, MGR-5 near the river mouth of Manggar River and MGR-11 near Penanas Island in the southern part of the survey area contained Zn levels of 0.06 and 0.07 mg/L, respectively, which are close to the threshold value for marine tourism but still above the threshold value for marine biota, i.e., 0.05 mg/L.

Similar to the seawater, the heavy metal content in the surface sediments is relatively low and does not exceed the marine sediment quality standard, according to WAC 173-204-320 (Washington State Department of Ecology, 2013). Table 2 demonstrates that while most sediment samples did not contain detectable levels of mercury (Hg), certain areas displayed inconsistent concentrations of mercury that exceeded the threshold value of 0.41 parts per million (ppm). These marine surface sediment samples from those areas showed mercury high concentrations above 4 ppm, with an average concentration of 14.58 ppm. The particularly high levels of mercury are found in

locations in close proximity to the estuary of Manggar River, as well as in the northern area of Manggar.

Valuable elements, such as Ti, Th, Fe, Cu, and Au, were analyzed by portable XRF scanning. These elements were found to be mostly high, particularly in samples near the Manggar River estuary (Samples MGR-4, 33, 34, 54, and MGR-64), as well as in the southern part of the survey area (Table 3). However, the concentration of Au should be cautiously evaluated due to our XRF equipment having Au composition as a part of its elements. Therefore, further analysis using more quantitative methods (AAS or ICP-MS equipment) is necessary.

Three parameters were considered in coastal characteristic mapping, including: beach morphology, lithological type, and coastline characteristics, in order to categorize and describe different aspects of a coastal area in Manggar (Figure 8). In terms of beach morphology and lithological type, the coastal area of Manggar can be divided into two types. The first type is the rocky beach, which is located in the northern part, from Burungmandi to Malanglepau Beaches. Along these beaches, the dominant

Table 2. Heavy metal concentration in the sediments

No	SAMPLE ID	Hg	As	Cu	Zn	Pb	Unit
							%
1	MGRS-1	4.13	10.2	10.1	21.3	18.5	PPM
2	MGRS-2	4.6	8.4	11.9	20	14.3	PPM
3	MGRS-10	ND	ND	11	ND	ND	PPM
4	MGRS-11	ND	5.2	ND	ND	ND	PPM
5	MGRS-12	14	3.8	9	ND	ND	PPM
6	MGRS-13	31	6.3	31	ND	ND	PPM
7	MGRS-14	ND	5.5	12	10	6.8	PPM
8	MGRS-15	ND	ND	15	ND	12.3	PPM
9	MGRS-16	ND	ND	ND	ND	6.7	PPM
10	MGRS-17	ND	2.5	14	ND	ND	PPM
11	MGRS-18	16	ND	11	ND	ND	PPM
12	MGRS-22	ND	2.2	16	ND	ND	PPM
13	MGRS-23	ND	7.3	12	ND	5.1	PPM
14	MGRS-28	ND	8	11	ND	ND	PPM
15	MGRS-29	ND	6.7	ND	ND	4.4	PPM
16	MGRS-3	ND	2.9	18	ND	9.9	PPM
17	MGRS-30	ND	4.4	14	ND	4.2	PPM
18	MGRS-32	12	21.1	21	41	31.7	PPM
19	MGRS-33	12	7.9	10	15	13.4	PPM
20	MGRS-34	6	16.1	11	26.1	23.7	PPM
21	MGRS-36	ND	2.6	13	ND	ND	PPM
22	MGRS-4	6	17.4	15	36.9	28.3	PPM
23	MGRS-42	ND	ND	13	ND	5.5	PPM
24	MGRS-43	ND	2.6	9	ND	ND	PPM
25	MGRS-45	14	3.1	12	ND	ND	PPM
26	MGRS-45	ND	3	9	ND	ND	PPM
27	MGRS-47	13	ND	9	ND	3	PPM
28	MGRS-48	19	7.4	16	ND	4.4	PPM
29	MGRS-50U	ND	11	11.1	28.2	16.6	PPM
30	MGRS-53	17	ND	13	ND	ND	PPM
31	MGRS-54	5	19.8	19	43.2	32.8	PPM
32	MGRS-55	ND	ND	10	ND	ND	PPM
33	MGRS-56	15	ND	13	ND	ND	PPM
34	MGRS-58	15	3.9	14	ND	ND	PPM
35	MGRS-59	23	ND	22	ND	ND	PPM
36	MGRS-60	26	ND	17	ND	ND	PPM
37	MGRS-61	19	ND	16	ND	ND	PPM
38	MGRS-62	17.5	ND	16	ND	ND	PPM
39	MGRS-63	17	ND	16	ND	ND	PPM
40	MGRS-9U	ND	2.5	11	ND	ND	PPM
Average		14.58	7.377	13.84	26.86	13.42	PPM
Threshold value (WAC 173-204-320)		0.41	57	390	410	450	PPM

Threshold value according to marine sediment quality standard for chemical criteria WAC 173-204-320

Table 3. Concentration of valuable elements in sediments

No	SAMPLE ID	Ti	V	Fe	Cu	Y	Zr	Au	Th	Unit
										%
1	MGRS-1	1576	14.9	5700	10.1	9.1	368	6.4	8	PPM
2	MGRS-2	2181	20	5975	11.9	15	866	ND	11	PPM
3	MGRS-3	613	4.6	1370	18	3	126	17	ND	PPM
4	MGRS-4	2417	28	11288	15	15.1	449	13	17	PPM
5	MGRS-10	81	ND	1054	11	ND	33	14	ND	PPM
6	MGRS-11	195	ND	760	ND	ND	227	49	33	PPM
7	MGRS-12	167	ND	1602	9	3.8	69	15	21	PPM
8	MGRS-13	419	6.3	2760	31	6.3	354	18	9	PPM
9	MGRS-14	470	6	2534	12	4.2	65	14	16	PPM
10	MGRS-15	525	5.6	2082	15	3.2	77	20	8	PPM
11	MGRS-16	141	ND	1064	ND	3.3	49	20	13	PPM
12	MGRS-17	105	ND	1559	14	2.3	41	25	ND	PPM
13	MGRS-18	100	ND	1188	11	2.4	23	17	ND	PPM
14	MGRS-22	353	ND	1359	16	3.3	80	21	ND	PPM
15	MGRS-23	150	3.6	2907	12	5.3	185	18	20	PPM
16	MGRS-28	472	ND	3666	11	3	145	24	ND	PPM
17	MGRS-29	166	ND	2702	ND	5.7	59	21	22	PPM
18	MGRS-30	131	3.8	1901	14	3.8	41	19	10	PPM
19	MGRS-32	2711	33	12546	21	17.5	334	15	20	PPM
20	MGRS-33	754	10.5	5082	10	6.4	114	ND	19	PPM
21	MGRS-34	2322	23	8003	11	14.7	497	21	18	PPM
22	MGRS-36	101	ND	1338	13	2.6	44	7	ND	PPM
23	MGRS-42	195	ND	1082	13	2.2	36	20	ND	PPM
24	MGRS-43	672	5.8	2095	9	3.4	147	17	9	PPM
25	MGRS-45	92	ND	905	12	2.9	45	21	22	PPM
26	MGRS-45	88	ND	842	9	3.3	41	18	18	PPM
27	MGRS-47	230	4	1815	9	3.2	32	17	8	PPM
28	MGRS-48	411	4.7	4552	16	5.8	303	28	ND	PPM
29	MGRS-50U	2115	20	7703	11.1	10.6	293	ND	11	PPM
30	MGRS-53	473	3.8	760	13	1.9	78	27	ND	PPM
31	MGRS-54	3334	34	11859	19	18.2	587	7.7	28	PPM
32	MGRS-55	171	ND	1308	10	3.1	43	11	ND	PPM
33	MGRS-56	279	4.1	1260	13	3	119	22	6	PPM
34	MGRS-58	57	ND	781	14	ND	52	19	37	PPM
35	MGRS-59	293	3.7	394	22	ND	60	35	ND	PPM
36	MGRS-60	555	3.9	552	17	1.9	202	31	ND	PPM
37	MGRS-61	649	5.5	456	16	2.1	204	33	ND	PPM
38	MGRS-62	552	3.7	436	16	ND	102	29	ND	PPM
39	MGRS-63	151	2.4	448	16	ND	28.4	23	ND	PPM
40	MGRS-9U	87	ND	1095	11	2.5	34	19	ND	PPM
Average		663.9	10.62	2920	13.84	5.709	166.3	20.33	16.7	

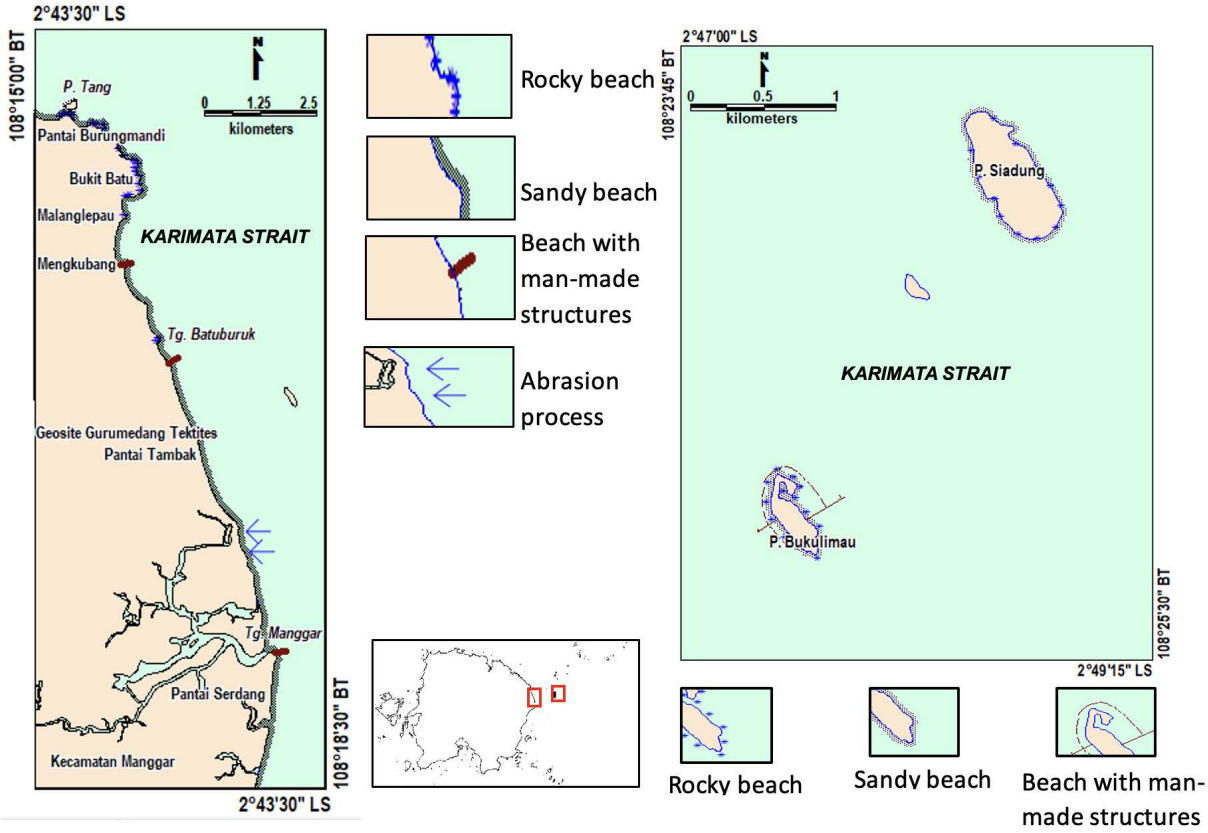

Figure 8. Coastal characteristics of Manggar, Siadung and Buku Limau Island

lithology is igneous rock, specifically Burungmandi Granodiorite of Cretaceous period (Baharuddin & Sidarto, 1995). This means that the beach in this area is characterized by the presence of rocks and a rugged shoreline. The second type is the flat beach, which occupies the southern area from Malanglepau to Serdang Beaches. The lithology composition of this area is different from the rocky beach. It is dominated by the Kelapakampit Formation and Quaternary alluvium. This means that the beach is relatively flat and composed of loose materials of gravel to cobble grains, sand, silt, clay, and Quaternary coral shells.

The characteristics of coastlines concerning lithology, which are influenced by the dominance of beach and sedimentation processes, can be classified into different types. The first type is a sandy beach, consisting of loose material in various sand sizes and coral shells. This type is prevalent in the surveyed area. The second type is a rocky beach made up of igneous rock granodiorite, found on the beaches from Burungmandi to Malanglepau and also in Batuburuk Cape. The third type is a beach with man-made structures, such as an unused pier and breakwater made of igneous rock boulders arranged in gabions. The unused pier is located in Mengkubang Beach and in the southern part of Batuburuk Cape, while the breakwater is situated at the estuary of Manggar River. The fourth type is characterized by the abrasion process, where rocks and other hard materials are continuously transported and fragmented by the action of waves and currents, leading to the erosion and smoothing of the coastline. This beach type occurs in the southern section of Tambak Beach.

Siadung and Buku Limau beaches have similar characteristics to Manggar Beach. Both have rocky beaches composed of coral reefs. They also have sandy beaches made up of coarse to fine-grained sand and contain rocks and coral fragments. Additionally, Buku Limau Beach has man-made structures such as piers and gabions as breakwaters made from igneous and coral boulders.

The rocky beaches of these small islands, made up of igneous rock and coral sand, provide valuable evidence about Belitong Geopark's geological history. Several geosites revealing outcrops of igneous rock, such as Batubesi, Burungmandi, and Baginda rock formations, can be observed. These islands also have coral reefs, which attract tourists. The symbiotic relationship between microfauna benthic foraminifera and coral results in the preservation of various genera, making it an appealing aspect of tourism. However, we have discovered a significant amount of broken foraminifera tests and lower diversity in this area, suggesting a decline in environmental quality compared to normal conditions. This degradation could be due to the high levels of

mercury found near the estuary of Manggar River and in the northern part of Manggar. Correspondingly, the decrease of Amphistegina in the northern region of Manggar Waters may be attributed to the elevated mercury level.

The presence of flat beaches and coral reefs in the southern part offers opportunities for studying geological processes more, such as beach formation. In addition, there is likely a relationship between sediment composition and marine biota, given the diversity of the marine ecosystem. It is also possible that the diversity of microorganisms is related to the mercury content in the sediments, as mercury can have an impact on the variety of foraminifera. Therefore, it is necessary to conduct further analysis of the elements in the marine sediments in order to obtain more dependable results.

Going through a comprehensive analysis of seawater, environmental factors, and sediments, these findings can be examined for developing strategies in order to protect and conserve the marine ecosystem. Similarly, the factors that influence the currents and their impacts on sediment transport, erosion, and deposition processes can be determined by understanding the variation in current speeds and directions. It is necessary for managing the risks of coastal erosion and sedimentation. The small islands surrounding the area, which have flat beaches, coral reefs, and interesting geological features such as rock outcrops, can also be developed as marine tourist destinations and activities. Thus, providing information on geological features and coastal erosion risks can contribute to sustainable marine tourism, ensuring that tourism activities do not harm the marine environment.

CONCLUSSIONS

The presence of flat beaches and coral reefs in the southern part, as well as a cluster of volcanic/plutonic rocks, can be a draw for visitors who are interested in the geological processes of the area. Even though it is not significant, the existence of microorganisms in the sediments indicates a diverse marine ecosystem. However, in contrast, the presence of mercury in the sediments in the northern part of Manggar and near the Manggar River estuary, as shown by the concentration analysis of elements, may have an adverse effect on the diversity of foraminifera in that particular area. Additionally, the small islands surrounding the area, with their flat beaches and interesting geological features, have the potential to be developed as attractive marine tourist destinations, particularly for activities related to marine tourism, like fishing, snorkeling, etc.

The northern part of Belitong Geopark experiences varying current speeds and directions. In the deeper part, the average speed is 0.671 m/s, while in the shallower section, the maximum speed reaches 0.764 m/s. In Manggar Waters, the currents move towards the north during low tide, while during high tide, they move towards the south. In terms of natural hazards, except for the southern part which is affected by abrasion processes, the current energy does not pose any risk to the geosites.

The thorough examination of various aspects of seawater, environmental factors, and sediment samples from this survey has provided a better understanding of the geological and environmental conditions and processes in the marine and coastal environment in Manggar Waters. It is expected to use the findings as the contribution to making cognizant decisions and implementing appropriate strategies for the protection and conservation of the marine ecosystem in the marine nature reserve. Moreover, the data acquired will support future research efforts and foster collaborations in order to gain a deeper comprehension of the geological aspects of Belitong Geopark.

ACKNOWLEDGEMENTS

We would like to extend our deep appreciation to the Indonesian government for their profound support in funding this survey by the financial year 2023. Additionally, we extend our heartfelt gratitude to the local government of East Belitung regency and Manggar district for kindly granting us permission to conduct the survey in their region. We would also like to acknowledge and commend the Manggar people for their warm hospitality and acceptance of our survey team. Moreover, we extend our sincere thanks to the Department of Geological Engineering at Padjadjaran University for affording their students the opportunity to carry out their practical work in the MGI's marine sedimentology laboratory.

REFERENCES

Baharuddin, and Sidarto, 1995. *Geological Map of Belitung Sheet, Sumatera*. Geological Research and Development Centre.

Belitong UGGp, 2021. *Belitong Geopark Information Center*. Available at https://belitonggeopark.net/beranda-1 as accessed on November 1, 2023.

Bhinekawati, R., Nelloh, L.A.M., and Abdurahman, O., 2020. The analysis of entrepreneurial intention in rural area: A case study of Bukit Peramun Geosite in Indonesia. *GeoJournal of Tourism and Geosites*, 28(1): 80–94. DOI: 10.30892/gtg.28106-453.

Clark, J. R., 1996. *Coastal Zone Management Handbook*. Lewis Publishers, New York.

Danish Hydraulic Institute (DHI), 2007. "MIKE21 Flow Model FM – Mud Transport Module User Guide". Danish Hydraulic Institute. Denmark.

Hallock, P., Lidz, B.H., Cockey-Burkhard, E.M., and Donnelly, K. B., 2003. Foraminifera as bioindicators in coral reef assessment and monitoring: the foram index. *Environmental Monitoring and Assessment*, 81(1–3): 221–238.

Hartoko, A. (2019). The myth and legend of Sadai and Gaspar Strait, Bangka Belitung (Banca-Billiton) and Oceanographic Conditions. *International Journal of GEOMATE*. Special Issue on Science, Engineering & Environment, 17(62): 212–218. DOI: 10.21660/2019.62.93965

Hutabarat, L.F., 2023. Pengembangan Geopark Nasional Indonesia menuju UNESCO Global Geopark sebagai diplomasi geotourism Indonesia. *Jurnal Ilmiah Hubungan Internasional*. 19(1): 94–106. DOI: 10.26593/jihi.v19i1.6000.94-106

Irlani, M., Widiastuti, E.L., Dewi, K.T., and Susanto, G.N., 2013. Struktur komunitas foraminifera bentik di Selat Karimata (Lembar Peta 1314), *Prosiding Semirata FMIPA Universitas Lampung.*

Javaux, E.J. and Scott, D.B., 2003. Illustration of modern benthic foraminifera from Bermuda and remarks on distribution in other subtropical/ tropical areas. *Paleontologia Electronica*, 6(4): 29 pp.

Oron, S., Abramovich, S., Almogi-Labin, A., Woeger, J., and Erez, J., 2018. Depth related adaptations in symbiont bearing benthic foraminifera: New insights from a feld experiment on *Operculina ammonoides*. *Scientific Reports,* 8: 9560, 11pp. DOI: 10.1038/s41598-018-27838-8.

Pitfield, P.E.J., 1987. Geochemistry of the Tin Islands granites of Indonesia in relation to those of Peninsular Malaysia. *Warta Geologi*, 13(3): 125–133.

Priem, H.N.A., Boelrijk, N.A.I.M., Hebeda, E.H., Verdurmen, E.A.Th., Verschure, R.H., and Bon, E.H., 1975. Isotope geochronology in the Indonesian tin belt. *Geologie en Mijnbouw*, 54(1): 61–70.

Sabri, F., Aulia, T., and Tresnanda, M., 2017. Analisis Banjir Belitung Timur. *Prosiding Seminar Nasional Penelitian dan Pengabdian pada Masyarakat: Inovasi Riset dan Teknologi Terapan untuk Mendukung Pembangunan Berkelanjutan*. Pangkalpinang.

Suparno, S., Arlius, Efriyeldi, and Putra, A., 2022. Marine Spatial Allocations of the Coastal and Small Islands Zoning Plan in West Sumatera Province. *Sumatra Journal of Disaster, Geography and Geography Education*, 6 (2): 22–30. DOI: 10.24036/sjdgge.v6i2.408.

UNESCO, 2021. *Belitong UNESCO Global Geopark*. Available at https://en.unesco.org/global-geoparks/belitong as accessed on November 1, 2023.

Washington State Department of Ecology, 2013. Sediment management standards: Marine sediment quality standards. *Washington Administrative Code (WAC)*. Title 173: Ch. 173-204: Sec. 173-204-320. Available at https://app.leg.wa.gov/WAC/default.aspx?cite=173-204-320 as accessed on November 1, 2023.

Wei, Z.X., Fang, G.H., Susanto, R.D., Adi, T.R., Fan, B., Setiawan, A., Li, S.J., Wang, Y.G., and Gao, X.M., 2015. Tidal elevation, current and energy flux in the area between the South China Sea and Java Sea. *Ocean Sci. Discuss.*, 12: 2831–2861. DOI: 10.5194/osd-12-2831-2015

Wicaksana, S., Sofian, I., and Pranowo, W., 2015. Karakteristik gelombang signifikan di Selat Karimata dan Laut Jawa berdasarkan rerata angin 9 Tahunan (2005-2013). Omni-Akuatika, 11(2): 33–40. DOI: 10.20884/1.oa.2015.11.2.37

Zukhri, N., Rosalina, E., and Christianingrum, C., 2021. Geopark Belitong: Environment based tourism branding in Belitung Island. *IOP Conference Series: Earth and Environmental Science*, 926(1): p. 012075. DOI: 10.1088/1755-1315/926/1/012075

Guide for Authors - Geoscience Publications
Bulletin of the Marine Geology

Writing should be submitted according to the following restrictions:

1. Manuscript should be written in English and be submitted online via journal website http://ejournal.mgi.esdm.go.id. Online Submission will be free. The author must login in order to make submission.
2. Manuscript should contains at least 2.000 words and at least 8 pages of manuscript that including embedded figures and tables, without any appendix, and the file should be in Microsoft Office (.doc/.docx) format. It should be prepared in A4 paper (21cm x 29.7cm) using 2.5 cm for left and right margins and 2 cm for top and bottom margins, additionally the paragraph should be used 1 line spacing, 11 TNR.
3. Title, Abstract, and Keywords should be written in English
   - Abstract should be written in English and Bahasa Indonesia version
   - Title should be less than 15 words, title case, small caps, centered, bold, font type Times New Roman (TNR), font size 16, and single spaced.
   - Abstract contains neither pictures nor tables, justified, in 11 TNR, single spaced, and should not exceed 250 words.
   - Keywords contain four to six words/phrases separated with coma and should be justified, 10 TNR and single spaced.
   - Please provide all email address of all authors for our database concern, however, in the published version, only the email address of the first author will be appeared.
4. Manuscript body consists of: Introduction, Method, Result, Discussion, and Conclusion completed by Acknowledgment and References in capital and bold.
5. Heading should be made in four levels. Level five cannot be accepted.
   - Heading 1: title caps, left aligned, bold, 14 TNR, single spaced
   - Heading 2: title case, left aligned, bold, 11 TNR, single spaced
   - Heading 3: title case, left aligned, italic, 11 TNR, single spaced
   - Heading 4 is not recommended, however, it could still be accepted with the format of: sentence case, left indent 5 mm, hanging indent 5 mm, italic, 11 TNR, single spaced
   - Heading 5 cannot be accepted in the manuscript.
6. Figure and table can be either in black and white or in color, they should be clearly readable and in a proportional measure to the overall page. Caption should be numbered, in 9 TNR and single spaced. For lay outing purpose, please provide the respective captioned figure/table with extension .tif/.jpg/.jpeg within a particular folder apart from the manuscript. Please note the figure source/citation/reference if it is taken and/or modified from previous publication.
7. Mathematical equation should be clearly written, numbered orderly, and accompanied with any information needed.
8. Header and footer including page number must not be used. All hypertext links and section bookmarks will be removed from papers. If you need to refer to an Internet email address or URL in your paper, you must type out the address or URL fully in Regular font.
9. Citation and Reference. Following are the detail organization of the references guidelines:
   a. References are written in alphabetical order according to the family name of the first author.
   b. If there is more than one references made by similar author, References are arranged in order of time, and then in alphabetical order.
   c. All the references should be cited in the text. In the text, reference is cited with author family name and the year of publication. If it is written by 2 authors, the family name of both authors are noted, followed by the year of publication, if it is written by more than 2 authors, the reference is cited with the first author family name, followed by *et al.,* and the year of publication. For example: (Kennett, 1981); (Usman and Panuju, 2013); (Susilohadi *et al.*, 2009). Several references are written in alphabetical order, for example: (Kennett, 1981; Susilohadi *et al.,* 2009; and Usman and Panuju, 2013).
   d. References are consist of paper, proceeding, or book that are published, or unpublished report including internal report, dissertation, or thesis.
   e. References can be taken from website, by writing the hyperlink, and the time when it is accessed. Wikipedia, personal blog, or non scientific website is not allowed to be taken into account.

f. References should be ten references in minimum, at least two of them were published in the last five years.

g. Only the family name of the authors are written, followed by the abbreviation of their first name and middle name (if available). If the reference is written by more than one author, all authors should be written, abbreviation (e.g. dkk, *et al,* or drr) is not allowed..

h. All the information of the references must be noted, including publisher, journal volume, number (if available), and page number.

- For book, the book title should be written in italic, for example:

  Kennett, J.P., 1981. *Marine Geology.* Prentice Hall, 813p.

- For periodicals, the name of the journal should be written in italic, for example:

  Susilohadi, S., Gaedicke, C., and Djajadihardja, Y.S., 2009. Structures and sedimentary deposition in the Sunda Strait, Indonesia, *Tectonophysics,* 467 (1): 55-71.

- (Tectonophysics is the name of the journal, 467 is the volume, 1 is issued number, 55 – 71 is page number)

  Usman, E., and Panuju, 2013. Study of Gas Potency Based on Gravity Anomaly Modeling And Seismic Profile Analysis at Banggai-Sula Basin. *Bulletin of the Marine Geology,* 28 (2): 51-60.

- For edited symposia, special issues, etc. published in periodical:

  Kenneth, S. J., 2009. Marine biogeochemistry in 2025. In: D. Glickson (Editor), *Oceanography in 2025: Proceedings of a workshop.* The National Academic Press, Washington D. C.: 130 – 134.

- For websites:

  <http://palaeo-electronica.org/2003_1/benthic/issue1_03.htm> [Accessed on 30 November 2011].

- Unpublished references:

  Darlan, Y., Kamiludin, U., Kurnio, H., Rahardian, R., Hutagaol, J. P., Sianipar, A. H., and Sinaga, A. C., 2005. *Eksplorasi prospektif gas biogenik kelautan di Perairan Muara Kakap dan sekitarnya - Kalimantan Barat.* Pusat Penelitian dan Pengembangan Geologi Kelautan, Bandung, Badan Penelitian dan Pengembangan Energi dan Sumberdaya Mineral, Departemen Energi dan Sumberdaya Mineral. Internal report, 104p. Unpublished.

SERTIFIKAT

Direktorat Jenderal Penguatan Riset dan Pengembangan,
Kementerian Riset, Teknologi, dan Pendidikan Tinggi

RISTEKDIKTI

Kutipan dari Keputusan Direktur Jenderal Penguatan Riset dan Pengembangan,
Kementerian Riset, Teknologi, dan Pendidikan Tinggi Republik Indonesia
Nomor: 21/E/KPT/2018, Tanggal 9 Juli 2018
Tentang Hasil Akreditasi Jurnal Ilmiah Periode I Tahun 2018

Nama Jurnal Imiah

Bulletin of the Marine Geology

E-ISSN: 2527-8843
Penerbit: Puslitbang Geologi Kelautan, Kementerian ESDM

Ditetapkan sebagai Jurnal Ilmiah

TERAKREDITASI PERINGKAT 2

TERAKREDITASI

Akreditasi berlaku selama 5 (lima) tahun, yaitu
Volume 31 Nomor 1 Tahun 2016 sampai Volume 35 Nomor 2 Tahun 2020

Jakarta, 9 Juli 2018
Direktur Jenderal Penguatan Riset dan Pengembangan

Dr. Muhammad Dimyati
NIP. 195912171984021001

MARINE GEOLOGICAL INSTITUTE

GEOLOGICAL AGENCY
MINISTRY OF ENERGY AND MINERAL RESOURCES
Jalan Dr, Junjunan No. 236, Bandung-40174, Indonesia
http://www.mgi.esdm.go.id, E-mail: ejournal.p3gl@gmail.com

ISSN 1410 - 6175
9 771410 617003